2017

Annual water balance model based on generalized proportionality relationship and its applications

Yin Tang
University of Central Florida

ANNUAL WATER BALANCE MODEL BASED ON GENERALIZED PROPORTIONALITY RELATIONSHIP AND ITS APPLICATIONS

by

YIN TANG
B.S. Beijing Forestry University, 2008
M.S. Beijing Forestry University, 2011

A dissertation submitted in partial fulfillment of the requirements
for the degree of Doctor of Philosophy
in the Department of Civil, Environmental and Construction Engineering
in the College of Engineering and Computer Science
at the University of Central Florida
Orlando, Florida

Spring Term
2017

Major Professor: Dingbao Wang

ABSTRACT

The main goal of this dissertation research is to derive a type of conceptual models for annual water balance at the watershed scale. The proportionality relationship from the Soil Conservation Service Curve Number method was generalized to annual scale for deriving annual water balance model. As a result, a one-parameter Budyko equation was derived based on one-stage partitioning; and a four-parameter Budyko equation was derived based on two-stage partitioning. The derived equations balance model parsimony and representation of dominant hydrologic processes, and provide a new framework to disentangle the roles of climate variability, vegetation, soil and topography on long-term water balance. Three applications of the derived equations were demonstrated. Firstly, the four-parameter Budyko equation was applied to 165 watersheds in the United States to disentangle the roles of climate variability, vegetation, soil and topography on long-term water balance. Secondly, the one-parameter Budyko equation was applied to a large-scale irrigation region. The historical annual total water storage change were reconstructed for assessing groundwater depletion due to irrigation pumping by integrating the derived equation and the satellite-based GRACE (Gravity Recovery and Climate Experiment) data. Thirdly, the one-parameter Budyko equation was used to model the impact of willow treatment on annual evapotranspiration through a two-year field experiment in the Upper St. Johns River marshes. An empirical relationship between the parameter and willow fractional coverage was developed, providing a useful tool for predicting long-term response of evapotranspiration to willow treatment.

To my beloved mother Xiaolin Zhu without whose never-failing love and all-out dedication, I would look more like a Ph.D.

仅以此博士论文献给我挚爱的母亲，感激母亲无尽的爱和毫无保留的付出。

ACKNOWLEDGMENTS

It is an unforgettable moment to thank everyone who provided the possibility to complete my dissertation.

No words can fully express my gratitude to my advisor Dr. Dingbao Wang. Guided by his brilliant thoughts, strict logic, inspiring blame, and unexhausted enthusiasm, I opened the door to the real research world. During the three-and-half-year studying time, he taught me how to critically think, how to face difficulties, and how to achieve better not just excellent. I really appreciate his great efforts, infinite patience, and his always supports.

I would like to thank Dr. Pedro F. Quintana-Ascencio for his kindness and guidance for our collaborated project. I would like thank Dr. John Fauth for his guidance in field works and I would like to thank my committee members, Dr. Arvind Singh, Dr. Kelly Kibler and Dr. David M. Sumner for the constructive comments and the time taken from their busy schedule. I would like to thank Dr. Tingju Zhu for his trust and encouragement.

I also want to thank Dr. Xi Chen, Dr. Seoyoung Kim, Dr. Debapi Ghosh, Mr. Han Xiao, Mr. Milad Hooshyar, Mr. Marwan Kheimi and all past and present members of Dr. Dingbao Wang's research group for their support and help. I would like to thank Danny Goodding, Luz M. Castro Morales and other students who help conduct the field experiments. I would like to thank Dr. Karim Alizad, Ms. Paige Hovenga, Ms. Sevil Ranjbar, Ms. Cigdem Ozkan, Mr. Daljit Sandhu, Mr. Tonmoy Sarker, and Mr. Shiblu Sarker for their friendship.

This research was funded in part under Award NA10OAR4170079 from the Florida Sea Grant, the project of "Evaluation of the Role of Transpiration by Carolina Willow (Salix caroliniana) in the Water Budget of Upper St. Johns River Marshes" funded by St. Johns River

Water Management District (SJRWMD), and the CGIAR Research Program on Water, Land and Ecosystems (WLE) through the project "Enhancing groundwater simulation in the IMPACT-Water model for assessment of groundwater irrigation sustainability and food production impacts" led by the International Food Policy Research Institute (IFPRI).

I would like to thank Dr. Zhiqiang Zhang, my master thesis advisor for his always trust and guidance. I would like to thank Dr. Shenping Wang for her care and supports. I am grateful to Dr. Xincai Liu, Dr. Guoyong Leng. Dr. Xuejun Zhang, Mr. Xiaozhou Zhang, Ms. Guohua Liu, Mr. Jinbin Xu of Land Surface Processes and Global Change Research Group at the Institute of Geographic Sciences and Natural Resources Research, Chinese Academy of Sciences for their supports, encouragement, and friendship. My sincere thanks to Dr. Qiuhong Tang for his supports and encouragement for pursuing my doctoral degree.

Finally, I would like to thank my family, my cousin Hui Zhu and my aunt Hua Tang for giving me the opportunity to pursue my doctoral degree in the United States. I would like to thank my friend Yuan Chen, Yangming Xu, Wenjun Li, Ka Yeung for the great tolerance and kind company.

TABLE OF CONTENT

LIST OF FIGURES xi
LIST OF TABLES xiv
CHAPTER 1: INTRODUCTION 1
1.1 Annual Water Balance Equation 1
1.2 Annual Water Balance Model 2
1.2.1 Physical annual water balance model 2
1.2.2 Empirical Budyko model 3
1.2.3 Conceptual L'vovich-Ponce-Shetty model 4
1.3 Proportionality Relationship 6
1.3.1 Soil conservation service curve number methods 6
1.3.2 Generalized proportionality relationship 6
1.3.3 Theoretical background of generalized proportionality relationship 7
1.4 Research Questions and Dissertation Outline 7
CHAPTER 2: ONE-PARAMETER BUDYKO EQUATION 9
2.1 Introduction 9
2.2 Hydrologic Models across Varying Time Scales 11
2.2.1 Budyko hypothesis for mean annual water balance 11
2.2.2 "abcd" model for monthly water balance 12
2.2.3 SCS direct runoff model at the event scale 13
2.3 Generalized Proportionality Hypothesis 13
2.4 Proportionality Application for Mean Annual Water Balance 14
2.4.1 Lower bound of E/P 17
2.4.2 Vegetation and rainfall frequency control on ε 19
2.5 A Temporal Pattern for Darwinian Hydrologic Models 21
2.6 Conclusions and Future Research 21
CHAPTER 3: FOUR-PARAMETER BUDYKO EQUATION 23

3.1 Introduction 23
3.2 Methodology 27
3.2.1 Proportionality relationships for two-stage partitioning of precipitation 27
3.2.2 Deriving a four-parameter Budyko equation 28
3.2.3 Study watersheds and data sources 30
3.2.4 Estimating H, λ, β, and γ 33
3.2.5 Evaluating the roles of watershed properties in mean annual water balance 33
3.3 Results 35
3.3.1 Estimated parameters 35
3.3.2 Controlling factors for parameters 37
3.3.3 Principal Component regression for the four parameters 44
3.4 Discussions 45
3.4.1 Parsimonious model and process control 45
3.4.2 Interdependence of model parameters 46
3.4.3 Comparison with one-parameter Budyko equation 47
3.5 Conclusion 49
CHAPTER 4: RECONSTRUCTION OF ANNUAL GROUNDWATER STORAGE CHANGE IN LARGE-SCALE IRRIGATION REGION 52
4.1 Introduction 52
4.2 Study Area and Data Sources 55
4.2.1 Study area 55
4.2.2 Precipitation 57
4.2.3 Potential evapotranspiration 58
4.2.4 Terrestrial water storage change 58
4.2.5 Evaporation and soil moisture storage change 59
4.2.6 Observed groundwater level 59
4.3 Methodology 60
4.3.1 Annual total water storage change by Budyko model 60

4.3.2 Reconstructed annual groundwater storage change and groundwater depletion ……62
4.4 Results 64
4.4.1 Annual terrestrial water storage change by Budyko model 64
4.4.2 Reconstructed annual groundwater storage change 70
4.5 Discussion 72
4.5.1 Annual terrestrial water storage change by Budyko model 72
4.5.2 Reconstructed annual groundwater storage change and groundwater depletion ……73
4.6 Conclusion..... 74
CHAPTER 5: EFFECT OF HERBICIDES ON EVAPOTRANSPIRATION IN RIPARIAN WILLOW MARSHES 76
5.1 Introduction 76
5.2 Field experiment and data collection 78
5.2.1 Field experiment..... 78
5.2.2 Data collection..... 80
5.3 Methods..... 83
5.3.1 Daily evapotranspiration by Penman-Monteith equation..... 83
5.3.2 Seasonal variations of *LAI* and *ET* 85
5.3.3 Annual evapotranspiration model 86
5.4 Results 87
5.4.1 Daily evapotranspiration by the Penman-Monteith equation..... 87
5.4.2 Seasonal variations of *LAI* and *ET* 92
5.4.3 Annual evapotranspiration model 92
5.5 Discussion 94
5.5.1 Performance of daily ET estimation..... 94
5.5.2 Impact of willow removal on *ET* 95
5.5.3 Impact of willow removal on annual water yield..... 96
5.5.4 Linking vegetation fractional coverage to annual *ET* 97

5.6 Conclusion..... 98
CHAPTER 6: CONCLUSION AND FUTURE WORK.....100
APPENDIX A: CURRICULUM VITAE 104
APPENDIX B: LIST OF PUBLICATIONS 106
REFERENCES……..108

LIST OF FIGURES

Figure 2.1: The theoretical lower and upper bounds of the Budyko curve and observed E/P and E_p/P data in watersheds: (a) around the world (*Zhang et al.*, 2004), and (b) MOPEX dataset. Equation (2.14) is plotted in both cases with the respective best fitted values for ε. 18

Figure 2.2: a) The vegetation control (NDVI) on the Horton index, and the fitted red line represented by $NDVI = 0.81 - \mathrm{e} - 12.82(1.05 - \mathrm{H})$; b) the vegetation and rainfall frequency (αR) control on $\lambda = E_0/W$, and the fitted red line represented by $\alpha R \cdot NDVI = 0.43 - 0.32\lambda$. 20

Figure 3.1: The aridity index and study watersheds. 32

Figure 3.2: The histogram of estimated (a) H, (b) λ, (c) β, and (d) γ for study watersheds. 36

Figure 3.3: Correlations between (a) λ (i.e., the ratio between initial evaporation and total wetting) and H (i.e., ratio between evaporation and total wetting), and (b) β (the ratio between initial wetting and total wetting) and γ (the ratio between total wetting to its potential). 36

Figure 3.4: Correlations between H and four controlling factors with linear correlation coefficients higher than 0.5: (a) average interval between rainfall events; (b) average slope; (c) $NDVI_{max}$; and (d) permanent wilting point. 40

Figure 3.5: Correlations between λ and four controlling factors with linear correlation coefficients higher than 0.5: (a) average interval between rainfall events; (b) average slope; (c) $NDVI_{max}$; and (d) permanent wilting point. 41

Figure 3.6: Correlations between β and two controlling factors with linear correlation coefficients higher than 0.5: (a) difference between filed capacity and residual soil moisture; and (b) saturated hydraulic conductivity. 42

Figure 3.7: Correlations between γ and three controlling factors with linear correlation coefficients higher than 0.5: (a) the computed effective soil water storage capacity; (b) number of rainfall events on an annual basis; and (c) precipitation timing with respect to potential evaporation as a measure of seasonality. 43

Figure 3.8: The observed E/P versus $\emptyset$ for the 165 study watersheds. Two watersheds (USGS gage #01421000 and #06606600) are located on the blue solid line which represents the single-parameter Budyko equation (i.e., equation 11) with $\varepsilon = 0.48$. The green dashed line and the red dash-dotted line represent the four-parameter equation (i.e., equation (8)) with the parameter sets for watersheds #01421000 and #06606600, respectively. 48

Figure 4.1: Indus River and its tributaries, observation wells and reservoir in Punjab, Pakistan. 56

Figure 4.2: Time series of annual values during 1980-2015 for: (a) precipitation from PREC/L and GLDAS-1; (b) potential evaporation from CRU and GLDAS-1; (c) evaporation from LSMs; (d) GRACE-derived terrestrial water storage change; (e) soil moisture storage change from LSMs; and (f) observed groundwater level change and estimated groundwater

storage change using the small specific yield (S_y) value of 0.07, large S_y of 0.25, and average S_y of 0.14 in Punjab, Pakistan..... 65

Figure 4.3: The annual evaporation ratio versus annual aridity index in Punjab during 2004-2010 and 18 fitted Budyko curves based on (a) precipitation from PREC/L and (b) precipitation from GLDAS-1, and potential evaporation from CRU and GLDAS-1, evaporation from 3 LSMs, terrestrial water storage change from 3 GRACE data sources..... 68

Figure 4.4: The 18 time series of Budyko-modeled terrestrial water storage change (ΔTWS) from 1980 to 2015 in Punjab and the comparison of ensemble mean of 18 Budyko-modeled ΔTWS based on precipitation from GLDAS-1, potential evaporation from CRU and GLDAS-1, evaporation from 3 LSMs, and parameters estimated by 3 GRACE data sources with the ensemble mean of GRACE-derived ΔTWS. 69

Figure 4.5: The 18 time series of the reconstructed annual groundwater storage change (ΔGWS) from 1985 to 1994 and the ensemble mean, and the ground-based ΔGWS. 70

Figure 4.6: The cumulative sum of the reconstructed annual groundwater storage change and the total number of tube wells during 1980-2013 in Punjab, Pakistan (data source: PDS (1988; 1996; 2005; 2015))..... 71

Figure 5.1: The schematic diagram of a designed experiment block consisting of three plots. ... 79

Figure 5.2: (a) The locations for Moccasin Island (MI) and Sweetwater Canal (SWC) experimental sites in the Upper St. Johns River Basin (USJRB); (b) the centroids of three plots (A, B, and C) in MI North and MI South blocks and weather tower (black star); and (c) the centroids of the plots in SWC East and SWC West blocks and weather tower..... 80

Figure 5.3: Mean monthly wind speed at the two towers located in the Moccasin Island and Sweetwater Canal sites during 9/1/2014-8/31/2016. 88

Figure 5.4: Estimated daily leaf area index (LAI) averaged over the control plots, the plots treated by mixed herbicide, and the plots treated by Clearcast herbicide during July 1-14 in (a) 2014, (b) 2015, and (c) 2016..... 89

Figure 5.5: (a) Daily Penman-Monteith (PM) evapotranspiration (ET) averaged over the control plots; and (b) the cumulative difference (control minus treated) of daily evapotranspiration for plots treated by mixed herbicide and the plots treated by Clearcast herbicide. Blue vertical lines indicate the herbicide application dates. The green solid lines represent the slopes of cumulative ET difference..... 91

Figure 5.6: (a) Mean monthly evapotranspiration (ET) computed by Penman-Monteith (PM) equation; and (b) mean monthly leaf area index over the control and treated plots during 9/1/2014-8/31/2016..... 92

Figure 5.7: The relationship between ε in equation (5) for annual evapotranspiration and the willow fractional coverage (C_w) in April are fitted by $\varepsilon = 0.34\ln(Cw) - 0.48$..... 93

Figure 5.8: The comparison of spatial average values of daily evapotranspiration (*ET*) computed by Penman-Monteith (PM) equation with satellite-based potential evapotranspiration (E_p) by Prestiley-Taylor (PT) equation from USGS. 95

Figure 5.9: Annual water yield (precipitation minus evapotranspiration) versus leaf area index. 97

LIST OF TABLES

Table 1.1: Budyko-type equations. 4

Table 3.1: Summary of identified watershed properties and data sources. 31

Table 3.2: The values of R^2 for four basic functions between each parameter and individual factor. The maximum R^2 among a set of parameter-factor relationships is highlighted as bold. 39

Table 4.1: Estimated parameters and the model performance of Budyko-modeled annual terrestrial water storage changes during 2004-2010. 67

Table 5.1: The dates and herbicides sprayed for treated plots. 80

Table 5.2: The measured variables at the weather stations and towers with sensors or by field work. 81

Table 5.3: The land surface elevation (Z_i), latitude (φ_i), and height (z_{mi}) for weather stations and towers, and the calibrated extinction coefficient (k) for each plot. The four control plots are highlighted in bold. 82

CHAPTER 1: INTRODUCTION

Water balance is one of the fundamental research topics in hydrology, and is required for solving theoretical and practical hydrological problems at different spatial (e.g., lakes, watersheds, groundwater basin) and temporal (e.g., monthly, seasonal, annual) scales. This dissertation is mainly focused on annual water balance at watershed scale. An understanding of annual water balance is extremely important for studies on the long-term hydrological responses to environmental change and anthropogenic activities. An annual water balance equation provides a framework to estimate hydrologic fluxes such as evaporation which is challenging to measure directly.

1.1 Annual Water Balance Equation

The study of water balance is the application of the principle of mass conservation, often referred to as the continuity equation. This states that, for any arbitrary volume and during any period of time, the difference between total input and output will be balanced by the change of water storage within the volume. Taking the closed watershed as a control volume (i.e., no inflow from adjacent watersheds), the annual water balance at watershed scale in its general form may be represented by:

$$P = E + Q + \Delta S \tag{1.1}$$

where P is the annual total rainfall and snow which is actually received at the ground surface, and surface and subsurface water inflow into the watershed; E and Q are annual evapotranspiration and total runoff which are outflow, respectively; and ΔS is the total water storage change including the changes in surface water body, soil water content, and groundwater storage.

With negligible ΔS, the annual water balance may be rewritten:

$$P = E + Q \quad (1.2)$$

This equation opened up an entire new era in hydrology and it is still in use even today (*L'vovich*, 1979). Based on this equation, the global annual water balance has been examined (*Budyko*, 1970, 1974; *Baumgartner and Reichel*, 1975; *Korzun et al.*, 1978). This equation is also called as one-stage partitioning of annual precipitation (*Wang and Tang*, 2014).

In order to describe the soil link in the water balance, *L'vovich* (1979) separated the total runoff into surface runoff and base flow, and the annual water balance equation (1.3) may be written:

$$P = Q_d + W \quad (1.3a)$$

$$W = Q_b + E \quad (1.3b)$$

$$Q = Q_d + Q_b \quad (1.3c)$$

where Q_d is surface runoff; Q_b is base flow; and W is total wetting of the area. This equation is in line with equation (1.4), moreover, it includes the surface runoff and base flow and the soil link (i.e., total wetting). This annual water balance equation is also called the two-stage partitioning of annual precipitation (*Sivapalan et al.*, 2011).

1.2 Annual Water Balance Model

1.2.1 Physical annual water balance model

The physical models have been developed to describe the complete annual water balance (i.e., equation (1.1)). Detailed processes have been incorporated into this type of model to quantify the role of the controlling factors on annual water balances. *Eagleson* (1978a, b) expressed annual water balance as a function of climate, soil, and vegetation by developing a comprehensive hydrologic model, which includes submodels for surface water storage, unsaturated storage,

groundwater flow, and infiltration. *Milly* (1994) investigated the interaction between soil water storage capacity and climate seasonality and intermittency through a stochastic model of soil moisture balance (i.e., equation (1.1)) (*Milly*, 1993). *Woods* (2003) extended the Milly's model to include water storage and release by the plant canopy and saturated soil zone. Based on the Milly's model, *Potter et al.* (2005) found that both soil water storage capacity and infiltration capacity are important controlling factors on annual water balance. *Yokoo et al.* (2008) investigated the role of climate, soil properties and topography in mean annual water balance through a physically-based water balance model. These physically-based models explicitly represent the processes related to the role of controlling factors and provide the continuous simulation. However, the required amounts of data and large number of parameters limit their practical applications (Ponce and Shetty, 1995).

1.2.2 Empirical Budyko model

With negligible long-term water storage change, annual precipitation (P) is partitioned into evaporation (E) and runoff (Q) (i.e., Equation (1.2)). Based on a large number of observations, the climate aridity index, defined as the ratio between mean annual potential evaporation (E_p) and P (i.e., $\emptyset = \frac{E_p}{P}$), has been found to be the first order control on this partitioning (*Budyko*, 1974). Nonparametric equations have been proposed for representing this relationship as shown in Table 1.1. The Budyko framework provides a simple but effective tool to estimate long-term evaporation and runoff and to evaluate their responses to climate change (e.g., *Berghuijs et al.*, 2014a). For the purpose of simplicity, the impacts of climate variability, vegetation, soil and topography on annual water balance were lumped into a single parameter under Budyko framework. Several one-parameter Budyko equation have been proposed or derived as shown in Table 1.1. The parameter

can be treated as a random variable due to the varying controlling factors among watersheds (Greve et al., 2015). The one-parameter Budyko equations have been used for quantifying the contribution of climate change and land use change to long-term streamflow changes (e.g., Roderick and Farquhar, 2011; Wang and Hejazi, 2011; Jiang et al., 2015). Although this framework is empirical it has been widely used due to its solid and efficiency.

TABLE 1.1: BUDYKO-TYPE EQUATIONS.

Budyko equation	**Parameter**	**References**
$E = P\left[1 - exp\left(-\frac{E_p}{P}\right)\right]$	None	(Schreiber, 1904)
$E = E_p \cdot tanh\left(\frac{P}{E_p}\right)$	None	(Ol'dekop, 1911)
$E = \left\{P\left[1 - exp\left(-\frac{E_p}{P}\right)\right] \cdot E_p \cdot tanh\left(\frac{P}{E_p}\right)\right\}^{0.5}$	None	(Budyko, 1958)
$E = \frac{P}{\left[1 + \left(\frac{P}{E_p}\right)^2\right]^{0.5}}$	None	(Turc, 1954; Pike, 1964)
$\frac{E}{P} = \left[1 + \left(\frac{E_p}{P}\right)^{-n}\right]^{-1/n}$	n	(Bagrov, 1953; Mezentsev, 1955; Choudhury, 1999; Yang et al., 2008)
$\frac{E}{P} = 1 + \frac{E_p}{P} - \left[1 + \left(\frac{E_p}{P}\right)^{\omega}\right]^{1/\omega}$	ω	(Fu, 1981; Zhang et al., 2004)
$\frac{E}{P} = \frac{1 + w\frac{E_p}{P}}{1 + w\frac{E_p}{P} + \left(\frac{E_p}{P}\right)^{-1}}$	w	(Zhang et al., 2001)
$\frac{E}{P} = \frac{1 + E_p/P - \sqrt{\left(1 + E_p/P\right)^2 - \frac{4\varepsilon(2-\varepsilon)E_p}{P}}}{2\varepsilon(2-\varepsilon)}$	ε	(Wang and Tang, 2014)

1.2.3 Conceptual L'vovich-Ponce-Shetty model

In order to quantify the each component in Equation (1.3), L'vovich (1979) proposed the proportional curves to describe the competitions between base flow and evaporation, and surface

runoff and base flow. For example, the renewable resources of soil wetting which do not manage to evaporate or be used for transpiration go to feed base flow. Ponce and Shetty (1995) provided two equations to describe the proportional curves:

$$\frac{P-\lambda_s W_p}{W_p-\lambda_s W_p} = \frac{Q_d}{P-\lambda_s W_p} \tag{1.4a}$$

$$\frac{E-\lambda_u E_p}{E_p-\lambda_u E_p} = \frac{Q_b}{W-\lambda_u E_p} \tag{1.4b}$$

where λ_s and $\lambda_u$are the initial surface-runoff abstraction and base flow abstraction coefficients, respectively; W_p is the potential total wetting, and Ep is the potential evaporation. Then the surface runoff and base flow may be solved:

$$Q_d = \frac{\left(P-\lambda_s W_p\right)^2}{P+(1-2\lambda_s)W_p} \tag{1.5a}$$

$$Q_b = \frac{\left(P-\lambda_u E_p\right)^2}{P+(1-2\lambda_u)E_p} \tag{1-5b}$$

Given annual precipitation and a set of initial abstraction coefficients λ_s and λ_u and W_p and Ep, the annual surface runoff, base flow, total runoff and evaporation are quantified. This conceptual model seems to provide a solution to balance the complexity of physical models and the parsimony of empirical Budyko equations since more processes have been incorporated than the empirical Budyko models and less parameters and data are required than the physical models. However, the behaviors of total runoff and evapotranspiration haven't been explicitly described in this framework.

1.3 Proportionality Relationship

1.3.1 Soil conservation service curve number methods

Rainfall at the event scale is partitioned into direct runoff (Q_d) and soil wetting (W), where soil wetting includes initial abstraction (I_a) and continuing abstraction (F_a). The initial abstraction I_a is the amount of water lost before direct runoff is generated, such as infiltration and rainfall interception by vegetation. After initial abstraction, the remaining water of $P - I_a$ is partitioned into F_a and Q_d. The potential for continuing abstraction (S) is a function of soil properties, land-use and land-cover, and the antecedent soil moisture condition. Given that Q_d does not compete for I_a, the potential for direct runoff is ($P - I_a$). The proportionality hypothesis of the SCS method is that the ratio of continuing abstraction to its potential is equal to the ratio of direct runoff to its potential value (SCS, 1972):

$$\frac{F_a}{S} = \frac{Q_d}{P - I_a} \text{ subject to } P = F_a + Q_d \quad (1.6)$$

This proportionality equation was obtained based on observed data from a large number of watersheds (SCS, 1985).

1.3.2 Generalized proportionality relationship

Ponce and Shetty (1995) proposed the generalized proportionality relationship as follows. A certain amount of water (Z) is partitioned into X and Y, such as wetting and direct runoff in the SCS model. X is constrained by its potential value denoted as X_P (i.e., S in the SCS model), and X has a priority to meet the initial water demand of X_0 like I_a. Y is constrained by total water availability of $Z - X_0$. The partitioning of Z is quantified by the generalized proportionality hypothesis:

$\frac{X-X_0}{X_P-X_0} = \frac{Y}{Z-X_0}$ subject to $Z = X + Y$ (1.7)

The generalized proportionality relationship has been proved to be applicable to any time period, from event to long-term average scale (Wang and Tang, 2014).

1.3.3 Theoretical background of generalized proportionality relationship

Wang et al. (2015) demonstrated that the proportionality relationship for both one-stage and two-stage partitioning of precipitation can be seen as a result of the application of the thermodynamic principle of Maximum Entropy Production (MEP). Hooshyar and Wang (2016) provided the physical basis of the Soil Conservation Service Curve Number method (i.e., equation (1.6)) and its proportionality hypothesis from the infiltration excess runoff generation perspective through an analytical solution of Richards' equation.

1.4 Research Questions and Dissertation Outline

Essentially, the one-stage and two-stage partitioning of annual precipitation are the same, the related functional forms to them looks quite different. It can be seen that the existing models to describe the behaviors of annual water balance are either too simple or too complicated. The generalized proportionality relationship seems to be a compromise solution to balance the complexity of physical models and the parsimony of empirical Budyko equations. These give rise to the following specific research questions:

(1) Can the functional forms describing the one-stage and two-stage partitioning of annual precipitation be similar?

(2) Is the generalized proportionality relationship a compromised solution to balance the complexity of physical models and the parsimony of empirical Budyko equations? or Is it possible

to explicitly to describe the behaviors of total runoff and evapotranspiration under two-stage partitioning of precipitation framework?

(3) If the compromised solution exists, what is its applicability for theoretical and practical hydrological problems?

The dissertation is subdivided into different chapters, answering in part one or more of the research questions formulated above. Chapter 2 derives the one-parameter Budyko equation from the generalized proportionality relationship for the one-stage partitioning of annual precipitation. Chapter 3 includes the derivation of the four-parameter Budyko-type equation based on the proportionality relationships for the two-stage partitioning of annual precipitation and the theoretical application on disentangling the roles of climate variability, vegetation, soil and topography on long-term water balance. Chapter 4 and Chapter 5 gives the practical applications of the derived one-parameter Budyko equation for reconstructing the annual total water storage change and groundwater storage change in large-scale irrigation region and evaluating the long-term impacts of willow treatment on annual evapotranspiration in the Upper St. Johns River marshes. Chapter 6 concludes with a summary of the research questions and corresponding answers, and provides an outlook on prospective research inspired by the findings.

CHAPTER 2: ONE-PARAMETER BUDYKO EQUATION

2.1 Introduction

In hydrologic problems, conservation of mass (i.e., water balance) should always hold regardless of the time scale of interest. Yet, identifying the water balance behavior over various temporal scales remains a challenging research task. One reason for this is that the roles of controlling factors on rainfall partitioning vary with temporal scale. For example, rainfall intensity and topography are important factors for runoff generation at short-time scales (Dunne and Black; 1970; Beven and Kirkby, 1979), while climate aridity index is the dominant controlling factor affecting the ratio between evaporation and precipitation (Budyko, 1974). To deal with this problem, various conceptual hydrologic models have been developed for capturing these dominant controls on rainfall partitioning specific to a particular temporal scale, i.e., long-term, monthly, or event scale (Blöschl and Sivapalan, 1995).

Hydrologic models can be categorized as being either Newtonian or Darwinian. The Newtonian approach builds a mechanistic model of hydrologic processes (e.g., evaporation, infiltration, surface runoff and base flow) and their coupled components including initial conditions, boundary conditions, and model parameters. Hydrologic behavior is derived from Newton's laws of motion, specifically the momentum equation, and other conservation equations (mass and energy). For example, the infiltration process can be modeled by the Richards equation, which combines the continuity equation with Darcy's law, which represents the momentum equation. The Darwinian approach is not concerned with the physical processes in isolation, and instead aims to explain the hydrologic behavior as a system (Harman and Troch, 2014). The Darwinian approach involves identifying simple and robust spatial or temporal patterns in

hydrologic behavior from a population of watersheds and postulating a theory for connecting the observed patterns – both similarities and variations - to the processes that created them (Harman and Troch, 2014). Spatial or temporal patterns are also called emergent behaviors in complex systems, and many examples, such as self-similar phenomena, are encountered in other fields of the geophysical sciences (Harte, 2002; Gentine et al., 2010).

The Darwinian approach is exemplified by three hydrologic models, which were developed based on empirical data from a large number of watersheds: the Budyko curve for long-term or climatological water balance (Budyko, 1974), the "abcd" model for monthly or daily water balance (Thomas, 1981), and the Soil Conservation Service (SCS) curve number method for event-scale hydrologic runoff (SCS, 1972). These hydrologic models have been successfully applied for water resources assessment at gauged and ungauged watersheds (Yadav et al., 2007). Due to the variable roles of controlling factors on rainfall partitioning across time scales, these models originated from distinct concepts and are based on different representations of the hydrologic physical processes. As a result, the structure and mathematical representations of these models are quite different, particularly between the Budyko model and the SCS model. The Budyko model is based on the concept of water and energy limits, which demonstrates that water is the limiting factor on evaporation when energy is unlimited, and vice versa. By contrast, the SCS model is based on the proportionality concept of direct runoff and continuing abstraction which represents post-ponding infiltration.

For a given watershed, physical properties such as vegetation, soil, and topography co-evolve under climate driving forces (Sivapalan, 2005). Hydrological responses, such as evaporation and runoff, across time scales are signatures from the co-evolution of natural systems

(Newman et al., 2006; Wagener et al., 2010; Gentine et al., 2012; Wang and Wu, 2013; Harman and Troch, 2014). Commonality, or linkage, exists among the behavior of rainfall partitioning across time scales and serves as an indicator of co-evolution. Therefore, the purpose of this paper is to recognize the general signature of rainfall partitioning by identifying the commonality of the three hydrologic models at the long-term, monthly, and event scales. The identified commonality, i.e., the generalized proportionality hypothesis, provides a hydrologic principle independent of any time scale from the Darwinian view, analogous to the role of the mass conservation principle from the Newtonian view. As a result of this study, a new single-parameter Budyko equation is derived for mean annual water balance, and a theoretical lower bound of the Budyko curve is identified.

2.2 Hydrologic Models across Varying Time Scales

2.2.1 Budyko hypothesis for mean annual water balance

In the mean annual or climatological water balance at the watershed scale, if water storage change is negligible, mean annual precipitation (P) is partitioned into runoff (Q) and evaporation (E). Budyko (1958) postulated that the partitioning of precipitation, to the first order, was determined by the competition between available water (P) and available energy measured by potential evaporation (E_p). Based on the data from a large number of watersheds, Budyko (1974) proposed a relationship between the mean annual evaporation ratio (E/P) and the mean annual potential evaporation ratio or climate aridity index (E_p/P):

$$\frac{E}{P} = \left[\left(1 - \exp\left(-\frac{E_p}{P}\right)\right)\frac{E_p}{P}\tanh\left(\frac{E_p}{P}\right)^{-1}\right]^{0.5} \quad (2.1)$$

To incorporate the impact of other factors on water balance, various functional forms have been proposed or derived in the literature as shown in Table 1 (e.g., Turc, 1954; Mezentsev, 1955; Pike, 1964; Fu, 1981; Milly, 1994; Zhang et al., 2001; Milly and Dunne, 2002; Yang et al., 2008; Gerrits

et al., 2009; Wang and Hejazi, 2011). These models have advanced the understanding of the controls of vegetation, soil water storage, and climate seasonality on the water balance. The Budyko hypothesis for mean annual water balance results from the co-evolution of watershed vegetation and soils with climate (Gentine et al., 2012; Troch et al., 2013).

2.2.2 "abcd" model for monthly water balance

The "abcd" model is a nonlinear monthly water balance model that was originally proposed by *Thomas* (1981) for national water assessment. This model has been utilized for monthly streamflow predictions taking rainfall and potential evaporation as inputs (*Alley*, 1985; *Li and Sankarasubramanian*, 2012). The "abcd" model defines W_t as available water and Y_t as evaporation opportunity. Available water is the summation of precipitation during month t and soil water storage at the beginning of month t; evaporation opportunity is the summation of actual evaporation during month t and soil water storage at the end of month t. Evaporation opportunity (Y_t) is postulated as a nonlinear function of available water (W_t):

$$Y_t = \frac{W_t+b}{2a} - \sqrt{\left(\frac{W_t+b}{2a}\right)^2 - \frac{W_t b}{a}} \qquad (2.2)$$

The parameter a ($0 \leq a \leq 1$) represents the propensity for runoff to occur before the soils are fully saturated; the parameter b is the upper bound of storage in the unsaturated zone above the groundwater table (*Thomas*, 1981). Equation (2.3) is the key component of the "abcd" model and was proposed simply because the limits of the derivative of *Y* should be 1 and 0 (*Thomas*, 1981). *Sankarasubramanian and Vogel* (2002) modified the original model for understanding the role of soil water storage capacity on the annual water balance. The "abcd" model has been used to test the effectiveness of model calibration (*Vogel and Sankarasubramanian*, 2003) and diagnose model structure and performance (*Martinez and Gupta*, 2011).

2.2.3 SCS direct runoff model at the event scale

Rainfall at the event scale is partitioned into direct runoff (Q_d) and soil wetting (W), where soil wetting includes initial abstraction (I_a) and continuing abstraction (F_a). The initial abstraction I_a is the amount of water lost before direct runoff is generated, such as infiltration and rainfall interception by vegetation. After initial abstraction, the remaining water of $P - I_a$ is partitioned into F_a and Q_d. The potential for continuing abstraction (S) is a function of soil properties, land-use and land-cover, and the antecedent soil moisture condition. Given that Q_d does not compete for I_a, the potential for direct runoff is $(P - I_a)$. The proportionality hypothesis of the SCS method is that the ratio of continuing abstraction to its potential is equal to the ratio of direct runoff to its potential value (*SCS*, 1972):

$$\frac{F_a}{S} = \frac{Q_d}{P - I_a} \tag{2.3}$$

This proportionality equation was obtained based on observed data from a large number of watersheds (*SCS*, 1985).

2.3 Generalized Proportionality Hypothesis

The proportionality hypothesis of the SCS method has been generalized by *Ponce and Shetty* (1995) as follows. A certain amount of water (Z) is partitioned into components X and Y (e.g., wetting and direct runoff in the SCS model). The quantity X is constrained by its potential value denoted as X_P (i.e., S in the SCS model), and X has a priority to meet the initial water demand of X_0, similar to I_a. The quantity Y is constrained by the total water availability of $Z - X_0$. The partitioning of Z is quantified by the generalized proportionality hypothesis:

$$\frac{X - X_0}{X_P - X_0} = \frac{Y}{Z - X_0} \tag{2.4}$$

The generalized proportionality hypothesis has been successfully applied for modeling the two-stage partitioning of rainfall and abstraction at the inter-annual scale (*Ponce and Shetty*, 1995; *Sivapalan et al.*, 2011).

In this paper, it is hypothesized that the generalized proportionality concept is applicable to any time period, from event to long-term average scale. To illustrate this, we show that the generalized proportionality is the commonality of three Darwinian hydrologic models across three time scales: the SCS model at the event scale, the "abcd" model for monthly water balance, and the Budyko hypothesis for long-term water balance. The generalized proportionality hypothesis provides a methodology to develop Darwinian models that are independent of temporal scale, and therefore serves a purpose similar to the water balance principle from the Newtonian view.

2.4 Proportionality Application for Mean Annual Water Balance

For mean annual water balance, water storage change is negligible and precipitation is partitioned into evaporation and runoff. At the first stage of the partitioning, precipitation is partitioned into wetting and direct runoff (L'vovich, 1979); at the second stage of the partitioning, wetting is partitioned into evaporation and base flow from groundwater discharge (Sivapalan et al., 2011). Total runoff is the summation of direct runoff and base flow. As shown in Figure 1, a portion of wetting is only available for direct evaporation, such as that which occurs due to vegetation interception and water storage in top soils. Evaporation from this portion of wetting is defined as initial evaporation (E_0). Following the initial abstraction concept of the SCS method, initial evaporation is represented as a percentage of wetting:

$$E_0 = \lambda W \tag{2.5}$$

where λ is the initial evaporation ratio and λW is the amount of water storage which is not available for competition between runoff and evaporation. The remaining rainfall ($P - \lambda W$) is partitioned into continuing evaporation ($E - E_0$) and total runoff (Q). Continuing evaporation is defined as the portion of evaporation that is lost through competition with runoff. For example, the interaction between root zone depth and the shallow water table dynamics affects the magnitude of continuing evaporation.

As precipitation increases unbounded, continuing evaporation is bounded by atmospheric evaporation demand and asymptotically approaches a constant value of $E_p - \lambda W$, where E_p is mean annual potential evaporation aggregated from daily or monthly values. Runoff increases unbounded with precipitation, but is constrained by $P - \lambda W$. Applying the generalized proportionality, we obtain:

$$\frac{E-E_0}{E_p-\lambda W} = \frac{Q}{P-\lambda W} \tag{2.6}$$

Substituting equation (2.5) and $Q = P - E$ (assuming no storage change on long time scales) into equation (2.6):

$$\frac{E-\lambda W}{E_p-\lambda W} = \frac{P-E}{P-\lambda W} \tag{2.7}$$

The ratio between evaporation and wetting is called the Horton index, $H = E/W$ (*Horton*, 1933; *Troch et al.*, 2009), and is a catchment signature that is predominantly controlled by vegetation (*Troch et al.*, 2009; *Voepel et al.*, 2011). Dividing the numerator and denominator of both sides of equation (2.7) by P and substituting in H, we obtain:

$$\frac{E/P-\frac{\lambda}{H}E/P}{E_p/P-\frac{\lambda}{H}E/P} = \frac{1-E/P}{1-\frac{\lambda}{H}E/P} \tag{2.8}$$

The ratio between λ and H is denoted as $\varepsilon = \lambda/H$. Based on the definitions of λ and H, ε can be interpreted as the ratio between initial evaporation and total evaporation, E_0/E. A quadratic function for $\frac{E}{P}$ is obtained by manipulating equation (2.8):

$$\varepsilon(2-\varepsilon)\left(\frac{E}{P}\right)^2 - \left(1+\frac{E_p}{P}\right)\frac{E}{P} + \frac{E_p}{P} = 0 \tag{2.9}$$

Since $\frac{E}{P}$ is positive and less than 1, the root for $\frac{E}{P}$ is obtained as:

$$\frac{E}{P} = \frac{1+E_p/P-\sqrt{\left(1+E_p/P\right)^2-4\varepsilon(2-\varepsilon)E_p/P}}{2\varepsilon(2-\varepsilon)} \tag{2.10}$$

Equation (2.10) quantifies $\frac{E}{P}$ as a function of $\frac{E_p}{P}$ with a single parameter, ε. This equation is a single-parameter Budyko-type equation. The parameter ε is the ratio of two dimensionless numbers, i.e., the ratio of the initial evaporation ratio to the Horton index. When $\varepsilon = 1$, equation) represents the upper bound of the Budyko curve, i.e., $\frac{E}{P} = \frac{E_p}{P}$ when $\frac{E_p}{P} \leq 1$, and $\frac{E}{P} = 1$ when $\frac{E_p}{P} > 1$.

Like the Budyko-type equations in Table 2.1, equation (2.10) satisfies the boundary conditions:

$$\frac{E}{P} \to 0 \text{ when } \frac{E_p}{P} \to 0 \tag{2.11a}$$

$$\frac{E}{P} \to 1 \text{ when } \frac{E_p}{P} \to \infty \tag{2.11b}$$

Observed data from real watersheds are typically located clustered around the deterministic Budyko curve (equation 2.1), which overlaps with the curve given by equation (2.10) when ε is approximately 0.6. When $\varepsilon = \frac{2-\sqrt{2}}{2} \approx 0.29$, the functional form of equation (2.11) is the same as Fu's equation, with the parameter $\omega = 2$ (*Fu*, 1981).

TABLE 2.1: THREE BUDYKO-TYPE EQUATIONS WITH A SINGLE-PARAMETER.

Budyko-type equations	Parameter	References
$\frac{E}{P}=\left[1+\left(\frac{E_P}{P}\right)^{-n}\right]^{-1/n}$	n	[*Turc*, 1954; *Mezentsev*, 1955; *Pike*, 1964; *Choudhury*, 1999; *Yang et al.*, 2008]
$\frac{E}{P}=1+\frac{E_p}{P}-\left[1+\left(\frac{E_p}{P}\right)^{\omega}\right]^{1/\omega}$	ω	[*Fu, 1981*; *Zhang et al.*, 2004; *Yang et al.*, 2007]
$\frac{E}{P}=\frac{1+w\frac{E_p}{P}}{1+w\frac{E_p}{P}+\left(\frac{E_p}{P}\right)^{-1}}$	w	[*Zhang et al.*, 2001]

2.4.1 Lower bound of E/P

It should be noted that equation (2.10) can mathematically simulate the entire domain between the upper bound and the horizontal axis ($E/P = 0$). However, since initial evaporation (E_0) cannot exceed total evaporation (E), the physical range of ε is between 0 and 1 ($0 \leq \varepsilon \leq 1$). When ε approaches zero, the limit of equation (2.10) can be obtained:

$$\lim_{\varepsilon \to 0} \frac{E}{P} = \left[1+\left(\frac{E_p}{P}\right)^{-1}\right]^{-1} \tag{2.12}$$

Equation (2.12) is the same as the Turc equation with $n = 1$ (*Turc*, 1954) and the equation by *Zhang et al.* (2001) with $w = 0$. Setting $\varepsilon = 0$ is equivalent to setting $E_0 = 0$, in which case equation (2.12) reduces to the following:

$$\frac{E}{E_p} = \frac{Q}{P} \tag{2.13}$$

As a result, the lower bound of the Budyko curve corresponds to the condition when the ratio of evaporation to potential evaporation equals the runoff coefficient. The lower bound is equivalent to the constraint of $\frac{E}{E_p} \geq \frac{Q}{P}$.

The theoretical lower bound of E/P is compared with reported data from real watersheds in the literature. Figure 2.1a plots the data for over 470 watersheds around the world from Zhang et al. (2004), and the lower bound is found to accurately constrain the vast majority of the data points. The best fit for these data points is achieved with equation (2.10) when ε=0.58, as is also shown in Figure 2.1a, where the fitted relationship overlaps with the deterministic Budyko curve given by equation (2.1). An additional 246 watersheds from the Model Parameter Estimation Experiment (MOPEX) dataset (Duan et al., 2006) provide a second dataset for verifying the lower bound, as is shown in Figure 2.1b, along with the best fit curve of equation (2.10) where ε=0.55. This second dataset is also nearly entirely constrained by the theoretical lower bound; of the 246 watersheds in this dataset, 242 are located above the lower bound determined by the proportionality hypothesis. The reported watershed data in other studies, using the equations in Table 2.1, are also located above the lower bound with a few exceptions (*Yang et al.*, 2007; *Roderick and Farquhar*, 2011; *Donohue et al.*, 2011).

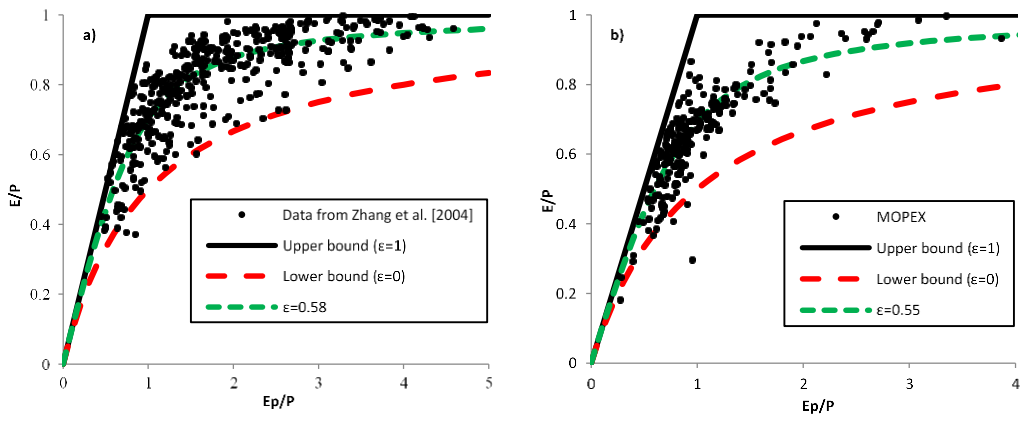

FIGURE 2.1: THE THEORETICAL LOWER AND UPPER BOUNDS OF THE BUDYKO CURVE AND OBSERVED E/P AND E_P/P DATA IN WATERSHEDS: (A) AROUND THE WORLD (*ZHANG ET AL.*, 2004), AND (B) MOPEX DATASET. EQUATION (2.14) IS PLOTTED IN BOTH CASES WITH THE RESPECTIVE BEST FITTED VALUES FOR ε.

2.4.2 Vegetation and rainfall frequency control on ε

As discussed earlier, the parameter ε in equation (2.10) has a physical meaning from the process perspective. From the soil wetting perspective, ε can be interpreted as the ratio between initial evaporation ratio (λ) and the Horton index (H). From the evaporation perspective, ε is the ratio between initial evaporation and total evaporation, where initial evaporation is the component of the wetting which is not available for runoff competition. Here, the physical control on ε is analyzed through the dimensionless numbers λ and H.

The Horton index provides a measure of water use efficiency of vegetation in response to change in precipitation (*Brooks et al.*, 2011). The Horton index is relatively constant from year to year despite fluctuations in annual precipitation, indicating that vegetation adapts to lower water availability by increasing water use efficiency (*Troch et al.*, 2009). In this study, soil wetting is computed by taking the difference between precipitation and direct runoff, which is obtained by base flow separation (*Sivapalan et al.*, 2011); bimonthly Normalized Difference Vegetation Index (NDVI) for the MOPEX watersheds are obtained from the satellite remote sensing data (*Tucker et al.*, 2005). Figure 2.2a presents the relation between average value of annual maximum NDVI and the Horton index, and the pattern is the same as the one reported by *Voepel et al.* (2011). Water use efficiency of vegetation, represented by the Horton index, is close to 1 in water-limited regions.

The initial evaporation ratio (λ) is the ratio of initial evaporation (E_0) to total soil wetting (W). Vegetation affects both soil wetting and initial evaporation. W increases with NDVI as shown in *Voepel et al.* (2011); and E_0 may also increase with NDVI since interception loss increases with vegetation coverage. Over shorter time scales, E_0 is affected by the frequency of rainfall events. To evaluate the impact of rainfall variability on λ, the long-term average fraction of rainy days is

computed for the MOPEX watersheds. The fraction of rainy days is computed from daily rainfall data as the ratio between the number of rainy days (N_R) and the total number of days in a year (N). As shown in Figure 2.2b, the initial evaporation ratio increases when $\alpha_R \cdot NDVI$ declines. Therefore, soil wetting increases faster than initial evaporation when NDVI increases.

In summary, the dominant controlling factors on ε are vegetation and rainfall. The physical meaning of ε is the ratio of initial evaporation, which is not through the competition process with runoff such as evaporation from vegetation interception and top soil, to total evaporation. The magnitude of ε decreases with increasing α_R. The control of vegetation on ε is complex because both λ and H decline with increasing NDVI. The relationship between ε and NDVI is non-monotonic since vegetation affects the processes of wetting, initial evaporation, and total evaporation.

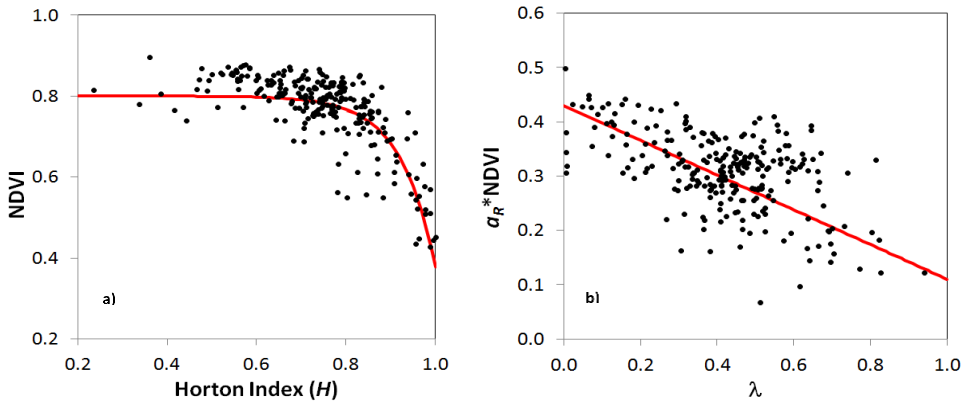

FIGURE 2.2: A) THE VEGETATION CONTROL (NDVI) ON THE HORTON INDEX, AND THE FITTED RED LINE REPRESENTED BY $NDVI = 0.8\left(1 - \mathrm{E}^{-12.82(1.05-\mathrm{H})}\right)$; B) THE VEGETATION AND RAINFALL FREQUENCY (α_R) CONTROL ON $\lambda = E_0/W$, AND THE FITTED RED LINE REPRESENTED BY $\alpha_R \cdot NDVI = 0.43 - 0.32\lambda$.

2.5 A Temporal Pattern for Darwinian Hydrologic Models

Dividing by W_t on both sides of equation (2.14), the key equation of the "abcd" model can be written as:

$$\frac{Y_t}{W_t} = \frac{1+\frac{b}{W_t}-\sqrt{\left(1+\frac{b}{W_t}\right)^2-4a\frac{b}{W_t}}}{2a} \tag{2.15}$$

This equation has the same functional form as equation (2.10). Over a monthly period, W_t is partitioned into Y_t and runoff; and b is the potential value of Y_t. Therefore, the concept of the "abcd" model is the same as the SCS and Budyko models, and equation (2.10) can be obtained from the generalized proportionality principle. As the above mentioned, the generalized proportionality is the commonality between the SCS and Budyko models, since the Budyko equation can be derived from the generalized proportionality hypothesis originating from the SCS model. In summary, the generalized proportionality hypothesis is identified as the commonality of the three Darwinian hydrologic models: the Budyko model for mean annual water balance, the "abcd" model for monthly water balance, and the SCS model for direct runoff at the event scale.

2.6 Conclusions and Future Research

In this work, the generalized proportionality hypothesis has been identified as the commonality of three hydrologic models across a range of time scales: the Budyko model at the long-term scale, the "abcd" model at the monthly scale, and the SCS model at the event scale. The Newtonian hydrologic modeling approach is independent of time scale; the generalized proportionality provides a hydrologic principle independent of time scales from Darwinian view. This commonality among rainfall partitioning across time scales is a signature of the co-evolution of climate, vegetation, soil, and topography as well as hydrologic responses. A single-parameter

Budyko-type equation was derived based on the generalized proportionality hypothesis: the ratio of continuing evaporation to its potential equals the ratio of runoff to its potential.

The temporal pattern of water balance or proportionality hypothesis emerges from the analysis of observed data based on the Darwinian approach. Reliable generalization of the pattern calls for identifying the underlying mechanisms based on the Newtonian approach in order to go beyond pattern to process. This research provides a basis for the synthesis of Newtonian and Darwinian approaches, presents opportunities for important progress in hydrologic research (*Sivapalan*, 2005; *Harman and Troch*, 2014; *Chen et al.*, 2013), and could also expedite progress in other disciplines of geosciences (*Harte*, 2002).

In practice, spatial or temporal patterns and process-based equations could co-exist in hydrologic model development. Laws or patterns based on the Darwinian approach could provide one component of a developed hydrologic model when Newtonian modeling is not achievable for some processes due to the limitation of observations or knowledge of mechanisms. Future research will investigate the linkage of rainfall partitioning between the event scale and long-term scale from a hydrologic processes view. Model structures, capturing temporal or spatial patterns and obeying the Newtonian laws, could be developed for reliable predictions.

CHAPTER 3: FOUR-PARAMETER BUDYKO EQUATION

3.1 Introduction

The partitioning of precipitation into evaporation and runoff at the long-term scale is one of the important research topics in watershed hydrology. With negligible long-term water storage change, mean annual precipitation (*P*) is partitioned into evaporation (*E*) and runoff (*Q*); and climate aridity index, defined as the ratio between mean annual potential evaporation (E_p) and P (i.e., $\emptyset = \frac{E_p}{P}$), is the first order control on this partitioning (Budyko, 1974). Nonparametric equations have been proposed for representing the evaporation ratio (*E*/*P*) as a function of climate aridity based on observations (e.g., Budyko, 1958; Pike, 1964). The Budyko framework provides a simple but effective tool to estimate long-term evaporation and runoff and to evaluate their long-term responses to climate change (e.g., Berghuijs et al., 2014a).

Besides climate aridity index, other factors also play a role in the partitioning of long-term precipitation, such as climate variability, vegetation, soil and topography. The climate variability includes the inter-annual rainfall variability, seasonality of precipitation and potential evaporation, and rainfall intensity, duration and frequency (Eagleson, 1978a; Milly, 1994; Potter et al., 2005; Jothityangkoon and Sivapalan, 2009; Gerrits et al., 2009; Feng et al., 2012; Biswal, 2016). The reported factors related to vegetation in the previous studies include vegetation type and coverage, temporal dynamics of vegetation, and rooting depth (Zhang et al., 2001; Donohue, et al., 2007; Donohue, et al., 2012; Li et al., 2013; Ye et al., 2015; Zhang et al., 2016), and these factors are interdependent. Soil properties, such as soil water storage capacity and infiltration capacity, are found to be important factors affecting the mean annual water balance (Sankarasubramanian and Vogel, 2002; Yokoo et al., 2008), since soil water storage capacity is a factor controlling saturation

excess runoff generation and infiltration capacity controls the production of infiltration excess runoff. A negative correlation between slope and long-term evaporation ratio has been reported in the literature (Yang et al., 2007).

Process-based models have been developed to quantify the role of the controlling factors on annual water balances. Eagleson (1978b) expressed annual water balance as a function of climate, soil, and vegetation by developing a comprehensive hydrologic model, which includes submodels for surface water storage, unsaturated storage, groundwater flow, and infiltration. Milly (1994) investigated the interaction between soil water storage capacity and climate seasonality and intermittency through a stochastic model of soil moisture balance (Milly, 1993). Woods (2003) extended the Milly's model to include water storage and release by the plant canopy and saturated soil zone. Based on the Milly's model, Potter et al. (2005) found that both soil water storage capacity and infiltration capacity are important controlling factors on annual water balance. Yokoo et al. (2008) investigated the role of climate, soil properties and topography in mean annual water balance through a physically-based water balance model. These physically-based models explicitly represent the processes related to the role of controlling factors; however, the practical application of these models is limited because of the complex numerical solutions required (Zhang et al., 2001).

For the purpose of simplicity, the impacts of climate variability, vegetation, soil and topography on mean annual water balance can be lumped into a single parameter. Therefore, Budyko equations with one parameter have been proposed or derived to quantify the lumped effect of watershed properties on long-term water balance (e.g., Fu, 1981; Choudhury, 1999; Zhang et al., 2004; Yang et al., 2008; Wang and Tang, 2014). The parameter can be treated as a random

variable due to the varying controlling factors among watersheds (Greve et al., 2015). The one-parameter Budyko equations have been used for quantifying the contribution of climate change and land use change to long-term streamflow changes (e.g., Roderick and Farquhar, 2011; Wang and Hejazi, 2011; Jiang et al., 2015).

The one-parameter Budyko equations are based on the one-stage partitioning concept, i.e., precipitation is partitioned into evaporation and runoff assuming negligible long-term water storage change. Surface runoff and base flow are not differentiated in the one-stage partitioning; but they are hydrologic responses at different time scales. Surface runoff is a quick response to a rainfall event, while base flow is the delayed discharge from groundwater storage. The controlling factors on surface runoff generation at the event scale include rainfall intensity and depth, initial soil moisture condition, soil infiltration capacity, and soil storage capacity (Horton, 1933; Dunne and Black, 1970). Base flow are affected by hydrogeological properties such as the processes of recharge and evaporation, slope, and soil properties (Brutsaert and Nieber, 1977). Since these two runoff generation processes are not represented in the one-stage partitioning. It is a challenge to disentangle the role of various watershed properties in the long-term water balance using one-parameter Budyko equations.

To balance the complexity of process-based models and the parsimony of one-parameter Budyko equations, the concept of two-stage precipitation partitioning proposed by L'vovich (1979) can be used to develop a multiple-parameter Budyko equation. At the first stage, precipitation is partitioned into total wetting and fast (or direct) runoff; and at the second stage, the total wetting is further partitioned into evaporation and slow runoff (or base flow). The two-stage partitioning framework explicitly represents the infiltration process (i.e., soil wetting),

surface runoff, and base flow. The competition between evaporation and runoff in the one-stage partitioning is decomposed into two competitions. The first competition between surface runoff and soil wetting occurs at the shorter time scale; while the second competition between slow runoff and evaporation occurs at the longer time scale. These two competitions can be modeled by the proportionality relationship generalized from the Soil Conservation Service curve number (SCS-CN) method for estimating direct runoff at the event scale (Ponce and Shetty, 1995). The applicability of the proportionality model for the two-stage partitioning has been tested in the MOPEX watersheds throughout a wide range of climate aridity index (Sivapalan et al., 2011). The generalized proportionality relationship can be derived as an optimal solution of entropy production from the system perspective (Wang et al., 2015; Zhao et al., 2016). Recently, Hooshyar and Wang (2016) showed the derivation of the proportionality relationship underpinning the SCS-CN method from an analytical solution to Richards' equation under shallow water table environment.

The objective of this paper is to derive a four-parameter Budyko equation by applying the proportionality relationship to the two-stage partitioning of mean annual precipitation. Two parameters are related to fast runoff, and two parameters are related to slow runoff. The roles of climatic variability, vegetation, soil and topography in long-term water balance are evaluated in gauged watersheds. Meanwhile, the principal component regressions between the four parameters of the derived Budyko equation and watershed properties provide a practical method for quantifying long-term evaporation and runoff in ungauged watersheds.

3.2 Methodology

3.2.1 Proportionality relationships for two-stage partitioning of precipitation

The generalized proportionality relationship is briefly described here and more detailed information is referred to Sivapalan et al. (2011) and Chen and Wang (2015). In the generalized proportionality framework, the available water of Z (e.g., precipitation) is partitioned into X (e.g., infiltration) and Y (e.g., runoff) during a certain time interval (e.g., a rainfall event). This partitioning has two properties: (1) when Z approaches to infinity, X approaches to its upper bound denoted by X_p (e.g., infiltration capacity) but Y approaches to infinity; (2) the competition between X and Y starts after the initial demand of X, denoted as X_i, has been satisfied. The partitioning of Z into X and Y is quantified by the following proportionality relationship:

$$\frac{X-X_i}{X_p-X_i}=\frac{Y}{Z-X_0}, \text{ subject to } Z=X+Y \tag{3.1}$$

This generalized proportionality relationship has been applied to the two-stage partitioning of mean annual water balance (L'vovich, 1979; Wang et al., 2015). At the first stage, P is partitioned into soil wetting (W) and direct runoff (Q_d), and this partitioning is quantified by the following equation:

$$\frac{W-W_i}{W_p-W_i}=\frac{Q_d}{P-W_i}, \text{ subject to } P=W+Q_d \tag{3.2}$$

where W_i is defined as initial wetting which does not compete with direct runoff (e.g., infiltration before generating direct runoff); and W_p is mean annual soil water storage capacity or the potential of W. At the second stage, W is partitioned into E and base flow (Q_b), and the corresponding proportionality relationship is shown in equation (3.3):

$$\frac{E-E_i}{E_p-E_i}=\frac{Q_b}{W-E_i}, \text{ subject to } W=E+Q_b \tag{3.3}$$

where E_p is potential evaporation, and E_i is defined as initial evaporation which does not compete with base flow (e.g., vegetation interception and evaporation from the top soil layer).

3.2.2 Deriving a four-parameter Budyko equation

Following the procedure for deriving the one-parameter Budyko equation in Wang and Tang (2014), a four-parameter Budyko equation can be derived from proportionality relationships for two-stage partitioning of precipitation. Firstly, equations (3.4a) and (3.4b) are obtained:

$$Q_d = \frac{(P-W_i)^2}{P+W_p-2W_i} \quad (3.4a)$$

$$Q_b = \frac{(W-E_i)(E-E_i)}{E_p-E_i} \quad (3.4b)$$

Substituting equations (3.4a) and (3.4b) into water balance equation (P-E=Q_d+Q_b) and multiplying 1/P at the both sides, one obtains:

$$1-\frac{E}{P} = \frac{(P-W_i)^2}{P^2+W_pP-2PW_i} + \frac{(W-E_i)(E-E_i)}{E_pP-E_iP} \quad (3.5)$$

To solve E/P from equation (5), the following four dimensionless numbers are defined:

$$H = E/W \quad (3.6a)$$

$$\lambda = E_i/W \quad (3.6b)$$

$$\beta = W_i/W \quad (3.6c)$$

$$\gamma = W/W_P \quad (3.6d)$$

where H is Horton index (*Horton*, 1933; *Troch et al.*, 2009); λ is the ratio of initial evaporation to total wetting; β is the ratio of initial wetting to total wetting; and γ is the ratio of total wetting to its potential. Substituting equations (3.6a–d) into equation (3.5) and letting $E_p/P = \emptyset$, a quadratic function is obtained after algebraic manipulation:

$$a\left(\frac{E}{P}\right)^2 - (b_1\emptyset + b_2)\frac{E}{P} + c\emptyset = 0 \quad (3.7)$$

where

$$a = \left[\left(2H\lambda - H + \lambda - \lambda^2\right)/\gamma + 2\beta H - 2\beta\lambda + 2\beta\lambda^2 - 4\beta H\lambda + \beta^2\lambda\right]/H^3 \quad (3.7.1)$$

$$b_1 = (\beta^2 + H/\gamma - 2\beta H)/H^2 \quad (3.7.2)$$

$$b_2 = \left(H - 2H\lambda - \lambda + \lambda^2 + \lambda/\gamma\right)/H^2 \quad (3.7.3)$$

$$c = 1/(H\gamma) - 1 \quad (3.7.4)$$

Since $\frac{E}{P}$ is between 0 and 1, the following root is the solution for $\frac{E}{P}$:

$$\frac{E}{P} = \frac{b_2 + b_1\emptyset - \sqrt{(b_2 + b_1\emptyset)^2 - 4ac\emptyset}}{2a} \quad (3.8)$$

When $E = E_i = W_i$, one obtains $H = \beta = \lambda$ and $a = b_1 = b_2 = c$; and equation (3.8) becomes $\frac{E}{P} = \frac{1+\emptyset-|1-\emptyset|}{2}$. When $0 \le \emptyset \le 1$, $\frac{E}{P} = \emptyset$ (i.e., the evaporation approaches to the energy supply limit); and when $\emptyset > 1$, $\frac{E}{P} = 1$ (i.e., the evaporation approaches to the water supply limit). Therefore, $E = E_i = W_i$ is corresponding to the upper bound of Budyko curve. When $E_i = 0$ and $W_i = W = P$, one can obtain, from equation (5), $\frac{E}{P} = [1 + (\emptyset)^{-1}]^{-1}$ which is the lower bound of Budyko curve (i.e., the minimum value of $\frac{E}{P}$ given a value of $\emptyset$) reported by Wang and Tang (2014). The lower bound is corresponding to the condition of zero initial evaporation and direct runoff, and precipitation is directly competed by continuing evaporation and base flow. Therefore, the lower bound of Budyko curve, based on the proportionality relationship, is corresponding to the condition when the ratio of evaporation to potential evaporation equals the runoff coefficient (i.e., $E/E_p = Q/P$). In equation (8), $E/P \to 1$ when $\emptyset \to \infty$; and $E/P = 0$ when $\emptyset = 0$. However, it should be noted that the

curves represented by equation (8) intercept with the upper limit line of Budyko curve (i.e., $\frac{E}{P} = \emptyset$ when $0 \leq \emptyset \leq 1$). The intersection point is at $\emptyset_0 = \frac{b_2 - c}{a - b_1}$ which is between 0 and 1.

3.2.3 Study watersheds and data sources

The derived four-parameter mean annual water balance equation is applied to the Model Parameter Estimation Experiment (MOPEX) watersheds (Duan et al., 2006), for which hydro-climatic data were obtained during 1983–2000. Daily precipitation data were obtained from the MOPEX dataset. Rainfall characteristics, including the average time interval between rainfall events denoted as t_b (Eagleson, 1978a), and the number of rainfall events (N), were quantified at the yearly basis using the daily precipitation data (Table 1). In this paper, a rainfall event is defined as a period with continuous daily rainfall greater than zero. Monthly potential evaporation data with a spatial resolution of 8 km were obtained from Zhang et al. (2010), and this dataset has been coupled with MOPEX data for water balance analysis in other studies (e.g., Wang and Alimohammadi, 2012). The seasonality of precipitation is measured by a dimensionless variable (δ_P^*) which describes whether or not the precipitation is in phase with the potential evaporation regime (Berghuijs et al., 2014b). When precipitation is out of phase with potential evaporation, δ_P^* equals –1; and δ_P^* equals 1 when precipitation is in phase with potential evaporation. Daily precipitation and monthly potential evaporation were aggregated to their annual values.

TABLE 3.1: SUMMARY OF IDENTIFIED WATERSHED PROPERTIES AND DATA SOURCES.

Watershed Property	Factor	Definition	Data Source / Methods
Precipitation variability	t_b	Average time interval between rainfall events, [day]	MOPEX
	N	Number of rainfall events, [year^{-1}]	
	$\delta_P{}^*$	Precipitation timing with respect to potential evaporation as a measure of seasonality [-]	(Berghuijs et al., 2014b)
Vegetation	$NDVI_{max}$	Mean annual maximum NDVI, [-]	(Tucker et al., 2005)
Topography	S	Average slope, [%]	NED
Soil	K_s	Saturated hydraulic conductivity, [mm/hour]	gSSURGO
	θ_{wp}	Permanent wilting point, [-]	
	$\theta_{fc} - \theta_r$	Difference between field capacity and residual soil moisture, [-]	
	S_b	Effective soil water storage capacity, [mm]	

Daily streamflow observations are available for the MOPEX watersheds. The observation data for base flow and direct runoff are not available. Base flow separation is a practical approach to estimate base flow from observed streamflow. The base flow separation approach is simple and robust but some base flow separation techniques are lack of physical meaning (Beven, 2011). In this study, the observed daily streamflow was separated into base flow and direct runoff by a one-parameter recursive filter (Lyne and Hollick, 1979). The performance of the digital filter method has been verified with physically-based methods such as isotope traces (Gonzales et al., 2009). This digital filter technique has been used and tested for the MOPEX watersheds in the previous studies by setting the filter parameter to 0.925 (Sivapalan et al., 2011; Brooks et al., 2011; Vopel et al., 2011; Chen and Wang, 2015). The base flow index (a ratio between base flow and total runoff) from the base flow separation technique was verified by comparison with the existing base flow index map (Santhi et al., 2008).

Data for watershed properties, including vegetation, topography and soil, were obtained from various sources (Table 1). The $NDVI_{max}$ is an index of vegetation structure and computed

using bimonthly NDVI (normalized difference vegetation index) data obtained from Tucker et al. (2005). Topographic characteristic, such as watershed mean slope (S), was computed based on Digital Elevation Model (DEM) with a 30–m resolution obtained from the National Elevation Dataset (NED). The following soil properties were extracted from the Gridded Soil Survey Geographic (gSSURGO) database (USDA, 2011): saturated hydraulic conductivity (K_s), sand fraction (ϕ_{sand}), clay fraction (ϕ_{clay}), field capacity (θ_{fc}), wilting point (θ_{wp}), and porosity (θ_s). Residual soil moisture (θ_r) was computed using ϕ_{clay}, ϕ_{sand} and θ_s (Rawls and Brakensiek, 1985). The shallow water table depth is also available and denoted as D_{lwt}. The weighted averages by soil layer depth were computed for each soil property and each soil type, and then the area-weighted averages were computed for each watershed.

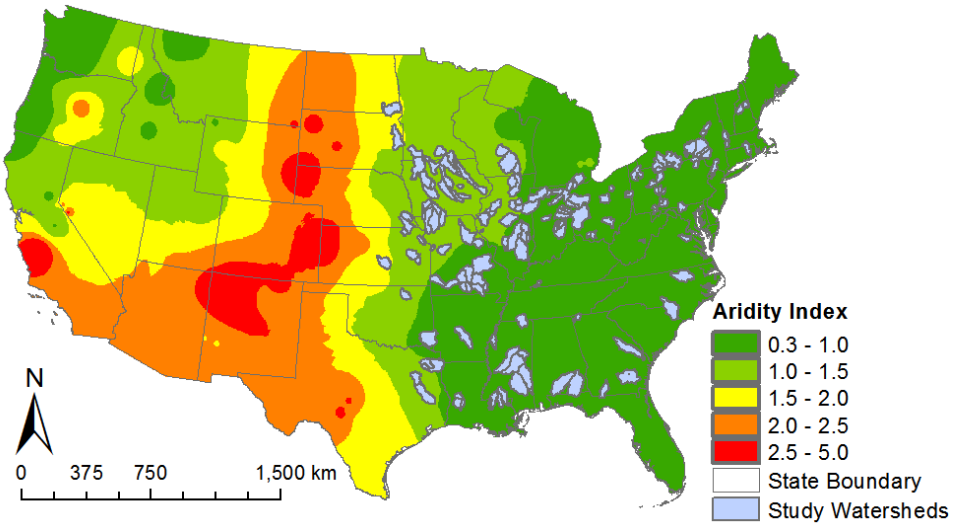

FIGURE 3.1: THE ARIDITY INDEX AND STUDY WATERSHEDS.

Considering the availability and quality of the data sources, particularly soil data, 165 watersheds were selected in this study. Over the study watersheds, the mean annual precipitation

ranges from 564 to 1669 mm/year; the climate aridity index ranges from 0.6 to 1.7 (shown as in Figure 1); and the magnitude of drainage area varies from 100 to 1000 km^2.

3.2.4 Estimating H, λ, β, and γ

Given observed precipitation, potential evaporation and streamflow, the values for E, W, E_i, W_p and W_i need to be quantified in order to estimate the values of the four parameters (H, λ, β, and γ). E is estimated as the difference between P and Q since storage change is negligible for long-term water balance. Based on the estimated Q_d by the base flow separation technique, W is estimated as the difference between P and Q_d. E_i is solved by substituting W, E, Q_b and E_p into equation (4b). W_p is estimated based on the soil data and daily rainfall data. For a given rainfall event, the effective soil water storage capacity is defined as S_b. Considering the data availability in the soil database of gSSURGO, S_b is approximated as:

$$S_b = \left(\theta_{fc} - \theta_r\right) D_{lwt} \tag{3.9}$$

The soil wetting capacity (W_p) for mean annual water balance is computed by the following equation:

$$W_p = S_b N \tag{3.10}$$

where N is the average number of rainfall events in a year. W_i is computed by substituting P, Q_d and W_p into equation (4a).

3.2.5 Evaluating the roles of watershed properties in mean annual water balance

The roles of precipitation variability, vegetation, soil and topography in long-term water balance are evaluated by exploring the dependence of the four parameters on the watershed properties. The controlling factors on each parameter are identified through correlation analysis. The linear correlation coefficient (r) between two variables is negligible when $|r|$ is less than 0.3

(Hinkle, 2003). In this study, watershed properties with $|r| \geq 0.5$ are selected as controlling factors for each parameter as shown in Table 1. Single-predictor analysis is used to evaluate the relationship between each identified controlling factor and individual parameter, and the candidate models include linear, power, exponential and natural logarithmic functions. The one with the maximum coefficient of determination (R^2) among the basic functions is selected for the further principal component regression (PCR) analysis.

PCR analysis is explained as follows. Principal component analysis (PCA) is applied to eliminate the potential multicollinearity among controlling factors for a parameter. PCA determines a set of uncorrelated linear combinations (called principal components) of the controlling factors. The determined principal components are used as the explanatory variables for multiple linear regression. Finally, the principal components in the developed multiple linear regression model are transformed back to the original controlling factors. For each parameter, the factor with the maximum R^2 for the identified basic function is selected as the first-order controlling factor. The identified basic function for the first-order controlling factor is used as the initial equation of PCR. The residuals between the calibrated and modeled parameter values by the initial equation are computed for identifying the second-order controlling factor. $|r|$ between the residuals and the remaining controlling factors are computed; and the factor with the highest $|r|$ is identified as the second-order controlling factor. Then, PCR is conducted for the first- and second-order controlling factors using the identified basic functions; and the computed residuals are used to identified the third-order controlling factor, and so forth. Through this procedure, PCR is conducted over the identified controlling factors for each parameter.

3.3 Results

3.3.1 Estimated parameters

The four parameters were estimated by the method described in section 2.4. Figure 3.2 shows the distributions of the estimated parameter values. The peaks are at 0.7–0.8 for the distribution of H (Figure 3.2a), 0.4–0.5 for the distribution of λ (Figure 3.2b), 0–0.1 for the distribution of β (Figure 3.2c), and 0.1–0.2 for the distribution of γ (Figure 3.2d). Compared with H and γ, the distributions of λ and β are more dispersed. For example, 74 (75) watersheds are located at the peak of H (γ); while 50 (53) watersheds are located at the peak of λ (β). H and λ are two parameters for slow runoff (equation 3.4b), and the difference between them is the numerator (equations 3.6a and 3.6b). Figure 3.3a shows the scatter plot for H and λ, and the correlation coefficient between them is 0.96. Due to this high correlation coefficient, the relationship between H and λ can be modeled by fitting a linear equation to the data points in Figure 3.3a, and the root mean square error for the linear regression (i.e., λ=1.55H–0.75) is 0.05. This linear relationship can be potentially used to reduce the number of parameters to three by eliminating λ. However, considering the scattering of the data points with lower value of H (i.e., watersheds in the humid region), the PCR analysis will be conducted for all the four parameters. β and γ are two parameters for quick runoff (equation 3.4a) and the difference between them is initial wetting (equation 3.6c) or wetting capacity (equation 3.6d). Figure 3.3b shows the scatter plot for β and γ, and the correlation coefficient between them is 0.75.

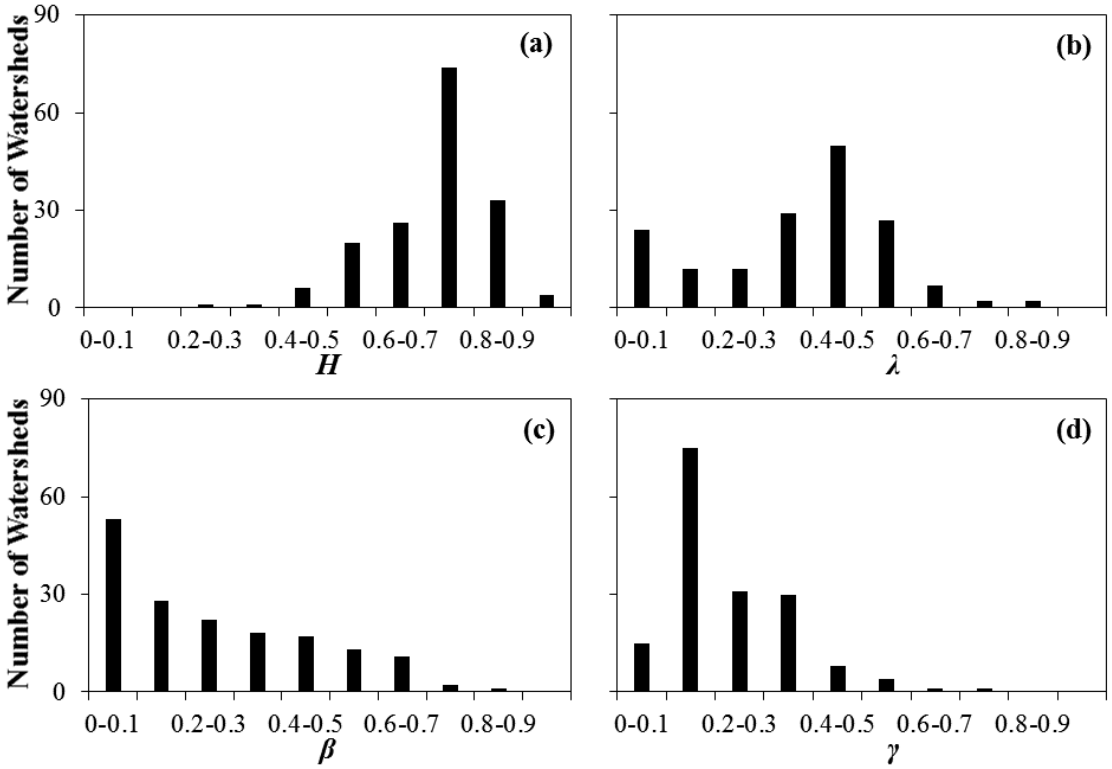

FIGURE 3.2: THE HISTOGRAM OF ESTIMATED (A) H, (B) λ, (C) β, AND (D) γ FOR STUDY WATERSHEDS.

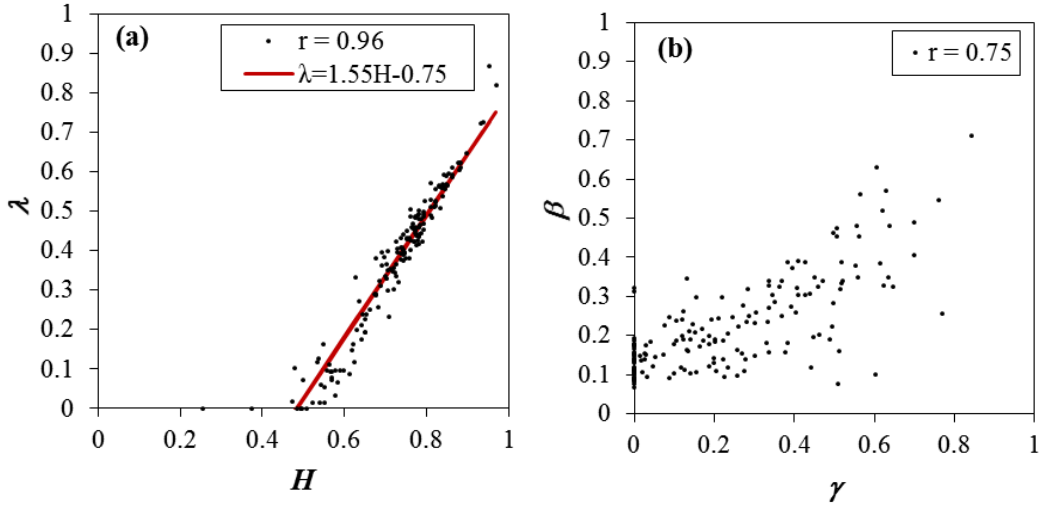

FIGURE 3.3: CORRELATIONS BETWEEN (A) λ (I.E., THE RATIO BETWEEN INITIAL EVAPORATION AND TOTAL WETTING) AND H (I.E., RATIO BETWEEN EVAPORATION AND TOTAL WETTING), AND (B) β (THE RATIO BETWEEN INITIAL WETTING AND TOTAL WETTING) AND γ (THE RATIO BETWEEN TOTAL WETTING TO ITS POTENTIAL).

3.3.2 Controlling factors for parameters

Based on the scatter plots and correlation analyses, controlling factors with the linear correlation coefficient higher than 0.50 are identified (shown in Table 1) for each parameter. H is a measure of vegetation water use efficiency (*Troch et al.*, 2009). Following the reported relationship between H and $NDVI_{max}$ by *Voepel et al.* (2011), a logarithmic function is selected in this study and $NDVI_{max}$ is transformed to $1 - NDVI_{max}/0.87$ for single-factor regression analysis. The result shows that H is strongly correlated with t_b ($r = 0.72$), S ($r = -0.65$), $NDVI_{max}$ ($r = -0.60$), and θ_{wp} ($r = 0.59$). H has positive correlations with t_b (Figure 4a) and θ_{wp} (Figure 4d), but negative correlations with S (Figure 4b) and $NDVI_{max}$ (Figure 4c). The maximum R^2 among the basic functions are 0.53 for t_b associated with the logarithmic relationship, 0.43 for S associated with the linear relationship, 0.43 for $1 - NDVI_{max}/0.87$ associated with the logarithmic relationship, and 0.38 for θ_{wp} associated with the logarithmic relationship (Table 2). Therefore, the scatter plots and single-predictor analysis for H suggest logarithmic functions for t_b, θ_{wp}, and $NDVI_{max}$, and a linear function for S.

Four controlling factors are identified for λ as shown in Figure 3.5. The results show that the correlations are positive with t_b ($r = 0.71$, Figure 3.5a) and θ_{wp} ($r = 0.51$, Figure 3.5d) but negative with S ($r = -0.63$, Figure 3.5b) and $NDVI_{max}$ ($r = -0.59$, Figure 3.5c). As we can see, the identified four controlling factors for λ are the same as the ones for H. This is consistent with significantly positive correlation between H and λ shown in Figure 3.3a. Moreover, the identified functional types are also the same, i.e., logarithmic functions for t_b, θ_{wp}, and $NDVI_{max}$ and a linear function for S (Table 3.2).

Two controlling factors are identified for β, i.e., $\theta_{fc} - \theta_r$ and K_s as shown in Figure 6. The correlation is positive with K_s (r = 0.61), but negative with $\theta_{fc} - \theta_r$ (r = –0.72). The scatter plots and single-predictor analysis suggest a logarithmic function for K_s, and a linear function for $\theta_{fc} - \theta_r$ (Table 3.2). S_b, N, and δ_P^* are identified as the controlling factors on γ (Figure 3.7); and the correlation coefficients are –0.80 for S_b, –0.57 for N, and –0.51 for δ_P^*. The scatter plots and single-predictor analysis suggest a power function for S_b, a logarithmic function for N, and an exponential function for δ_P^* (Table 3.2).

For comparison, Table 3.3 summarizes the controlling factors for annual water balance reported in the previous studies using MOPEX watersheds. The controls of vegetation and topography on H have been reported (*Brooks et al.*, 2011; *Voepel et al.*, 2011). Even though t_b and θ_{wp} were not reported as the controlling factors on H, their roles can be explained based on the meaning of Horton index, which represents water use efficiency of vegetation. H is higher in the drier environment with lower vegetation coverage (*Troch et al.*, 2009). Since t_b represents the duration of dry period, the water use efficiency of vegetation increases with t_b. More percentage of soil wetting is stored in the root zone for evaporation with the increase of θ_{wp}. As a result, H is positively correlated with t_b and θ_{wp} (Figure 4a and 4d). Snowiness is defined as the fraction of total annual precipitation that falls as snow (*Berghuijs et al.*, 2014a, b). The correlation coefficients between snowiness and H as well as λ are –0.46. Therefore, snowiness is not selected for further PCR analysis since the absolute value of its correlation coefficient is less than 0.5. However, it should be recognized that correlation between snowiness and H (λ) indeed exists. The control of precipitation seasonality, measured by δ_P^*, has been reported in the MOPEX watersheds (*Berghuijs et al.*, 2014b) and other watersheds (e.g., *Potter et al.*, 2005). The role of K_s and $\theta_{fc} -$

θ_r has also been reported (*Gentine et al.*, 2012), and the role of rainfall frequency or number of rainfall event has been reported in one-parameter Budyko equation (*Zanardo et al.*, 2012; *Wang and Tang*, 2014). The effective soil water storage capacity is the product of $\theta_{fc} - \theta_r$ and mean water table depth. The rooting zone depth and elevation have a small correlation coefficient (i.e., $|r|<0.5$) with the four parameters.

TABLE 3.2: THE VALUES OF R^2 FOR FOUR BASIC FUNCTIONS BETWEEN EACH PARAMETER AND INDIVIDUAL FACTOR. THE MAXIMUM R^2 AMONG A SET OF PARAMETER-FACTOR RELATIONSHIPS IS HIGHLIGHTED AS BOLD.

Parameter	**Factor**	**Basic Function**			
		Linear	**Exponential**	**Logarithmic**	**Power**
		R^2	R^2	R^2	R^2
H	t_b	0.52	0.47	**0.53**	0.49
	S	**0.43**	0.41	0.39	0.38
	$1-NDVI_{max}/0.87$	0.36	0.33	**0.43**	0.41
	θ_{wp}	0.35	0.32	**0.38**	0.35
λ	t_b	0.50	0.14	**0.51**	0.16
	S	**0.40**	0.15	0.36	0.13
	$1-NDVI_{max}/0.87$	0.35	0.09	**0.42**	0.14
	θ_{wp}	0.26	0.06	**0.28**	0.06
β	$\theta_{fc}-\theta_r$	**0.51**	0.20	0.49	0.17
	K_s	0.38	0.12	**0.47**	0.24
γ	S_b	0.64	0.74	0.74	**0.77**
	N	0.33	0.31	**0.35**	0.31
	$\delta_P{}^*$	0.26	**0.38**	-	-

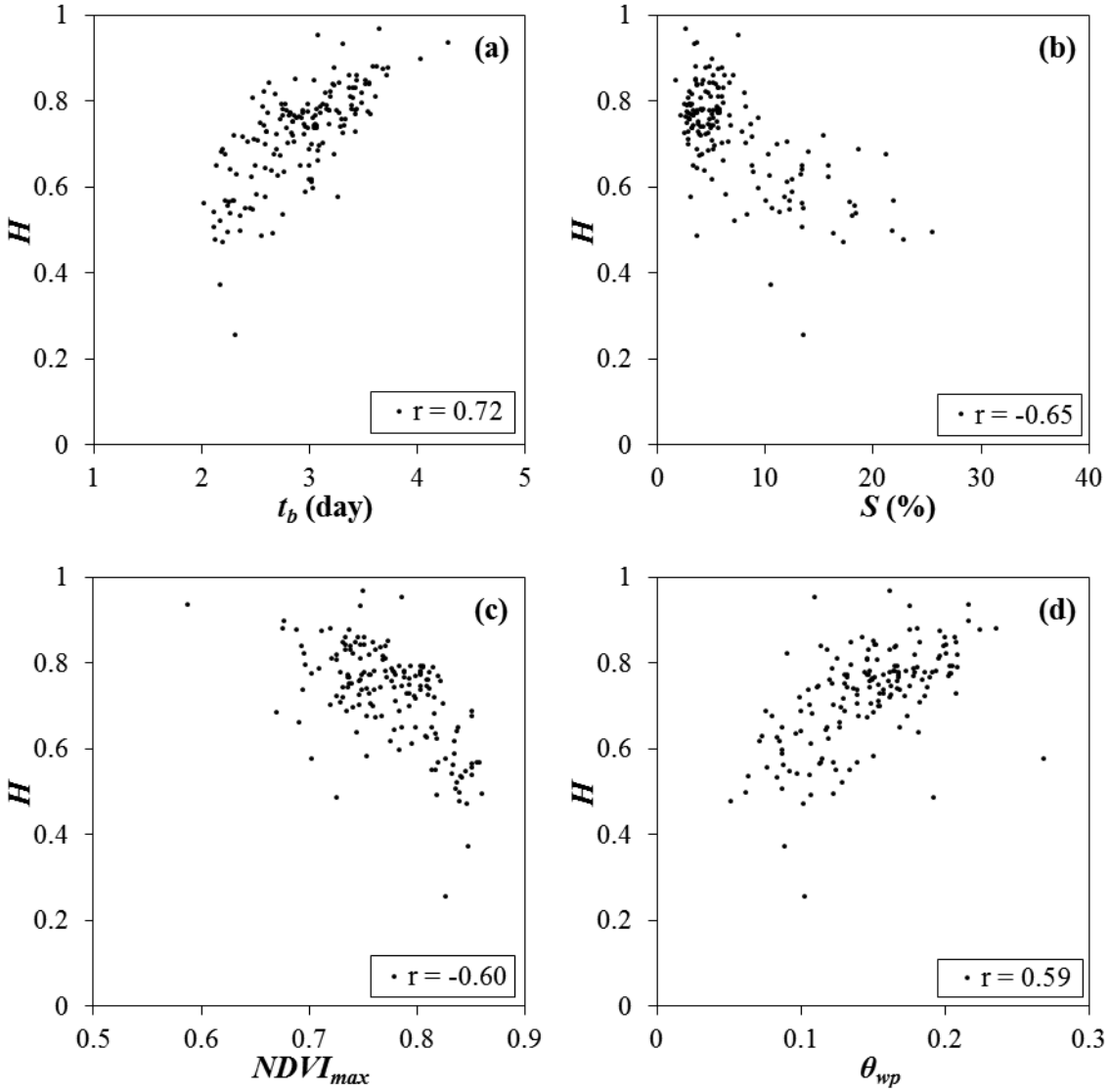

FIGURE 3.4: CORRELATIONS BETWEEN *H* AND FOUR CONTROLLING FACTORS WITH LINEAR CORRELATION COEFFICIENTS HIGHER THAN 0.5: (A) AVERAGE INTERVAL BETWEEN RAINFALL EVENTS; (B) AVERAGE SLOPE; (C) $NDVI_{MAX}$; AND (D) PERMANENT WILTING POINT.

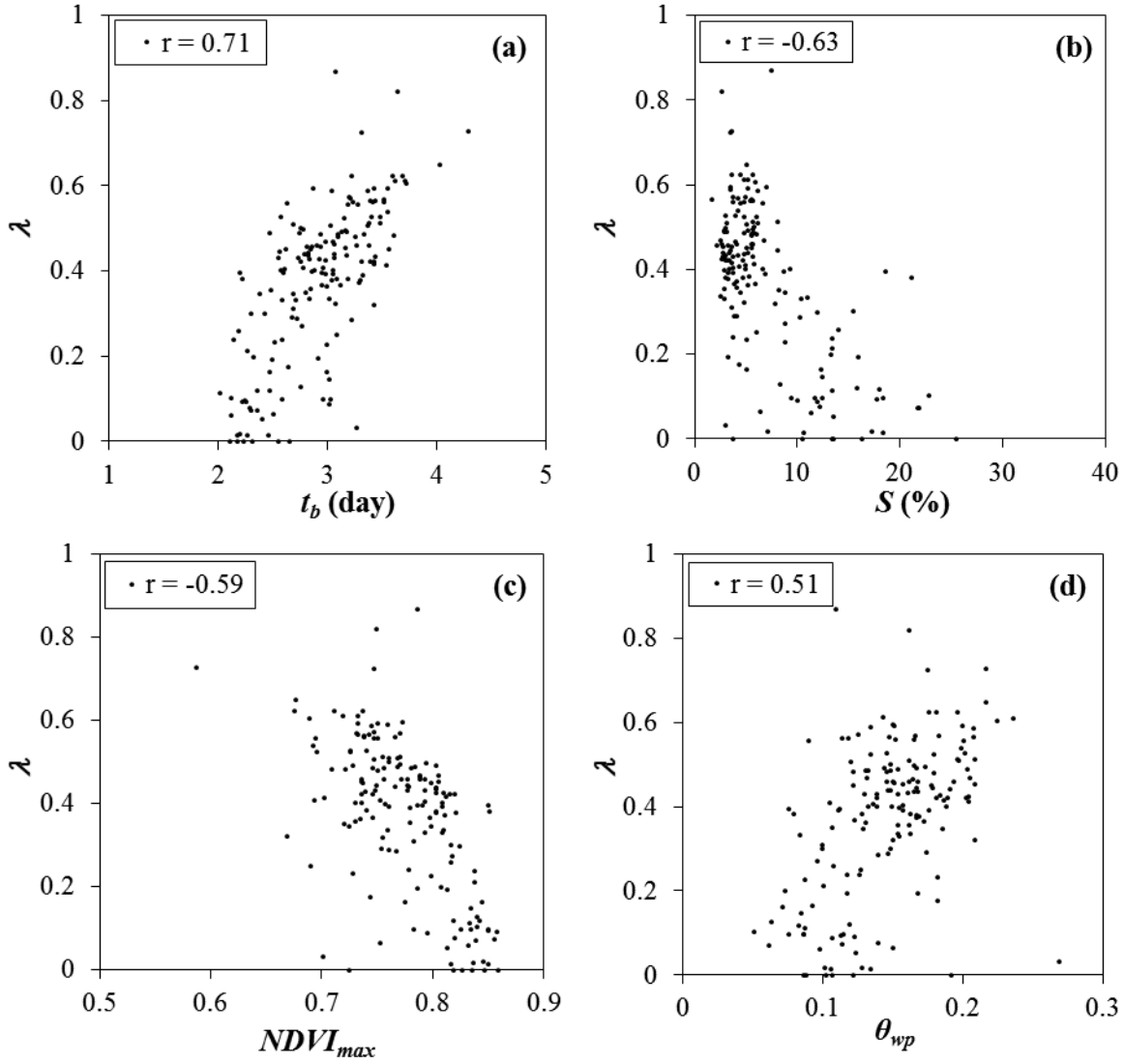

FIGURE 3.5: CORRELATIONS BETWEEN λ AND FOUR CONTROLLING FACTORS WITH LINEAR CORRELATION COEFFICIENTS HIGHER THAN 0.5: (A) AVERAGE INTERVAL BETWEEN RAINFALL EVENTS; (B) AVERAGE SLOPE; (C) $NDVI_{MAX}$; AND (D) PERMANENT WILTING POINT.

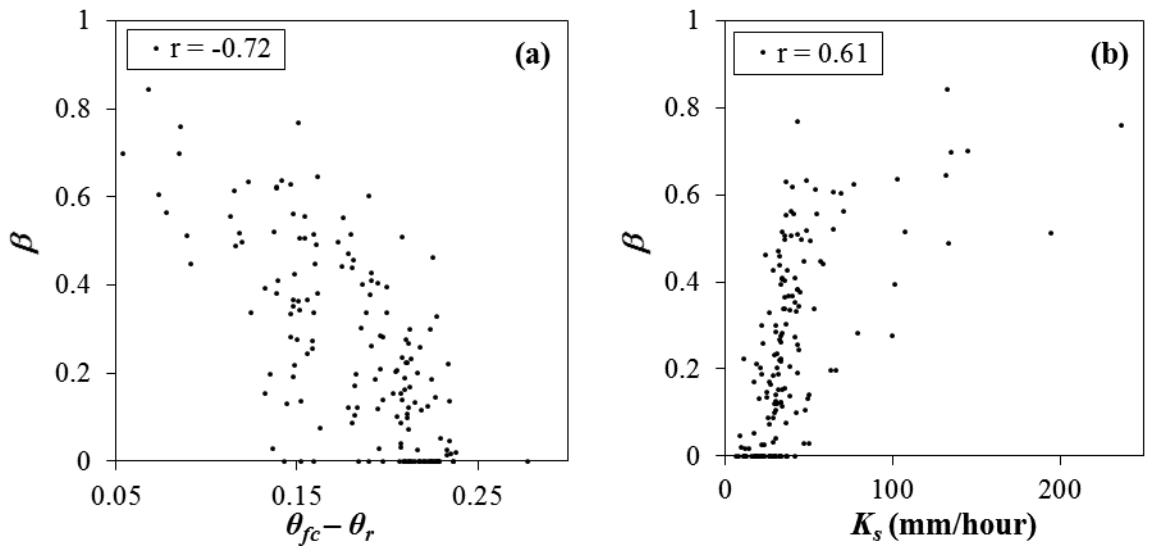

FIGURE 3.6: CORRELATIONS BETWEEN β AND TWO CONTROLLING FACTORS WITH LINEAR CORRELATION COEFFICIENTS HIGHER THAN 0.5: (A) DIFFERENCE BETWEEN FILED CAPACITY AND RESIDUAL SOIL MOISTURE; AND (B) SATURATED HYDRAULIC CONDUCTIVITY.

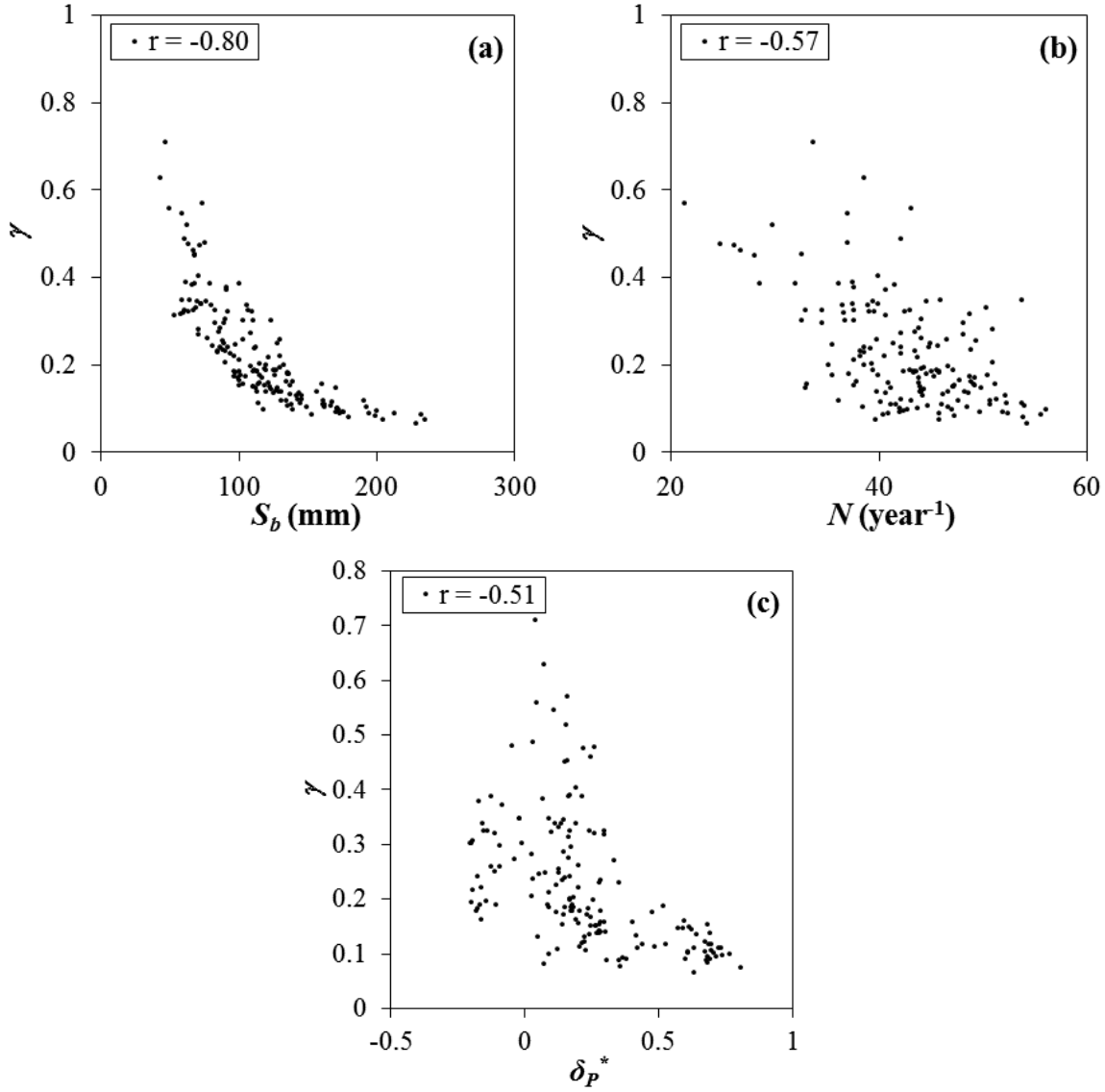

FIGURE 3.7: CORRELATIONS BETWEEN γ AND THREE CONTROLLING FACTORS WITH LINEAR CORRELATION COEFFICIENTS HIGHER THAN 0.5: (A) THE COMPUTED EFFECTIVE SOIL WATER STORAGE CAPACITY; (B) NUMBER OF RAINFALL EVENTS ON AN ANNUAL BASIS; AND (C) PRECIPITATION TIMING WITH RESPECT TO POTENTIAL EVAPORATION AS A MEASURE OF SEASONALITY.

3.3.3 Principal Component regression for the four parameters

PCR analysis is conducted for each of the four parameters for the developed mean annual water balance model, and the results are shown in Table 4. t_b is identified as the first-order control on H, and it explains about a half of the variation in H (P1 in Table 3.4). R^2 for H increases from 0.53 to 0.60 by adding the slope to PCR (P2). θ_{wp} is further added to PCR and R^2 increases to 0.62 (P3). The incorporation of $NDVI_{max}$ increases R^2 by 0.01 (P4). As the first-order controlling factor on λ, t_b explains 51% of the variation in λ (P5). The incorporation of the second-order (S) improves the R^2 by 0.05 and the third-order ($NDVI_{max}$) controlling factor increases R^2 by 0.02 and the forth-order (θ_{wp}) does not increase the value of R^2. Similarly, the first-order controlling factor, $\theta_{fc} - \theta_r$, explains 51% of the variation in β. By adding the second-order controlling factor (K_s), the value of R^2 increases to 0.56 (P10). Compared with other three parameters, the first-order controlling factor, S_b, largely explains the variation in γ (77% in P11). The second-order controlling factor (N) increases R^2 to 0.88 (P12), and δ_P^* further increases R^2 to 0.92 (P13). The equations representing the best-fit models for H, λ, β, and γ are P4, P7, P10, and P13, respectively.

It should be noted that the estimation of λ is affected by the uncertainty of potential evaporation. Therefore, the estimated value of λ may vary with the method for estimating potential evaporation. As a sensitivity analysis, the Hamon's equation (*Hamon*, 1961) is used to compute potential evaporation. Even though the coefficients of PCR equations are affected by the method for estimating potential evaporation, the same controlling factors and basic functions (Table 3.2) are identified for λ.

3.4 Discussions

3.4.1 Parsimonious model and process control

The controls of watershed properties, besides climate aridity index, on long-term water balance have been studied through single-parameter Budyko equations (e.g., Choudhury, 1999; Zhang et al., 2001) and physically-based models such as stochastic soil moisture balance models (Milly, 1994; Porporato et al., 2004). The single-parameter Budyko equations are simple and practical; but the roles of intra-annual climate variability, soil, vegetation, and topography are lumped to the single parameter. Relationships between the single parameter and one dominant controlling factor (Zhang et al., 2016) or multiple factors (Yang et al., 2007; Xu et al., 2013) have been developed by regression analysis for predicting mean annual evaporation and runoff. Physically-based models represent detailed hydrologic processes (e.g., surface water storage, unsaturated storage, and groundwater flow) and the roles other than climate have been explicitly described (e.g., Feng et al., 2012; Gentine et al., 2012); however, the practical application of these models are limited because of the complex solutions required. Compared with the single-parameter Budyko equations, the developed four-parameter Budyko equation extends the one-stage partitioning to two-stage partitioning by representing the fast process and slow process, explicitly. However, the four-parameter Budyko equation is practical for application since it is an explicit analytical equation as the single-parameter Budyko equations. Compared with the stochastic soil moisture balance models, the process representation in the four-parameter Budyko equation is limited and implicit since the two-stage partitioning is quantified by two proportionality relations. However, the dominant runoff generation mechanisms are conceptualized through surface runoff and base flow. Particularly, the proportionality relation has the physical basis at the

event scale (*Hooshyar and Wang*, 2016). Therefore, the developed four-parameter equation balances model parsimony and representation of dominant processes.

3.4.2 Interdependence of model parameters

There is interdependence amongst the four parameters for the proposed long-term water balance equation. The correlation coefficient between the two parameters (H and λ) for slow process is 0.96 (Figure 3a), and the correlation coefficient between the two parameters (β and γ) for fast process is 0.75. The cross correlation coefficients of parameters between slow and fast runoff are relatively smaller, i.e., –0.46 for H and γ, –0.38 for λ and γ, –0.13 for H and β, and –0.06 for λ and β. This interdependence can be explained by three reasons. One reason is that two watershed properties may be interdependent. As demonstrated by Li et al. (2014), climate, soil, vegetation, and topography may be constrained to be codependent in order to satisfy the Budyko curve. For example, the correlation coefficients are –0.57 for S and $\theta_{fc} - \theta_r$, –0.49 for $NDVI_{max}$ and θ_{wp}, –0.57 for S and t_b, and 0.49 for S_b and t_b. The second reason is that a watershed property could be a controlling factor on two parameters. For example, the identified controlling factors on the pair of H and λ. The third reason is the potential spurious correlation since total wetting is the denominator for both H and λ. The correlation coefficient between E_i and E is 0.88; while the correlation for H and λ is 0.96. Therefore, the spurious correlation indeed explains part of the correlation between H and λ. The interdependence of the four parameters indicates that it is a challenge, if not impossible, to fully isolate the impacts of individual factors on long-term water balance. The interdependence of model parameters needs to be considered in the studies for assessing climate change and land use change impacts on hydrologic responses.

3.4.3 Comparison with one-parameter Budyko equation

Compared with one-parameter Budyko equations, the proposed four-parameter equation differentiates slow and fast processes and the corresponding controlling factors. For example, Figure 8 compares the four-parameter equation with the one-parameter Budyko equation derived from one-stage precipitation partitioning based on proportionality relationship (Wang and Tang, 2014):

$$\frac{E}{P} = \frac{1+\emptyset-\sqrt{(1+\emptyset)^2-4\varepsilon(2-\varepsilon)}}{2\varepsilon(2-\varepsilon)} \tag{3.11}$$

The parameter ε equals to 0.48 for the two highlighted watersheds in Figure 8 (#01421000 located in New York and #06606600 located in Iowa), and the blue solid line represents equation (3.11) with ε = 0.48. However, the base flow index (i.e., the ratio between annual base flow and total runoff) is 0.67 for #01421000 and 0.78 for #06606600. Correspondingly, the parameter sets of the four-parameter equation for these two watersheds are quite different. The parameter set for #01421000 includes H = 0.68, λ = 0.38, β = 0.56, and γ = 0.45 (the green dashed line); and the parameter set for #06606600 includes H = 0.78, λ = 0.42, β = 0.26, and γ = 0.10 (the red dash-dotted line). The discrepancy of parameter sets between these two watersheds is due to the differences of watershed properties. For example, θ_{wp} and t_b in #06606600 are about twice of the values in #01421000. S is 4% in #06606600 and 21% in #01421000. The value of K_s is 22 mm/hour in #06606600 and 39 mm/hour in #01421000. $\theta_{fc} - \theta_r$ is 0.22 in #06606600 and 0.15 in #01421000. The value of δ_P^* in #06606600 is 0.7 indicating a relatively strong summer-dominant precipitation; but the value of δ_P^* is 0.2 in #01421000 indicating a relative uniform precipitation throughout the year.

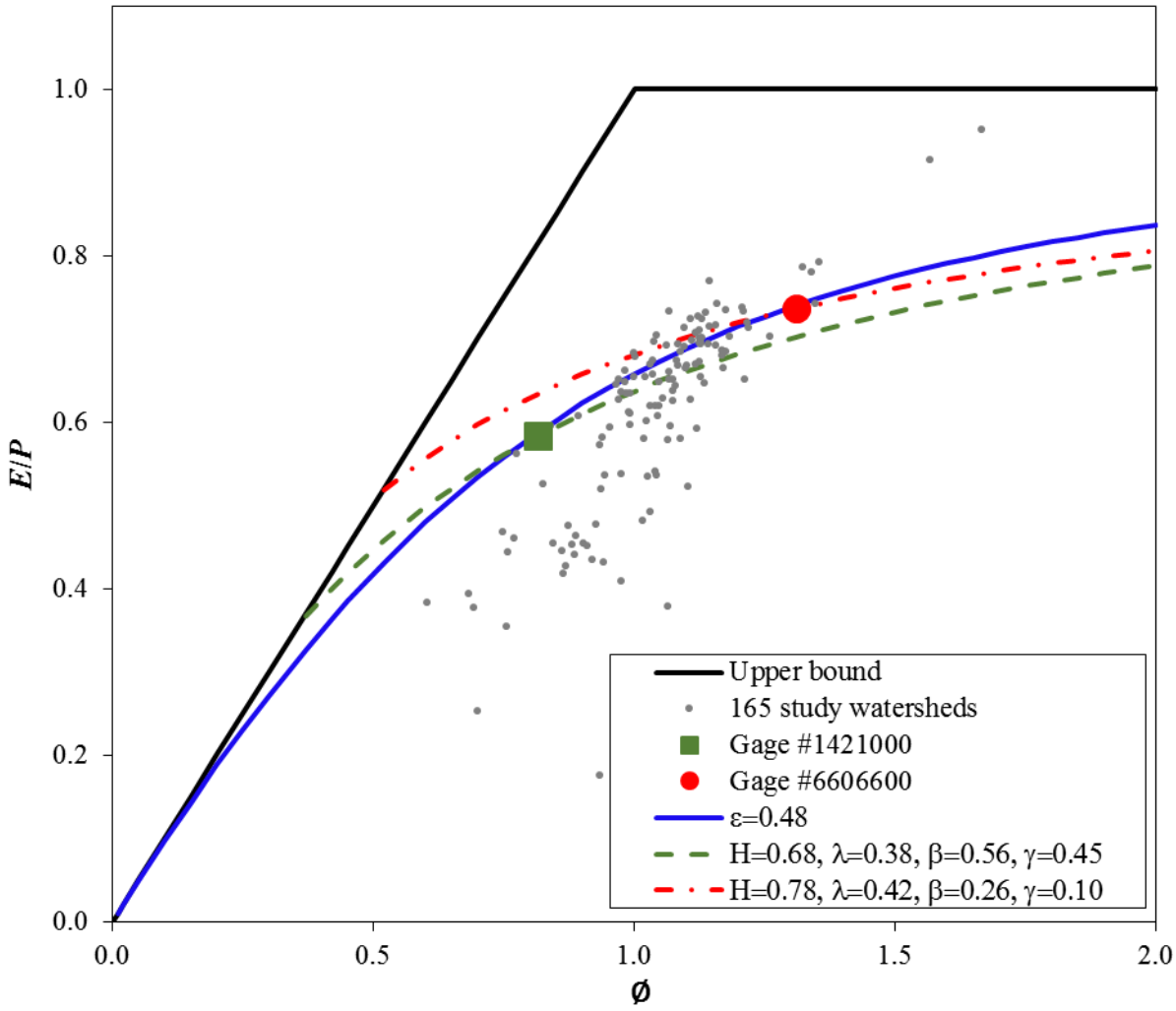

FIGURE 3.8: THE OBSERVED *E*/*P* VERSUS Ø FOR THE 165 STUDY WATERSHEDS. TWO WATERSHEDS (USGS GAGE #01421000 AND #06606600) ARE LOCATED ON THE BLUE SOLID LINE WHICH REPRESENTS THE SINGLE-PARAMETER BUDYKO EQUATION (I.E., EQUATION 11) WITH $\varepsilon = 0.48$. THE GREEN DASHED LINE AND THE RED DASH-DOTTED LINE REPRESENT THE FOUR-PARAMETER EQUATION (I.E., EQUATION (8)) WITH THE PARAMETER SETS FOR WATERSHEDS #01421000 AND #06606600, RESPECTIVELY.

The four-parameter Budyko curves intercept with the upper bound of Budyko curve at $\emptyset_0 = \frac{b_2 - c}{a - b_1}$ as discussed in section 2.2. $\emptyset_0$ is 0.36 for watershed #01421000 and $\emptyset_0$ is 0.52 for watershed #06606600. It indicates that a watershed with a specific parameter set is only possibly located in the region with Ø higher than or equal to a certain positive value ($\emptyset_0$). For example, the

watersheds with $H = 0.78$, $\lambda = 0.42$, $\beta = 0.26$, and $\gamma = 0.10$ can be only potentially located in the region with $\emptyset \geq 0.52$ if the proportionality relationships are valid. The existence of the lower bound of climate aridity index can be explained by the dependence of watershed properties on climate. Since the four parameters are controlled by watershed properties as shown in section 3.3 and watershed properties are controlled by climate, the parameters are not independent on climate. To demonstrate the dependence of parameters on climate, the correlation coefficients between $\emptyset$ and each parameter can be computed. By taking the study watersheds as samples, the correlation coefficients between $\emptyset$ and the parameters are 0.73 for H, 0.64 for λ, –0.17 for β, and –0.57 for γ. It should be noted that a feasible parameter set (i.e., combination of four parameter values) is associated with a unique curve in the figure. Once the values of the parameter set change, the corresponding curve will change.

3.5 Conclusion

Parsimonious hydrologic models provide transparent tools to quantify runoff responses to the changes in climate and land cover. Single-parameter Budyko equations have been developed and used for quantifying long-term runoff and evaporation responses to climate and understanding the physical controls on mean annual water balance. The roles of watershed properties including climate variability, soil, vegetation and topography are lumped into a single parameter in many studies. On the other hand, process-based hydrologic models have been developed for understanding the physical controls on long-term water balance. In this paper, a four-parameter equation is derived based on the two-stage partitioning of mean annual precipitation and proportionality relationships. At the first-stage partitioning, the ratio of continuing wetting to its potential equals to the ratio of surface runoff to its potential; and at the second-stage of partitioning,

the ratio of continuing evaporation to its potential equals to the ratio of base flow to its potential. The derived four-parameter equation provides a potential solution to balance model parsimony and representation of dominant processes, i.e., the fast and slow runoff processes.

The four parameters of the derived equation are estimated for 165 watersheds based on observations of precipitation, potential evaporation, streamflow, and soil properties. Then, the roles of watershed properties represented by the four parameters are evaluated based on correlation analysis. The two parameters (H and λ) related to slow process have positive correlations with rainfall variability (i.e., the average time interval between rainfall events) and soil property (i.e., permanent wilting point) and negative correlations with topography (i.e., slope) and vegetation (NDVI). For the fast process, β is found to be controlled by soil properties including the difference between field capacity and residual soil moisture, saturated hydraulic conductivity; while γ is controlled by effective soil water storage capacity, frequency of rainfall events, and precipitation seasonality. Therefore, the four-parameter equation provides a framework to systematically evaluate the role of controlling factors in long-term water balance.

Principal component regression analysis was then conducted to construct equations for linking the model parameters to the identified dominant controlling factors. These equations provide a model to assess long-term evaporation and runoff responses to climate and watershed property changes related to fast and slow processes in ungauged watersheds. Meanwhile, the proposed four-parameter equation can be used to reveal the interdependence of model parameters.

The principal component regression models are based on a subset of MOPEX watersheds (165) with climate aridity index ranging from 0.6 to 1.7. Therefore, the performance of the multiple linear regression models in the very humid or arid regions needs further investigation.

However, the four-parameter Budyko equation itself should be applicable to a wide range of hydro-climatic conditions, since the applicability of the proportionality model for two-stage partitioning has been verified in 377 MOPEX watersheds (Sivapalan et al., 2011).

CHAPTER 4: RECONSTRUCTION OF ANNUAL GROUNDWATER STORAGE CHANGE IN LARGE-SCALE IRRIGATION REGION

4.1 Introduction

Groundwater is the largest unfrozen freshwater source on the Earth (Aeschbach-Hertig and Gleeson, 2012). It is more widely accessible and less vulnerable to droughts than surface water (Foster and Chilton, 2003; Schwartz and Ibaraki, 2011). Groundwater is often the only available water resource for supporting and expanding food production, and has become the major source for irrigation in approximately 40% of cropland around the globe (Jury and Vaux, 2005). As a result, the worldwide 'explosion' of groundwater exploitation has been instrumental for ensuring global food supplies (Giordano, 2009). Global groundwater consumption for irrigation during 1967-2007 was estimated at 545 km3/year accounting for 56% of total groundwater withdrawals (Siebert et al., 2010; Margat and Gun, 2013). The flip side of the consumption has been severe groundwater depletion in many parts of the world (Hanasaki et al., 2008), threatening the sustainability of food production in the longer term and deteriorating groundwater dependent ecosystems (Konikow and Kendy, 2005; Gleeson et al., 2010). To address this issue, several efforts have been made for incorporating the irrigation into global land surface models in recent (e.g., Leng et al., 2014, 2015; Pokhrel et al., 2016).

The launch of the Gravity Recovery and Climate Experiment (GRACE) satellites in 2002 also provides an unprecedented opportunity to derive ΔGWS from the terrestrial water storage change (ΔTWS) for the large-scale irrigation regions. Information of TWS in different spatial scales can be extracted from the observed gravity field (Wahr et al., 1998; Swenson and Wahr, 2002; Jacob et al., 2012). The change of TWS captured GRACE represents the vertical integration

of changes in groundwater, soil moisture, surface water, snow, ice, and biomass (Tapley et al., 2004), and potential mass changes by anthropogenic activities (Tang et al., 2013). Owing to the complicated restoration of satellites' signal, GRACE-derived data to large-scale river basins (e.g., > 200,000 km^2) are associated with the bias caused by the measurement and aliasing of high-frequency mass variations in the monthly GRACE gravity field solutions (Wahr et al., 1998; Swenson and Wahr, 2002, 2006). The bias is corrected by the spatial smoothing, through which TWS anomaly relative to the mean value during a certain period over a specific area is computed (e.g., Han et al., 2005). The leakage error introduced by spatial smoothing contains the amplitude damping from mass inside and outside the basin (Klees et al., 2007; Longuevergne et al., 2010). Scaling factor is applied to restore power attenuated by leakage error (Swenson and Wahr, 2002; Chen et al., 2007), even though a single multiplicative factor may not be able to describe leakage error (Zhao et al., 2016).

GRACE-derived groundwater storage changes generally agree well with ground-based observations, especially for the seasonal variations in regions with abundant data of groundwater levels and soil moisture, such as the High Plains Aquifer (Strassberg et al., 2009) and the State of Illinois (Yeh et al., 2006) in the United States. GRACE-derived data as relatively reliable large-scale measurements have been widely used to assess groundwater depletion in extensively irrigated regions around the world (Feng et al., 2013; Rodell et al., 2009; Shamsudduha et al., 2012; Panda and Wahr, 2016). Moreover, GRACE-based TWS anomalies have been integrated with regional groundwater and surface water models to quantify hydrologic responses to droughts and anthropogenic activities (Scanlon et al., 2012; Sun et al., 2012; Niu et al., 2014; Castle et al., 2014; Huang et al., 2015; Humphrey et al., 2016), and model the TWS and groundwater storage changes

(e.g., Doll et al., 2014; Wada et al., 2014; Pokhrel et al., 2015). Additionally, the GRACE-based TWS anomalies have been also integrated with the statistical models to reconstruct the TWS and groundwater storage change (e.g., Long et al., 2014a). The integration with the sophisticated models (e.g., MODFLOW: Modular Groundwater Flow Model, and process-based hydrological models) limit the practical applications for reconstructing and the predicting the long-term groundwater storage change for the effective management of groundwater resources. It is challenging to reveal the hydrological interactions of the reconstructed TWS and groundwater storage changes with other water components for the integration of the statistical models.

At the long-term scale when TWS change is negligible in the natural watersheds, mean annual precipitation ($\bar{P}$) is partitioned into mean annual evapotranspiration ($\bar{E}$) and runoff ($\bar{Q}$); this partitioning was described by a parsimonious water balance model (i.e. Budyko equation), $\bar{E}/\bar{P} = f(\overline{E_p}/\bar{P})$ where $\overline{E_p}$ refers to mean annual potential evapotranspiration (Mezentsev, 1955; Budyko, 1958; Pike, 1964; Fu, 1981; Choudhury, 1999; Zhang et al., 2001; Donohue et al., 2007; Yang et al., 2008; Zhou et al., 2015). Wang and Tang (2014) derived a newly Budyko-type equation for the partitioning of annual precipitation and this functional form is similar with equations for the partitioning of precipitation at the event, monthly. Liu et al. (2016) indicated that the utility of assessing the partitioning depended on the catchment size. Wang (2012) pointed out the annual water storage carry-over can be significant and the intensified anthropogenic activities such as urbanization, groundwater exploitations, hydraulic engineering can also induce a large total water storage change (Du et al., 2016). When TWS change is substantial, the available water for partitioning into evapotranspiration (E) and runoff (Q) is the effective precipitation (P_{eff}) as the difference between precipitation (P) and ΔTWS (i.e., $P_{eff} = P\text{-}\Delta TWS$) (Wang, 2012; Du et al.,

2016). Therefore, it is possible to reconstruct Δ*TWS* using Budyko-type equations. Due to having few parameters, this Budyko-type model provides a practical way to describe the annual water balance from a hydrological respective.

Therefore, the objectives of this paper are to: 1) integrate the GRACE data with a Budyko model to practically and hydrologically reconstruct the long-term time series of Δ*TWS* and annual groundwater storage changes (Δ*GWS*) for the large-scale irrigation regions (e.g., Punjab in Pakistan); 2) quantify the groundwater depletion in the study area based on the reconstructed Δ*GWS*. The remaining of the paper is organized as follows. Section 2 provides background on study area and data sources. Section 3 describes the methodology such as the annual Budyko model, the parameters estimation, and the reconstruction of Δ*TWS* and Δ*GWS*. Results and discussion are presented in section 4 and section 5, and conclusions are drawn in section 6.

4.2 Study Area and Data Sources

4.2.1 Study area

The Punjab, located in the northern part of Pakistan, consists of vast alluvial plain traversed by the Indus River and its five tributaries including Chenab, Sutlej, Jhelum, Ravi, and Punjnad (Figure 1). The climate in the region is characterized by significant seasonal fluctuations in temperature and rainfall. The mean annual temperature during 1971-2000 is about 23.3 ℃, and the maximum temperature occurs in summer from May to August reaching as high as to 32.8 ℃ (MoWP, 2012). The mean annual precipitation during 1971-2000 is around 58 cm/year and about 70% of rainfall occurs during the monsoon season from June to September (MoWP, 2012). Correspondingly, about 60 percent of the annual river flow is concentrated in the monsoon season. The topographic slope declines from north to south and southwest, and the soils are moderately or

highly permeable (Greenman et al., 1967). Punjab contains a large unconfined aquifer with no lateral flow crossing the boundary (Swarzenski, 1968; Khan et al., 2016). The Chashma reservoir located on the Indus River (Figure 1) is the major reservoir, and the annual surface water storage is much smaller than groundwater and soil moisture storage change (MoWP, 2012). Therefore, surface water storage change is assumed to be negligible in this study.

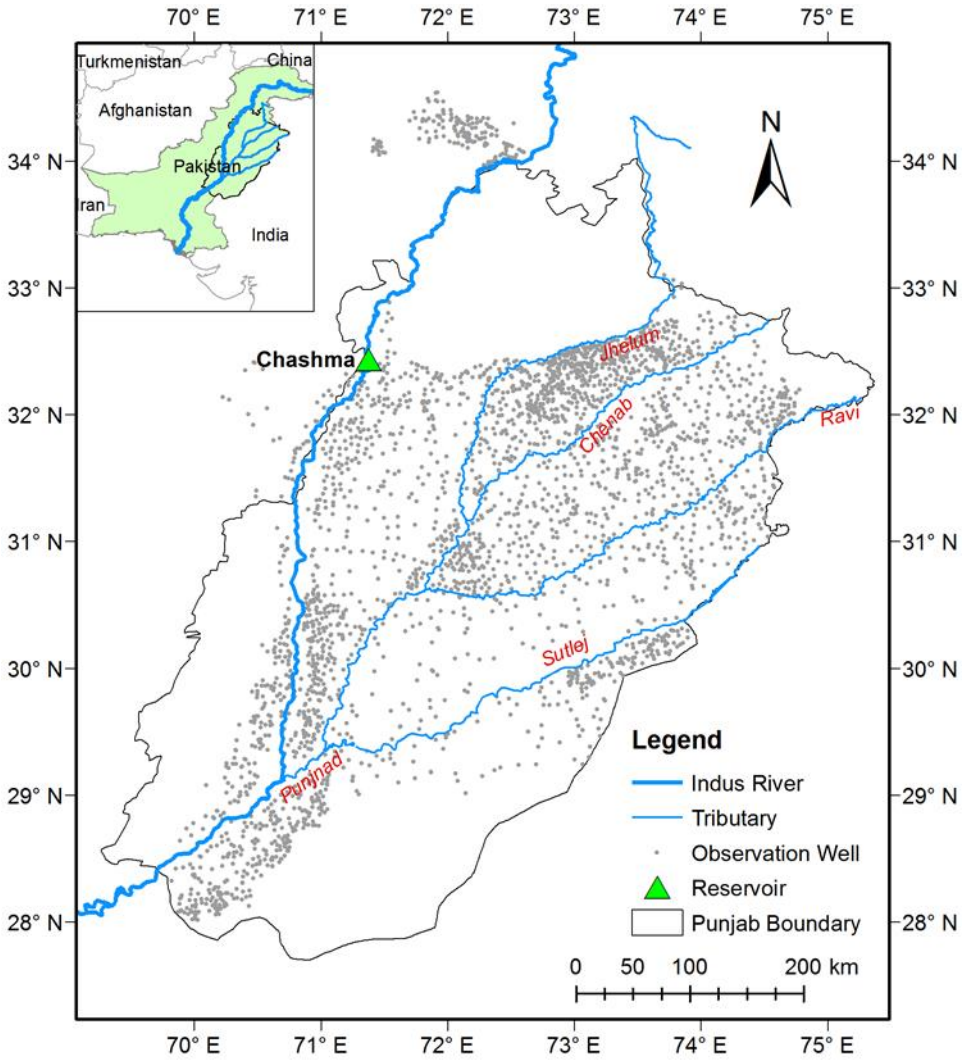

FIGURE 4.1: INDUS RIVER AND ITS TRIBUTARIES, OBSERVATION WELLS AND RESERVOIR IN PUNJAB, PAKISTAN.

As the major agricultural producer in the country, the Punjab provides 76% wheat, 83% gram, and 65% sugarcane of total national production during 2013-2014 (PDS, 2015). Irrigation becomes a prerequisite to support the intensive agriculture in this arid or semi-arid region and a consistent increase in both surface water and groundwater use has been modeled and reported (Wada et al., 2014). At the early stage, canal irrigation was introduced and became the predominant water supply, which relied on a vast surface network of canals spreading water from the Indus and its tributaries over large tracts of land. The water table has raised due to the relative plenty of precipitation and surface water irrigation and highly seepage soil (Siddiqi and Wescoat, 2013; Mekonnen et al., 2016). However, with the increase of water stress caused by rapid growth of population and instability of surface water resources, groundwater pumping started in the 1960s. Afterwards, the installations of private tube wells increased rapidly from 2,700 in 1960 to over 600,000 in 2001. Groundwater abstractions have increased from 10 billion m^3 in 1965 to 68 billion m^3 in 2002; and over 80 percent of groundwater is exploited through private tube wells (Bhutta and Alam, 2005). Groundwater is used on approximately 69% of irrigated areas, either alone or in conjunctive use with canal water (PDS, 2015). The continuous over-draft and unregulated pumping have been resulting in the observed groundwater depletion (Mekonnen et al., 2016).

4.2.2 Precipitation

In this study, precipitation data were obtained from the precipitation reconstruction over land (PREC/L) and the meteorological forcing for land surface models (LSMs) in the Global Land Data Assimilation System (GLDAS-1). Both PREC/L and forcing in GLDAS-1 contain monthly gridded precipitation data with a spatial resolution of 1 degree. The PREC/L dataset was generated by interpolating observations from more than 17,000 stations in the Global Historical Climatology

Network (GHCN) version 2 dataset and the Climate Anomaly Monitoring System (CAMS) dataset (Chen et al., 2002). The forcing dataset was derived by combining reanalysis data and observations (Sheffield et al., 2006). The spatial averages of monthly precipitation within the study area were computed for each dataset during1980-2016. Precipitation data from GLDAS-1 during 1995-1997 were removed due to the high uncertainty in the forcing dataset (Rui, 2015).

4.2.3 Potential evapotranspiration

A fully physical-based form of potential evapotranspiration was recommended to obtain the more reliable estimations (Donohue et al., 2010; McVicar et al., 2012). In this study, the FAO (Food and Agricultural Organization) Penman-Monteith equation for a clipped grass-surface without water stress (Allen et al., 1994, Ekström et al., 2007) was used to estimate E_p based on two meteorological data sets. The one data set was obtained from GLDAS-1 with spatial resolution of 1 degree during 1980-2016. The other is the Climatic Research Unit (CRU) dataset with spatial resolution of 0.5 degree from 1980 to 2014 (Harris et al., 2014). The CRU also provided the monthly E_p products across the world. The average monthly E_p over the study area was computed.

4.2.4 Terrestrial water storage change

The GRACE data are categorized into three levels. The raw data, collected from satellites, are calibrated, time-tagged, and labeled as Level-1 data. The Level-2 monthly gravity field data, based on the identical GRACE Level-1 data, were obtained from three data centers: Jet Propulsion Laboratory (JPL), Center for Space Research (CSR), and GeoForschungsZentrum Potsdam (GFZ). The Level-3 mass anomalies datasets are associated with the most up-to-date Level-2 gravity field estimates from JPL, CSR, and GFZ (i.e., RL05). The Level-3 gridded TWS anomalies provided by GRACE TELLUS (Landerer and Swenson, 2012) are used in this study. Monthly TWS changes

were estimated by the time derivative of the scaled TWS anomalies given the backward differentiation approximation (Long et al., 2014b). The scaled TWS anomalies were computed using the scaling factor provided by GRACE TELLUS. The measurement error and leakage error for the scaled TWS anomalies in Punjab were computed using the pseudo-code and gridded error data provided by GRACE TELLUS. The TWS anomalies for some months in 2002, 2003 and 2011-2015 were missing.

4.2.5 Evaporation and soil moisture storage change

Evapotranspiration and soil moisture storage (SMS) were obtained from the outputs of three LSMs in GLDAS-1 including Mosaic (Koster and Suarez, 1994; 1996), Noah (Ek et al., 2003), and Variable Infiltration Capacity (VIC) (Liang et al., 1994). Outputs of LSMs include monthly evapotranspiration and soil moisture data since 1979 at the spatial resolution of 1 degree. Evapotranspiration including soil evapotranspiration and transpiration was estimated from the energy budget in LSMs (Bonan, 1996). The soil depth of LSMs varies from 190 cm to 350 cm. The monthly SMS for each grid cell was computed by aggregating SMS of all the soil layers. Correspondingly, monthly SMS changes were computed as the difference of SMS in two consecutive months. The spatial averages of monthly evapotranspiration and SMS change were computed from 1980 to 2015. The annual evapotranspiration (E) and changes in SMS (ΔSMS) were computed by aggregating the monthly values. Owing to the high uncertainty in the forcing data of LSMs (Rui, 2015), data from 1995 to 1997 were removed from the analysis in this paper.

4.2.6 Observed groundwater level

The groundwater level observations during 1980-2012 were obtained from 2,377 wells (Figure 1) provided by the Salinity Control and Reclamation Projects Monitoring Organization

division of Water and Power Development Authority. The groundwater level observations were used to validate the Budyko-based estimation of ΔGWS. The groundwater level data in 1980-1983, 2005, and 2008 is only available for 20% of wells; therefore, groundwater level data during these years were removed in the analysis. The annual changes in groundwater level (Δh) were computed as the difference of observed heads in two consecutive years. The ground-based ΔGWS was estimated as the product of specific yield (S_y) and Δh. The values of S_y in Punjab range from 0.01 to 0.4 and most of the values fell between 0.07 and 0.25 (Greenman et al., 1967). In this study, the average S_y value of 0.14 is used to compute the ground-based ΔGWS.

4.3 Methodology

4.3.1 Annual total water storage change by Budyko model

4.3.1.1 Annual total water storage change by Budyko model

Several Budyko equations with a single parameter have been developed in the literature for long-term water balance (e.g., Fu, 1981; Yang et al., 2008). Recently, Wang and Tang (2014) developed a one-parameter Budyko equation based on the generalized proportionality relationship from the Soil Conservation Service (SCS) curve number method:

$$\frac{\bar{E}}{\bar{P}} = \frac{1+\frac{\overline{E_p}}{\bar{P}} - \sqrt{\left(1+\frac{\overline{E_p}}{\bar{P}}\right)^2 - 4\varepsilon(2-\varepsilon)\frac{\overline{E_p}}{\bar{P}}}}{2\varepsilon(2-\varepsilon)} \tag{4.1}$$

where $\bar{E}$, $\overline{E_p}$, and $\bar{P}$ are mean annual evapotranspiration, potential evapotranspiration, and precipitation, respectively; ε is a parameter defined as the ratio between mean annual initial evapotranspiration and total evapotranspiration. The initial evapotranspiration is defined as the portion of evapotranspiration which does not compete with runoff. Equation (4.1) approaches to its upper limit for $\varepsilon = 1$ and lower limit for $\varepsilon = 0$.

In Punjab, the groundwater storage change for irrigation substantially alters the annual terrestrial water storage change, and further affects the available water for annual water balance. To incorporate the considerably annual total water storage change, equation (4.1) is extended to the annual scale following the method proposed by Chen et al. (2013):

$$\frac{E}{P_{eff}} = \frac{1+\left(\frac{Ep}{P_{eff}}-\emptyset\right)-\sqrt{\left(1+\frac{Ep}{P_{eff}}-\emptyset\right)^2-4\varepsilon(2-\varepsilon)\left(\frac{Ep}{P_{eff}}-\emptyset\right)}}{2\varepsilon(2-\varepsilon)} \quad (4.2)$$

where ϕ is the lower bound for annual aridity index; ε has the same definition as in Equation (4.1); E and E_p are annual evapotranspiration, and potential evapotranspiration, respectively; P_{eff} is effective precipitation which is the difference of P and ΔTWS; and E/P_{eff} and E_p/P_{eff} are annual evapotranspiration ratio and aridity index, respectively. It has been noted that the equation (4.2) is only applicable for the steady-state water balance (e.g., natural and closed watershed at long-term scale) when the E was unknown. In another words, if E was given equation (4.2) can be applicable for the unsteady-state water balance (e.g., the administrative unit and watersheds with considerable inter-basin water transfer). In this study, E was provided by the energy balance from LSMs, thus, the equation (4.2) is applicable to Punjab.

4.3.1.2 Parameter estimation

The P_{eff} during high data quality period (2004-2010) were computed by the difference of P and the GRACE-derived ΔTWS; E/P_{eff} and E_p/P_{eff} during the same period were calculated. The two parameters (ε and ϕ) in equation (2) were estimated by minimizing the root-mean-square error (*RMSE*) between Budyko modeled and GRACE-derived ΔTWS. In order to evaluate the propagation of uncertainties in the inputs into the estimated parameters, different data sources for P, E_p, E and GRACE-derived ΔTWS were used. Combining P from 2 data sources, E_p from 2 data

sources, E from 3 LSMs, ΔTWS from 3 GRACE data centers, total 36 (i.e., 2 P × 2 E_p × 3 E × 3 ΔTWS) parameter-sets were estimated.

4.3.1.3 Reconstructed annual terrestrial water storage change

Based on equation (2), P_{eff} during 1980-2015 can be computed given estimated ε and ϕ and the available data of E, and E_p; then, ΔTWS were calculated by the difference of P_{eff} and P (i.e., P-P_{eff}). Corresponding to the estimated parameter-sets, 36 time-series of ΔTWS were reconstructed. The performance of each model estimation was evaluated by *RMSE* (equation 4.3) and the correlation coefficient (r) (equation 4.4) with respect to the corresponding GRACE-derived ΔTWS:

$$RMSE = \sqrt{\frac{\sum(M_i - O_i)^2}{N}} \tag{4.3}$$

$$r = \frac{\sum(O_i - \bar{O})(M_i - \bar{M})}{\sqrt{\sum(O_i - \bar{O})^2}\sqrt{\sum(M_i - \bar{M})^2}} \tag{4.4}$$

where N is the total number of years; $\bar{M}$ is the mean value of Budyko-modeled ΔTWS during 2004-2010 by equation (4.2); $\bar{O}$ is the mean value of GRACE-derived ΔTWS; and M_i and O_i are the modeled and observed values in the ith year, respectively. *RMSE* represents the error of Budyko-modeled ΔTWS due to the uncertainty of data sources. The value of r is a measure of the linear correlation between observed and modeled values, ranging from -1 to 1. A larger value of r suggests better performance on capturing the inter-annual variability of GRACE-derived ΔTWS (Zhang et al., 2014).

4.3.2 Reconstructed annual groundwater storage change and groundwater depletion

The ΔGWS can be derived by subtracting the annual ice and snow change, surface water storage change, soil moisture storage change from terrestrial water storage change. It is seen that

considering the surface water storage change for the regions with considerable dams and inter-region water transfer may reduce the uncertainties in the derived Δ*GWS*. The annual ice and snow change is negligible since Punjab is an alluvial plain, and the annual surface water storage change is relatively small (MoWP, 2012). Therefore, the long-term Δ*GWS* for Punjab was derived by only subtracting Δ*SMS* from the Budyko-modeled Δ*TWS*. The pair of Δ*SMS* and *E* used for modeling Δ*TWS* is from the same LSM. To minimize the impacts of return flow and recharge on the evaluation of Δ*GWS*, the annual values were computed based on water year, i.e., from October to September. Additionally, the irrigation demand in Punjab in October is minimum (Biemans et al., 2015). It can partially minimize the uncertainties in Δ*SMS* from LSMs where the irrigation is not considered (Feng et al., 2013). Based on 18 (i.e., 1 *P* from GLDAS-1× 2 E_p × 3 *E* × 3 Δ*TWS*) time series of Budyko-modeled Δ*TWS*, total 18 historical time series of Δ*GWS* were derived. The Budyko-derived Δ*GWS* were validated by comparing with the ground-based Δ*GWS* during 1985-1994. The performance was quantified by *RMSE* and *r*. In order to evaluate the historical groundwater depletion in Punjab, 18 time series of cumulative Δ*GWS* were computed during 1980-2015. Negative values of the cumulative Δ*GWS* suggest the depletion of groundwater. The slope of the trend line of the cumulative Δ*GWS* time series can be used to quantify the groundwater depletion rate. The average and standard deviation of the depletion rates of 18 time series were calculated.

4.4 Results

4.4.1 Annual terrestrial water storage change by Budyko model

4.4.1.1 Long-term time series of input data and their uncertainties

Multiple data sources for P, E_p, E, ΔTWS, and ΔSMS were used in this study. Figure 4.2a-e shows the comparison of each variable from different data sources and Figure 4.2f shows the uncertainties in ground-based ΔGWS caused by the uncertainties in S_y. As shown in Figure 4.2a, the difference of P between PREC/L and GLDAS-1 is substantial after 1999 (i.e., 15.6 cm/year). As shown in Figure 4.2b, the values of E_p based on meteorological data in GLDAS-1 are globally larger than the CRU estimations. The mean annual E_p is 154.2 cm/year for CRU dataset and 172.1 cm/year for GLDAS-1. The reported mean annual reference evapotranspiration estimated by Penman-Monteith equation in this region is around 165.0 cm/year during 1962-1991 (Ullah et al., 2001). The inter-annual variabilities of E from LSMs have the consistently decreasing trends during 1980-2015 (Figure 4.2c). The slope of the linear trend is -0.3 cm/year for Noah, -0.6 cm/year for VIC, and -0.4 cm/year for both Mosaic and the ensemble mean. The discrepancies of annual values exist individually, especially after 2010 and the standard deviation of E among LSMs is ±1.0 cm/year. The differences of simulated E among LSMs are mainly attributed to the discrepancy of model structure and parameterization (Chen et al., 1996). The fluctuations of ΔTWS from three GRACE centers (CSR, GFZ, and JPL) are comparable generally, but the amplitudes in the years of 2003, and 2011-2015 with missing data do not match very well among the three sources (Figure 4.2d). The variability among them is ±2.0 cm/year. The GRACE-derived TWS anomalies in Punjab have a leakage error of 5.7 cm and a measurement error of 1.2 cm. As shown in Figure 4.2e, the values of ΔSMS from LSMs compare favorably and the uncertainty is

±0.9 cm. The long-term cumulative sum of Δ*SMS* during 1980-2015 is relatively small (i.e., -0.8±1.0 cm), suggesting no trend in soil moisture storage as reported in northwestern India (Rodell et al., 2009).

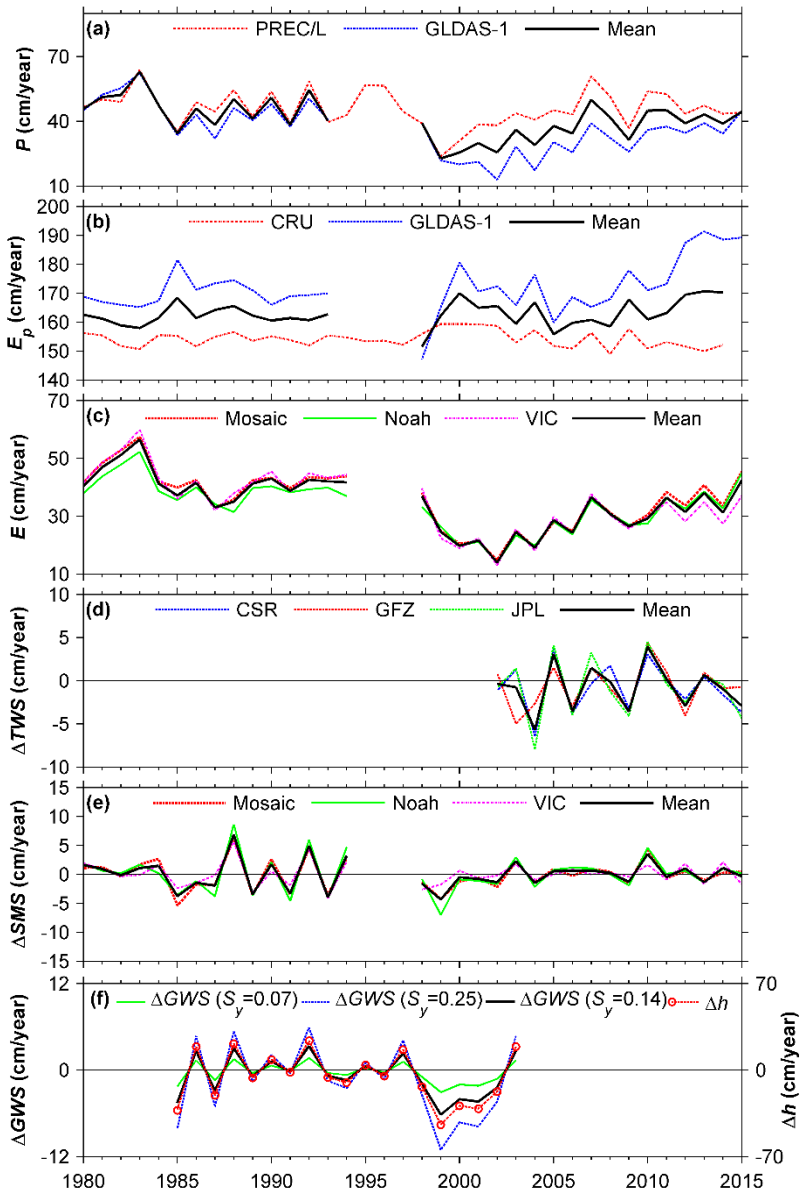

FIGURE 4.2: TIME SERIES OF ANNUAL VALUES DURING 1980-2015 FOR: (A) PRECIPITATION FROM PREC/L AND GLDAS-1; (B) POTENTIAL EVAPORATION FROM CRU AND GLDAS-1; (C) EVAPORATION FROM LSMS; (D) GRACE-DERIVED TERRESTRIAL WATER STORAGE CHANGE; (E)

SOIL MOISTURE STORAGE CHANGE FROM LSMS; AND (F) OBSERVED GROUNDWATER LEVEL CHANGE AND ESTIMATED GROUNDWATER STORAGE CHANGE USING THE SMALL SPECIFIC YIELD (S_Y) VALUE OF 0.07, LARGE S_Y OF 0.25, AND AVERAGE S_Y OF 0.14 IN PUNJAB, PAKISTAN.

The absolute values of ΔSMS are much larger than zero in most years before 1995, and the maximum value is 8.6 cm/year in 1988 from Noah. It is seen that the amplitudes of ΔSMS during 1988-1994 are much larger than other periods, and trend of ΔSMS during 1999-2002 is inconsistent with the P: the P declines but the ΔSMS increases. Figure 4.2f shows the ground-based ΔGWS computed using the small, large, and average values of S_y from 1985 to 2003. The considerable discrepancies exist among ΔGWS based on different S_y. The cumulative sum of ground-based ΔGWS by $S_y = 0.14$ is -15.0 cm during 1985-2003.

4.4.1.2 Estimated model parameters

The estimated values of ε and ϕ by 36 combinations of input data sources were summarized in Table 4.1. The estimated parameters range from 0.01 to 0.53 for ε and 0 to 1.56 for ϕ. The variations of the 36 estimated parameter sets are ±0.24 for ε and ±0.77 for ϕ. The large variability of ε is associated with P from GLDAS-1, while the large variability of ϕ is associated with P from PREC/L (Table 4.1). Figure 4.3a shows the annual evapotranspiration ratio versus annual aridity index during the high data quality period (2004-2010) and the corresponding 18 fitted Budyko curves based on P from PREC/L, E_p from CRU and GLDAS-1, E from 3 LSMs, and ΔTWS from 3 GRACE data sources. Figure 3b shows the other 18 fitted Budyko curves when P was from GLDAS-1. It is seen that climate aridity indices based on PREC/L are smaller than those based on GLDAS-1. ϕ represents a non-negative lower bound of annual aridity index for a given watershed and ε represents the controlling factors other than climate (e.g., vegetation and

storminess) on evapotranspiration (Donohue, et al., 2012; Trancoso et al., 2016). Budyko curves reach the lower bound when ε approaches to zero; and the upper bound is corresponding to ε=1 (Wang and Tang, 2014). Therefore, the variation of annual climate aridity indices cause the variability of estimated ϕ and the variation of annual evapotranspiration ratio leads to the variability of estimated ε.

TABLE 4.1: ESTIMATED PARAMETERS AND THE MODEL PERFORMANCE OF BUDYKO-MODELED ANNUAL TERRESTRIAL WATER STORAGE CHANGES DURING 2004-2010.

***P* Source**	***E_p* Source**	**LSMs *E***	**GRACE ΔTWS**	ε	ϕ	***RMSE* (cm)**	***r***
PREC/L	GLDAS-1	Mosaic	CSR	0.01	1.34	8.1	-0.63
PREC/L	GLDAS-1	Noah	CSR	0.01	1.41	8.3	0.77
PREC/L	GLDAS-1	VIC	CSR	0.01	1.31	9.3	-0.63
PREC/L	GLDAS-1	Mosaic	GFZ	0.01	1.35	7.3	0.11
PREC/L	GLDAS-1	Noah	GFZ	0.01	1.43	7.5	0.23
PREC/L	GLDAS-1	VIC	GFZ	0.01	1.32	8.4	-0.36
PREC/L	GLDAS-1	Mosaic	JPL	0.01	1.42	8.3	0.62
PREC/L	GLDAS-1	Noah	JPL	0.01	1.5	8.4	0.41
PREC/L	GLDAS-1	VIC	JPL	0.01	1.4	9.6	-0.34
PREC/L	CRU	Mosaic	CSR	0.01	1.41	8.0	-0.13
PREC/L	CRU	Noah	CSR	0.01	1.49	8.2	0.68
PREC/L	CRU	VIC	CSR	0.01	1.38	9.2	-0.24
PREC/L	CRU	Mosaic	GFZ	0.01	1.41	7.2	0.04
PREC/L	CRU	Noah	GFZ	0.01	1.49	7.3	0.62
PREC/L	CRU	VIC	GFZ	0.01	1.38	8.3	-0.10
PREC/L	CRU	Mosaic	JPL	0.01	1.47	8.3	-0.09
PREC/L	CRU	Noah	JPL	0.01	1.56	8.3	-0.12
PREC/L	CRU	VIC	JPL	0.01	1.46	9.5	-0.87
GLDAS-1	GLDAS-1	Mosaic	CSR	0.48	0	2.3	0.77
GLDAS-1	GLDAS-1	Noah	CSR	0.37	0	2.7	0.62
GLDAS-1	GLDAS-1	VIC	CSR	0.48	0	3.1	0.43
GLDAS-1	GLDAS-1	Mosaic	GFZ	0.52	0	1.2	0.89
GLDAS-1	GLDAS-1	Noah	GFZ	0.41	0	1.6	0.82
GLDAS-1	GLDAS-1	VIC	GFZ	0.53	0	2.1	0.61
GLDAS-1	GLDAS-1	Mosaic	JPL	0.51	0	2.9	0.84
GLDAS-1	GLDAS-1	Noah	JPL	0.4	0	2.9	0.71
GLDAS-1	GLDAS-1	VIC	JPL	0.52	0	3.9	0.42
GLDAS-1	CRU	Mosaic	CSR	0.48	0	2.3	0.76
GLDAS-1	CRU	Noah	CSR	0.37	0.02	2.7	0.62

GLDAS-1	CRU	VIC	CSR	0.48	0	3.1	0.42
GLDAS-1	CRU	Mosaic	GFZ	0.52	0	1.2	0.90
GLDAS-1	CRU	Noah	GFZ	0.4	0	1.6	0.82
GLDAS-1	CRU	VIC	GFZ	0.52	0	2.1	0.61
GLDAS-1	CRU	Mosaic	JPL	0.51	0	2.9	0.85
GLDAS-1	CRU	Noah	JPL	0.4	0	2.9	0.71
GLDAS-1	CRU	VIC	JPL	0.51	0	3.9	0.42

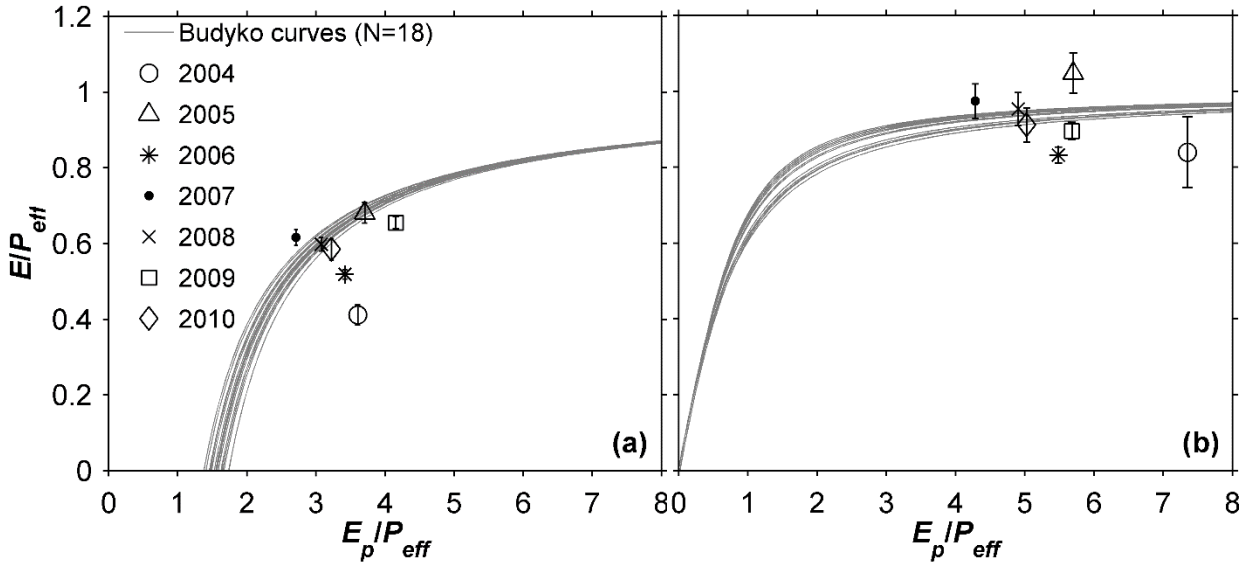

FIGURE 4.3: THE ANNUAL EVAPORATION RATIO VERSUS ANNUAL ARIDITY INDEX IN PUNJAB DURING 2004-2010 AND 18 FITTED BUDYKO CURVES BASED ON (A) PRECIPITATION FROM PREC/L AND (B) PRECIPITATION FROM GLDAS-1, AND POTENTIAL EVAPORATION FROM CRU AND GLDAS-1, EVAPORATION FROM 3 LSMS, TERRESTRIAL WATER STORAGE CHANGE FROM 3 GRACE DATA SOURCES.

4.4.1.3 Reconstructed annual total water storage change

Based on the estimated parameter sets, 36 time series of Δ*TWS* during 1980-2014 were reconstructed. The *RMSE* and *r* between Budyko-modeled and GRACE-derived Δ*TWS* vary from 1.2 cm to 9.6 cm and -0.87 to 0.90 (Table 4.1), respectively. The standard deviation of Budyko-modeled Δ*TWS* among 36 time series is ±11.3 cm/year. If the model performances and uncertainties were evaluated separately based on the individual precipitation source, all of the negative *r* are related to *P* from PREC/L, and the average *RMSE* and standard deviation of Budyk-

modeled Δ*TWS* for PREC/L (i.e., 8.3 cm for *RMSE* and 9.4 cm for standard deviation) are much larger than GLDAS-1 (i.e., 2.5 cm and 3.1 cm). Therefore, the following analysis is only focused on the results using *P* from GLDAS-1. Figure 4.4 shows the ensemble (i.e., 18) of Budyko-modeled Δ*TWS* based on *P* from GLDAS-1 and its ensemble mean during 1980-2015, and the ensemble mean of GRACE-derived Δ*TWS* from 2003 to 2015. The inter-annual variations in Budyko-modeled Δ*TWS* is in-phase during 2003-2010 but out-or-phase after 2010. *r* between the two ensemble means is 0.48 during 2003-2015 and 0.71 during the high data quality period (2004-2010). The absolute differences between Budyko-modeled and GRACE-derived Δ*TWS* have the minimum value of 0.7 cm in 2008 and the maximum value of 3.6 cm in 2006. In 5 out of 13 years, the Budyko-modeled Δ*TWS* underestimated the GRACE-derived Δ*TWS* (Figure 4.4).

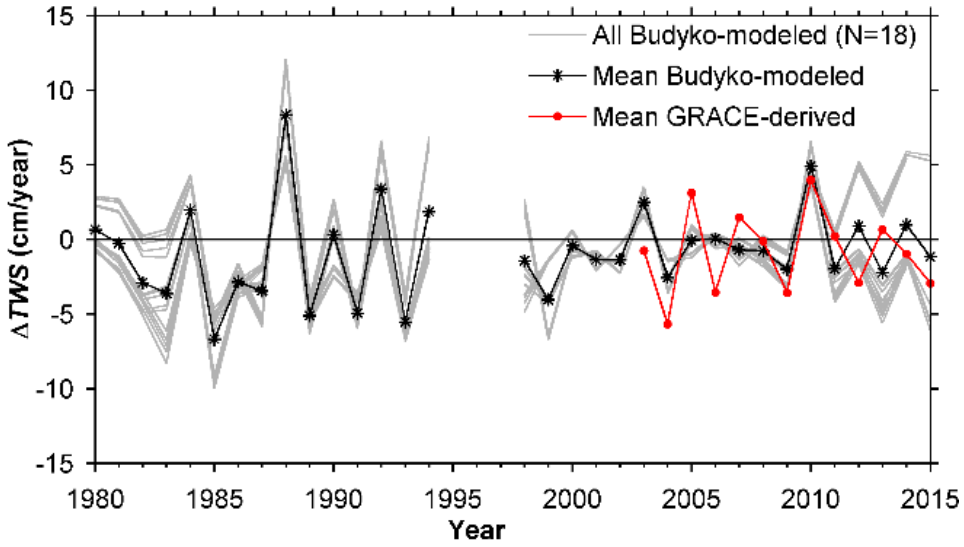

FIGURE 4.4: THE 18 TIME SERIES OF BUDYKO-MODELED TERRESTRIAL WATER STORAGE CHANGE (Δ*TWS*) FROM 1980 TO 2015 IN PUNJAB AND THE COMPARISON OF ENSEMBLE MEAN OF 18 BUDYKO-MODELED Δ*TWS* BASED ON PRECIPITATION FROM GLDAS-1, POTENTIAL EVAPORATION FROM CRU AND GLDAS-1, EVAPORATION FROM 3 LSMS, AND PARAMETERS ESTIMATED BY 3 GRACE DATA SOURCES WITH THE ENSEMBLE MEAN OF GRACE-DERIVED Δ*TWS*.

4.4.2 Reconstructed annual groundwater storage change

The Budyko-derived Δ*GWS* was computed by subtracting Δ*SMS* from the modeled Δ*TWS*. Considering the data availability and consistency, Figure 5 presents the ensemble (i.e., 18) of Budyko-derived Δ*GWS* and its ensemble mean, and the ground-based Δ*GWS* during 1985-1994. *RMSE* between them is 2.4 cm and *r* is 0.64 which indicates the strongly positive correlation exists. The absolute differences between the ensemble mean of Budyko-derived Δ*GWS* and ground-based Δ*GWS* range from 0.3 cm in 1988 and 4.6 cm in 1986. In 7 out of 10 years, the Budyko-derived Δ*GWS* were underestimated (Figure 4.5).

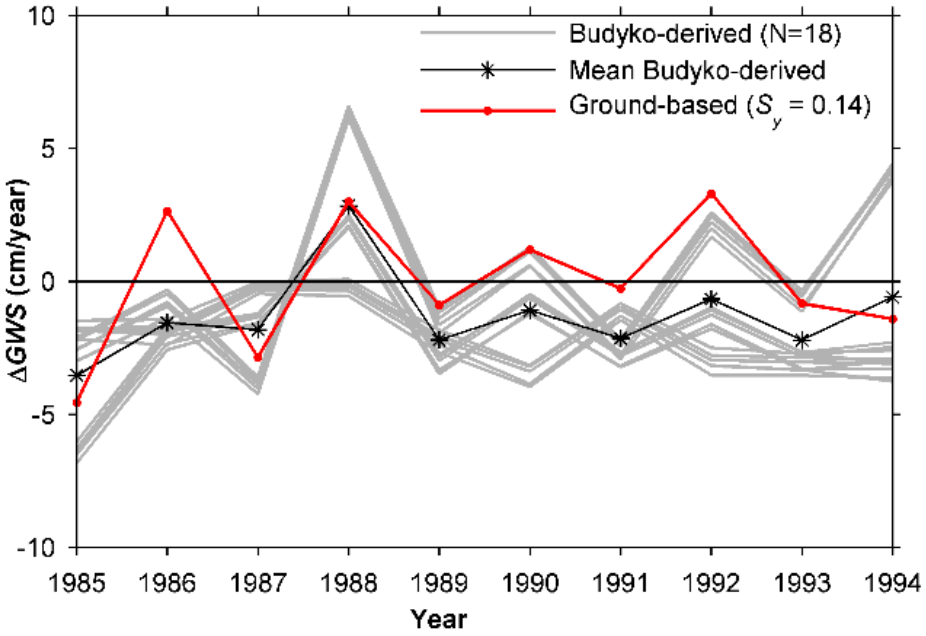

FIGURE 4.5: THE 18 TIME SERIES OF THE RECONSTRUCTED ANNUAL GROUNDWATER STORAGE CHANGE (Δ*GWS*) FROM 1985 TO 1994 AND THE ENSEMBLE MEAN, AND THE GROUND-BASED Δ*GWS*.

Based on reconstructed Δ*GWS*, we computed the cumulative sum of Δ*GWS* and evaluate the historical groundwater depletion in Punjab. As shown in Figure 4.6, the modeled cumulative sum of Δ*GWS* is -27.6 cm from 1980 to 2013 and the total number of tube wells approach to

1,012,541 in 2013. The modeled cumulative sum of Δ*GWS* during the entire study period (1980-2015) are -28.4±19.8 cm. The negative values of cumulative sum indicated the groundwater has been depleted in Punjab. The depletion rates are -0.7±0.6 cm/year during 1980-2015. The recent Budyko-derived depletion rates are -0.5±0.4 cm/year during 2000-2012, -0.6±0.2 cm/year during 2003-2010, and -0.8±0.2 cm/year during 2003-2007. On the contrary, the installed tube wells which are used to exploit groundwater in Punjab have a long-lasting increasing trend during 1980-2013 as the red dotted curve in Figure 4.6 shows.

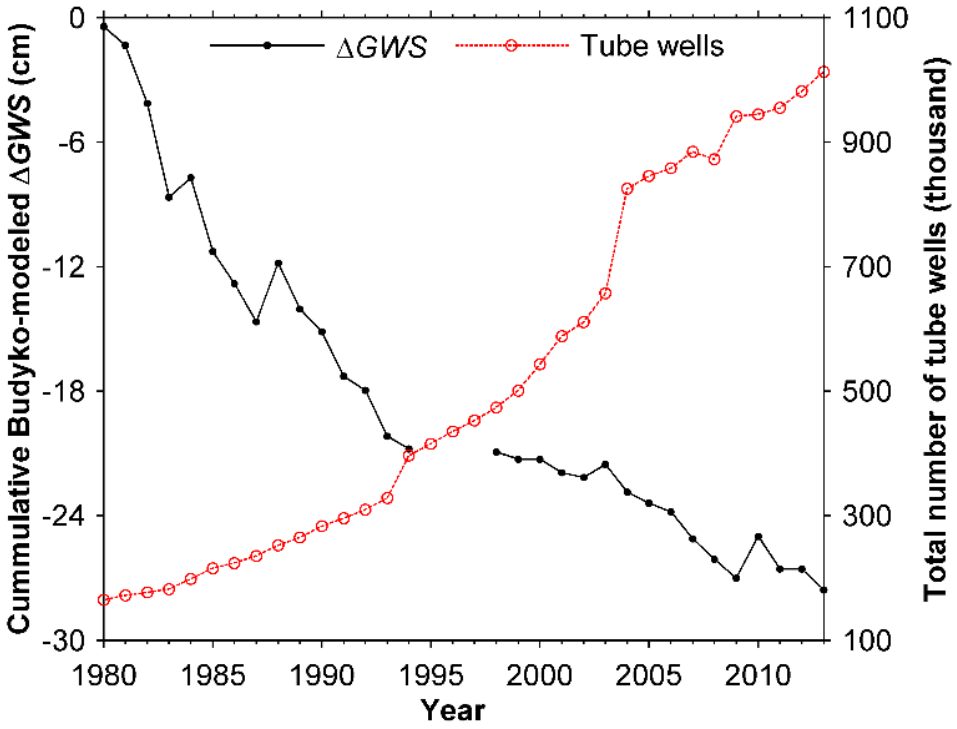

FIGURE 4.6: THE CUMULATIVE SUM OF THE RECONSTRUCTED ANNUAL GROUNDWATER STORAGE CHANGE AND THE TOTAL NUMBER OF TUBE WELLS DURING 1980-2013 IN PUNJAB, PAKISTAN (DATA SOURCE: PDS (1988; 1996; 2005; 2015)).

4.5 Discussion

4.5.1 Annual terrestrial water storage change by Budyko model

Although the Budyko-modeled Δ*TWS* favorably agree with the GRACE-derived one, the discrepancy of their annual-to-annual values exists as shown in Figure 4. The substantial discrepancies between GRACE-derived terrestrial water storage change and ground-based estimations were also reported in the High Plains Aquifer (Strassberg et al., 2009; Longuevergne et al., 2010) and Illinois (Yeh et al., 2006). These discrepancies may be attributed to the uncertainty in both Budyko-modeled (i.e., ±1.9 cm) and GRACE-derived Δ*TWS* (i.e., ±1.3 cm). The out-of-phase inter-annual variations between Budyko-modeled and GRACE-derived Δ*TWS* after 2010 potentially arises from the high uncertainties in GRACE-derived Δ*TWS* caused by missing data. The uncertainties in input variables as discussed in section 4.1.1 can be propagated into the Budyko-modeled Δ*TWS*. This propagation mainly causes the uncertainties in modeled Δ*TWS*. Taking the *P* as the representative example, the uncertainties in *P* before 1994 are much smaller than afterwards as shown in Figure 2a. Correspondingly, the standard deviation of 36 Budyko-modeled Δ*TWS* is ±8.6 cm/year during 1980-1994 and increases to 12.6 cm/year during 1998-2015. The uncertainty in *P* for a large-scale region is due to its high spatio-temporal heterogeneity (Daly et al., 1994; Herold et al., 2015). There are currently more than 20 precipitation products from different principal measurements or modeling sources such as CPC Unified (Climate Prediction Center Unified) (Xie et al., 2007; Chen et al., 2008), GPCP-1DD (Global Precipitation Climatology Project 1-Degree Daily Combination) (Huffman et al., 2001) and MSWEP(Multi-Source Weighted-Ensemble Precipitation) (Beck et al., 2017).

4.5.2 Reconstructed annual groundwater storage change and groundwater depletion

Compared with the performance of Budyko-modeled Δ*TWS* during the high data quality period, the *r* is smaller and the discrepancies is larger for Budyko-derived Δ*GWS*. The smaller *r* and larger discrepancies are potentially attributed to the uncertainty in ground-based Δ*GWS* (Sun et al., 2010) and Δ*SMS* from LSMs (Shamsudduha et al., 2012; Thomas et al., 2016). Strassberg et al. (2009) pointed out that the limited number of pumping tests might not represent the considerable spatial variability of S_y in such as large spatial region. As shown in Figure 2f, the substantial uncertainties exist among ground-based Δ*GWS* using different S_y. Due to lack of the irrigation in LSMs, there may be a high uncertainty in Δ*SMS* for irrigation region (Feng et al., 2013). This relatively high values of Δ*SMS* during 1985-1994 (Figure 2e) potentially caused the consistent underestimation of Δ*GWS* (Figure 5).

Based on the cumulative sum of the reconstructed Δ*GWS*, we comprehensively evaluate the groundwater depletion in Punjab by comparing the results in this study with the ground-based measurements and the previous findings. The slopes of the trend lines of both modeled and ground-based cumulative Δ*GWS* during 1985-2003 are -0.6 cm/year. The recent Budyko-derived changes in annual groundwater storage (i.e., -0.5±0.4 cm/year during 2000-2012, -0.6±0.2 cm/year during 2003-2010, and -0.8±0.2 cm/year during 2003-2007) are also close to the reported groundwater depletion in Punjab (-1.0 ± 0.4 cm/year during 2000-2012) (MacDonald et al., 2016), the Upper Indus Plain (-0.4 cm/year during 2003-2010) (Iqbal et al., 2016), and the adjacent Bengal Basin (-1.1±0.2 cm/year during 2003-2007) (Shamsudduha et al., 2012). The estimated depletion rates in Punjab are smaller than the finding in India such as -4.0±1.0 cm/year over the Indian States of Rajasthan, Punjab and Haryana (Rodell et al., 2009) and -2.0±0.3 cm/year across a 2,700,000

km^2 region centered on New Delhi (Tiwari et al., 2009). The ratio of area equipped with groundwater pumping for irrigation to total irrigation area in India is about 2 times larger than that in Punjab and Bengal basin (Siebert et al., 2010). As shown in Figure 6, the groundwater depletion has strongly negative correlation (r = -0.87) with the number of tube wells in Punjab.

4.6 Conclusion

In order to practically and hydrologically reconstruct the terrestrial water storage change and groundwater storage change, this study developed a two-parameter annual Budyko model. As a case study, the developed model integrated with the GRACE data was applied to the Punjab in Pakistan. The historical ΔTWS and ΔGWS during 1980-2015 were reconstructed using multiple input data sources. The model parameters were estimated by minimizing root-mean-square error of Budyko-modeled and GRACE-derived ΔTWS during the high data quality period (2004-2010). An ensemble (i.e., 36) of model parameter sets were estimated based on the combinations of input data sets (i.e., 2 precipitation sources × 2 E_p sources × 3 GRACE-derived ΔTWS × E from 3 land surface models). Due to the high uncertainty caused by P from PREC/L, 18 model parameter sets using P from GLDAS-1 were used to reconstruct the ΔTWS, from which ΔGWS were reconstructed by subtracting ΔSMS.

The modeled ΔTWS agree favorably with the GRACE-derived values (i.e., r = 0.71) during 2004-2010, and the modeled ΔGWS was validated (i.e., r = 0.64) by the ground-based observations during 1985-1994. However, the discrepancies of their annual-to-annual values exist. The differences of ΔTWS potentially arise from the uncertainties in both Budyko-modeled and GRACE-derived ΔTWS. The differences of ΔGWS mainly caused by the uncertainties in ground-based ΔGWS and ΔSMS from LSMs. The negative values (i.e., -28.4±19.8 cm) of the cumulative

sum of the reconstructed ΔGWS indicated the groundwater has been depleted in Punjab. The depletion rates are -0.7±0.6 cm/year during 1980-2015. The groundwater depletion has strongly negative correlation with the total number of tube wells in Punjab with a correlation coefficient of -0.87. The integration of the developed Budyko equation with the GRACE data provides a useful tool for the evaluation of the long-term groundwater depletion in the large-scale irrigation regions.

CHAPTER 5: EFFECT OF HERBICIDES ON EVAPOTRANSPIRATION IN RIPARIAN WILLOW MARSHES

5.1 Introduction

Evapotranspiration (*ET*), the second largest magnitude of global water balance after precipitation, highly affects water yields (i.e., runoff and percolation). Physically, *ET* is the transition of water from the liquid phase to the vapor phase (Brutsaert, 2005). Vegetation as an important water transition media, largely determines the magnitude of *ET* (Bosch and Hewlett, 1982); and the effect of vegetation change on *ET* has been evaluated in many studies (e.g., Zhang et al., 2001; Donohue et al., 2007). Vegetation management (e.g., herbicides) has been implemented to increase water yields for vegetated area (Brown et al., 2005; Li et al., 2017).

The Penman-Monteith (PM) equation has been widely used to estimate daily actual *ET* from both unstressed and stressed canopies. It originated from Penman (1948) equation and was substantially modified by Monteith (1965). Penman equation was developed for estimating evaporation from open water, combining energy balance equation with the aerodynamic equation for vapor transfer (Han et al., 2012). Monteith (1965) incorporated a canopy resistance term to describe the effect of vegetation on evapotranspiration. The accuracy of PM equation for estimating actual *ET* has been reported (Cleugh et al., 2007; Mu et al., 2007; Leuning et al., 2008). The key for accurate estimation of *ET* depends on the surface resistance, especially for forest surfaces (Beven, 1979; Choudhury, 1997; Zhang et al., 2016). For well-watered surfaces, the actual *ET* is equal to potential evaporation denoted as E_p (Brutsaert and Parlange, 1998).

Annual *ET* at the catchment scale has been found to be dominantly dependent on annual precipitation (*P*) and atmospheric water demand (Schreiber, 1904; Ol'dekop, 1911). Atmospheric

water demand can be computed by potential evaporation or energy supply represented by water equivalent of net radiation (R_n) for a moist surface (Budyko, 1958; Choudhury, 1999). Budyko (1958) proposed a deterministic relationship to model annual *ET* as the geometric mean of empirical equations by Schreiber (1904) and Ol'dekop (1911). Pike (1964) had also proposed a similar function by replacing the air temperature in Turc (1954) equation with E_p based on open water evaporation by Penman equation. Although functional forms were different, the estimated annual *ET* by Budyko and Tuck-Pike equations did not differ greatly (Dooge, 1992; Choudhury, 1999). Single parameter Budyko equations have also been proposed or derived to incorporate the impact of non-climatic controlling factors on evapotranspiration (Fu, 1981; Choudhury, 1999; Zhang et al., 2004; Yang et al., 2008). Recently, Wang and Tang (2014) derived a one-parameter Budyko equation by applying the proportionality relationship, generalized from Soil Conservation Services (SCS) curve number method (SCS 1972), to the partitioning of mean annual precipitation. These annual *ET* models with a parameter provide practical tools to evaluate the long-term impact of landscape change (e.g., afforestation and vegetation treatment) on annual evapotranspiration.

Riparian herbaceous marshes are critical ecosystems with many important ecohydrological functions including floral and faunal biodiversity, carbon storage, surface water storage, groundwater recharge, and flood mitigation (Ross et al., 2006; Ahn et al., 2007; Budny and Benscoter, 2016). The headwater region of the Upper St. Johns River (USJR) in east-central Florida contains 1200 km^2 of herbaceous mashes, shrub swamps, and forested wetlands. Due to shortened hydro-periods, reduced fire frequency, and other changes in disturbance (e.g., burning, mowing, and water level fluctuation) over the past 40 years (Quintana-Ascencio et al., 2013), woody shrubs, primarily Carolina willow (*Salix caroliniana Michx.*), have invaded into areas that

were historically herbaceous marshes (Hall 1987; Ponzio et al., 2006). The expansion of willow increased the potential for less water yield by increasing evapotranspiration (*ET*) rate and reducing runoff and percolation (Hibbert, 1967; Li et al., 2017). The *ET* rate for herbaceous marshes during the growing season ranges from 3 mm day^{-1} to 4.2 mm day^{-1} (Mao et al., 2002; Siedlecki et al., 2016). The reported willow *ET* rate during the growing season is 6.71±4.83 mm day^{-1} based on measurements of eddy covariance, lysimeter, and sap-flow (Hall et al., 1998; Schaeffer et al., 2000; Pauliukonis and Schneider, 2001; Nagler et al., 2005; Guidi et al., 2008). To address the ecological and hydrological consequences of willow expansion, vegetation management, such as herbicide, can be potentially applied to the USJR marshes (Likens et al., 1970).

The objectives of this study were to 1) evaluate the impact of willow (Carolina willow, *Salix caroliniana Michx.*) removal on *ET* after a two-year field experiment in which herbicides were applied in two USJR marshes; 2) quantify the relationship between annual water yield and leaf area index of willow; and 3) develop a single-parameter annual *ET* model for quantifying the long-term response of *ET* to willow management. The daily *ET* estimations were computed by PM equation, and the seasonality of *ET* was analyzed based on monthly *ET* aggregated from daily values. A one-parameter Budyko equation was developed to model annual *ET* and water yield as a function of willow fractional coverage.

5.2 Field experiment and data collection

5.2.1 Field experiment

We used a randomized complete block design (Clewer and Scarisbrick, 2001), with each block including three plots (Figure 1). The plot size was 150 m by 150 m, and there was a 50 m buffer between adjacent plots. The experiments were conducted at two sites, i.e., Moccasin Island

(MI) and Sweetwater Canal (SWC) in the USJR marshes (Figure 2a). Each site included two blocks. Totally, there were four blocks and twelve plots in this study.

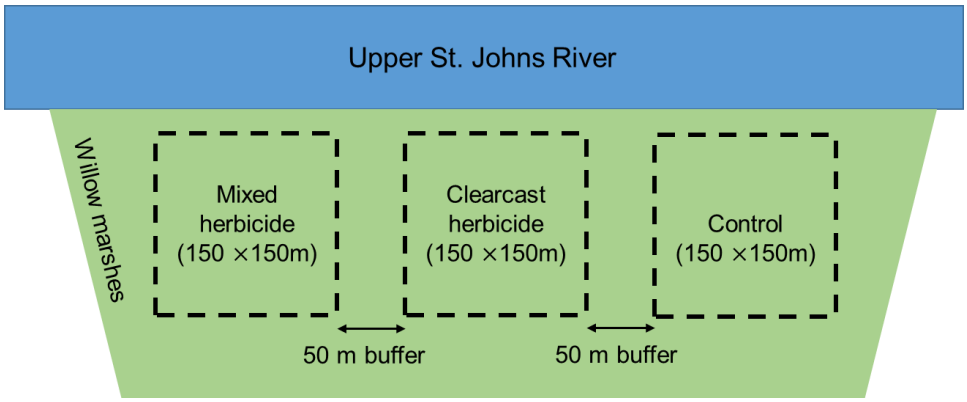

FIGURE 5.1: THE SCHEMATIC DIAGRAM OF A DESIGNED EXPERIMENT BLOCK CONSISTING OF THREE PLOTS.

Two of the three plots in each block were aerially sprayed with herbicides and the remaining untreated plot was taken as the control (Figure 1). The control plots included North C, South B, East A, and West B (Table 1). The first round was in August 2014, and the second round was in July 2015. Clearcast herbicide was applied to North B, South C, East C, and West C for both rounds of the treatment. For the plots of North A, South A, East B, and West A, Aquasweep herbicide was applied at the fist treatment, and Ecomazapyr herbicide was applied at the second treatment due to the limited effectiveness of Aquasweep.

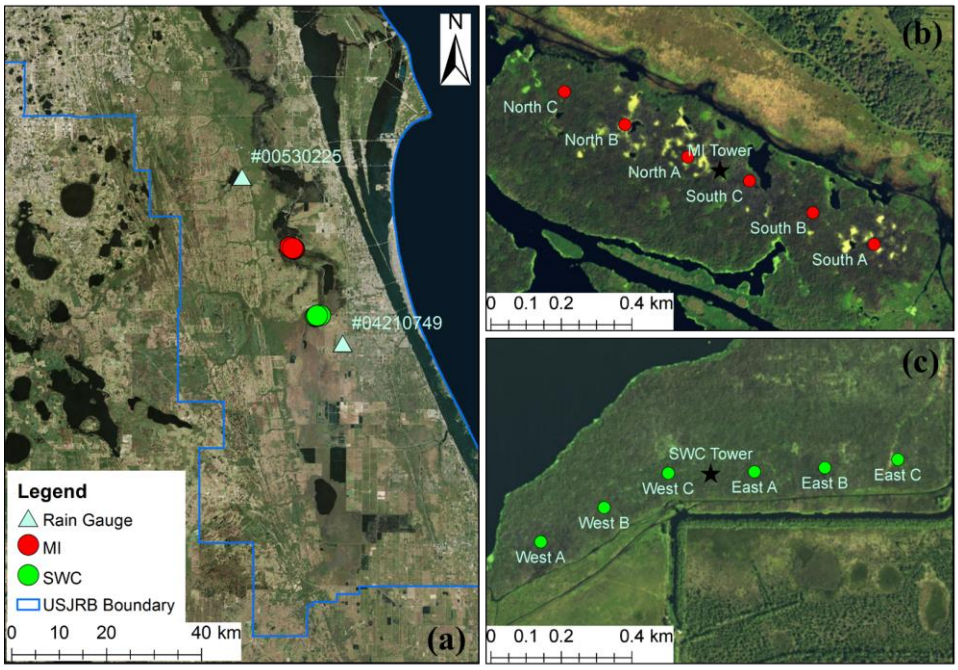

FIGURE 5.2: (A) THE LOCATIONS FOR MOCCASIN ISLAND (MI) AND SWEETWATER CANAL (SWC) EXPERIMENTAL SITES IN THE UPPER ST. JOHNS RIVER BASIN (USJRB); (B) THE CENTROIDS OF THREE PLOTS (A, B, AND C) IN MI NORTH AND MI SOUTH BLOCKS AND WEATHER TOWER (BLACK STAR); AND (C) THE CENTROIDS OF THE PLOTS IN SWC EAST AND SWC WEST BLOCKS AND WEATHER TOWER.

TABLE 5.1: THE DATES AND HERBICIDES SPRAYED FOR TREATED PLOTS.

Plot	First Treatment		Second Treatment	
	Date	Herbicide	Date	Herbicide
North A, South A, East B, West A	8/21/2014	Aquasweep	7/15/2016	Ecomazapyr
North B, South C, East C, West C	8/21/2014	Clearcast	7/15/2016 or 7/21/2016	Clearcast

5.2.2 Data collection

Field measurements were initiated in May, 2014 and ended in September, 2016. We installed twelve weather stations at a height of about 2 m, located at the center of each plot. Two weather towers were installed at a height of about 7 m, above tree canopy, and were located at the

middle of the blocks in each site (Figure 2b and Figure 2c). Air temperature, solar radiation, relative humidity, and wind speed with a 30-minute interval were recorded during 7/1/2014-8/31/2016 at each weather station and weather tower (Table 2). Missing data for these meteorological variables due to sensor failure were less than 5% of the entire period. We used interpolation to fill the data gap. Daily values of mean air temperature, maximum and minimum temperature, solar radiation, wind speed, and relative humidity were computed from the 30-minute records. The land surface elevation, latitude, and height of each weather station and weather tower were measured during the installation of sensors (Table 3). We measured the heights of willow stands in September 2014 and the willow fractional coverage during the early growing season in the April of 2015 and 2016.

TABLE 5.2: THE MEASURED VARIABLES AT THE WEATHER STATIONS AND TOWERS WITH SENSORS OR BY FIELD WORK.

Variable	Description	Measurement Period
T	Air temperature	7/1/2014-8/31/2016
R_h	Relative humidity	7/1/2014-8/31/2016
R_s	Solar radiation	7/1/2014-8/31/2016
U	Wind speed	7/1/2014-8/31/2016
z_{mi}	Height of weather/tower station	5/2014
Z_i	Land surface elevation of weather/tower station	5/2014
φ_i	Latitude of weather/tower station	5/2014
h_c	Height of willow stands	9/2014
C_w	Willow fractional coverage	4/2015 and 4/2016

TABLE 5.3: THE LAND SURFACE ELEVATION (Z_I), LATITUDE (Φ_I), AND HEIGHT (Z_{MI}) FOR WEATHER STATIONS AND TOWERS, AND THE CALIBRATED EXTINCTION COEFFICIENT (K) FOR EACH PLOT. THE FOUR CONTROL PLOTS ARE HIGHLIGHTED IN BOLD.

Site	Z_i (m)	φ_i (°N)	z_{mi} (m)	K
North A	1.83	28.20	1.88	0.30
North B	2.13	28.20	1.92	0.14
North C	1.52	28.20	1.87	0.18
South A	2.13	28.20	1.89	0.44
South B	2.43	28.20	1.89	0.31
South C	1.83	28.20	1.88	0.26
East A	2.13	28.07	1.82	0.39
East B	1.83	28.07	1.84	0.40
East C	1.52	28.07	1.93	0.50
West A	1.83	28.07	1.88	0.22
West B	1.52	28.07	1.89	0.29
West C	2.13	28.07	1.94	0.28
Tower in MI	1.68	28.20	7.00	-
Tower in SWC	1.83	28.07	7.94	-

The daily potential evapotranspiration (E_p) for 2014-2015 were obtained from Caribbean-Florida Water Science Center at U.S. Geological Survey (USGS). The daily E_p in this dataset were computed by Priestley-Taylor (PT) equation based on Geostationary Operational Environmental Satellites (GOES) with a spatial resolution of 2 km (Jacobs et al., 2008). We extracted the E_p data for the pixels covering the four blocks: pixel (28.20°N, 80.83°W) for MI North, pixel (28.20°N, 80.81°W) for MI South, pixel (28.08°N, 80.76°W) for SWC East, and pixel (28.08°N, 80.77°W) for SWC West, respectively. We used the daily precipitation data from rain gauges #0530225 (near to MI) and #04210749 (near to SWC) provided by the St. Johns River Water Management District (Figure 2a). The annual value of flux variable (e.g., precipitation) referred to a water year was aggregated from daily values. We denoted a water year as September 1st to August 31st.

5.3 Methods

5.3.1 Daily evapotranspiration by Penman-Monteith equation

The daily evapotranspiration at each experimental plot was computed by the Penman-Monteith equation (Monteith, 1965; Allen et al., 1998):

$$\lambda ET = \frac{\Delta(R_n - G) + \rho_a c_p \frac{(e_s - e_a)}{r_a}}{\Delta + \gamma(1 + \frac{r_s}{r_a})} \quad (5.1)$$

where ET is the estimated daily actual evapotranspiration (mm day^{-1}); λ is latent heat of vaporization (MJ kg^{-1}) which is dependent on temperature; Δ represents the slope of the relationship between saturation vapor pressure and air temperature (kPa °C^{-1}); R_n is the daily net radiation (MJ m^{-2} day^{-1}) which is the difference of net longwave radiation and net shortwave radiation and 0.17 is used for albedo considering willow land cover (Blanken and Rouse, 1994); G is the ground heat flux assumed to be negligible for daily calculation; ρ_a is the mean air density at constant pressure (kg m^{-3}); c_p is the specific heat of air at constant pressure and the value of 1.013×10^{-3} (MJ kg^{-1} °C^{-1}) was recommended by Allen et al. (1998); e_s is the saturation water vapor pressure at a given air temperature (kPa) and e_a is the actual water vapor pressure (kPa) which is derived from e_s and relative humidity; γ is the psychrometric constant (kPa °C^{-1}); r_a is the aerodynamic resistance (s m^{-1}) which determines the transfer of heat and water vapor from the evaporating surface into the air above the canopy; and r_s is the bulk surface resistance for vapor flow through the land surface (s m^{-1}).

5.3.1.1 Aerodynamic resistance

We estimated the aerodynamic resistance to heat transfer from the surface to the air above canopy (e.g., tower) by an approximation under neutral stability conditions (Garratt and Hicks, 1973; Brutsaert and Stricker, 1979):

$$r_a = \frac{\mathrm{LN}\left[\frac{z_m - d}{z_{om}}\right] \mathrm{LN}\left[\frac{z_h - d}{z_{oh}}\right]}{k^2 u_z} \quad (5.2)$$

where z_m is the height of wind measurements (m); z_h is the height of humidity measurements (m) and both z_m and z_h are approximated to the height of wind speed measurement at the towers in this study; d is the zero plane displacement height (m); z_{om} is the roughness height governing momentum transfer (m); z_{oh} is the roughness height governing transfer of heat and vapor (m); k is von Karman's constant and equals 0.41 (-); and u_z is the wind speed measured at the towers (m s^{-1}). According to Allen et al. (1989), z_{om} is ten times of z_{oh}. z_{om} was estimated as 0.123 times of h_c which is the mean vegetation height; therefore, z_{oh} was computed as 0.0123 h_c (i.e., $z_{om} = 0.123h_c$ and $z_{oh} = 0.0123\ h_c$). The average measured willow heights (h_c) were 4.2 m for MI North, 4.6 m for MI South, 4.8 m for SWC East and 5.1 m for SWC West. The displacement height d is defined as the height at which mean wind velocity is zero due to large obstacles such as canopy and grass surface. We designated d as 0.9 times the height of weather station below canopy (i.e., $d = 0.9z_{m,below}$) since the measured average daily wind speed was 1 m/s at the towers and 0.1 m/s at the weather stations.

5.3.1.2 Surface resistance

Surface resistance was estimated as the canopy resistance for well-watered, actively growing willow stands:

$$r_s = \frac{r_I}{0.5\mathrm{LAI}} \quad (5.3)$$

where r_I is the average value of minimum daytime stomatal resistance for a single leaf; LAI is the index of the leaf area (m^2 of leaf area per m^2 of soil surface). The minimum stomatal resistance of willow without water stress is about 100 s m^{-1} (Glenn et al., 2008) which is close to the value for alfalfa and grass canopy (Monteith, 1965, 1981). Szeicz and Long (1969) recommended

considering only one half of the leaf area as being effective in evapotranspiration since typically the upper half of canopy of a dense vegetation surface receives the majority of net radiation. Allen et al. (1989) defined the half of LAI as the active (sunlit) leaf area index for estimating reference evapotranspiration.

The LAI for willow varied with time, vegetation height, and treatment. Therefore, we estimated the daily LAI values for each experimental plot through the measured solar radiation above and below canopy. It is based on the inversion of the expanded Beer-Lambert equation (Monsi and Saeki, 1953; Bréda, 2003):

$$LAI = -\frac{1}{k}\mathrm{LN}(I/I_0) \quad (5.4)$$

where I is the solar radiation transmitted below canopy (MJ m^{-2} day^{-1}); I_0 is the solar radiation above canopy measured at the towers (MJ m^{-2} day^{-1}); k is the extinction coefficient and can be calibrated based on direct measurements of LAI by allometry or litter fall (Vose and Swank, 1990; Smith et al., 1991; Burton et al., 1991). In this study, k is calibrated by matching the average of estimated daily *LAI* during 7/1/2014-7/31/2014 from equation (4) to the reported value (i.e., 3.2) of *LAI* in July (Schaeffer et al., 2000).

5.3.2 Seasonal variations of *LAI* and *ET*

We computed the monthly *ET* by aggregating the daily values and monthly *LAI* by the average of daily values, and then evaluated the impacts of willow removal on the seasonality of *LAI* and *ET*. Based on the observed data for the control plots and previous studies (Milly, 1994; Berghuijs et al., 2014; Luo et al., 2002), the intra-annual variability of *ET* and *LAI* follows a simple sine curve and can be modeled by the following sine model:

$$LAI(t) = \overline{LAI}[1 + \delta_{LAI}\mathrm{SIN}(2\pi(t - s_{LAI})/\tau_{LAI})] \quad (5.5)$$

$$ET(t) = \overline{ET}[1 + \delta_{ET}\text{SIN}(2\pi(t - s_{ET})/\tau_{ET})] \quad (5.6)$$

where t is the time (days); s is a phase shift (days), τ is the duration of the seasonal cycle (days), δ is a dimensionless seasonal amplitude. The duration of seasonal cycle is 1 year (i.e., $\tau_{LAI} = \tau_{ET} = 365$). $LAI(t)$ is the leaf area index as a function of t, with the time-averaged value of $\overline{LAI}$. $ET(t)$ is the leaf area index as a function of t, with the time-averaged value of $\overline{ET}$. τ and δ were estimated by minimizing the squared errors and coefficient of determination (R^2) was computed by comparison with the observed monthly time series. The model with a larger R^2 indicates that the monthly series has a relatively regular cyclic variation.

5.3.3 Annual evapotranspiration model

The annual *ET* model in this study is based on a one-parameter Budyko equation derived by Wang and Tang (2014) but the annual E_p referred in the annual *ET* model is estimated by water equivalent of net radiation instead of the values estimated by empirical or energy balance equations (e.g., Priestley-Taylor equation) considering the well-watered surface during the entire experimental period (Budyko, 1958; Choudhury, 1999):

$$ET = \frac{P+R_n-\sqrt{(P+R_n)^2-4\varepsilon(2-\varepsilon)P\times R_n}}{2\varepsilon(2-\varepsilon)} \quad (5.7)$$

where P is annual rainfall; ET is annual evapotranspiration; R_n is water equivalent of annual net radiation; and ε is a model parameter which represents the control of landscape characteristics on ET. ε ranges from 0 to 1. ε=0 is corresponding to the lower bound of ET; and ε=1 is corresponding to the upper bound of ET. The value of ε was estimated based on the measurements of annual P, R_n, and ET during the study period. Annual P was obtained from daily data at rain gauges (Figure 2a). Annual R_n is the annual value of water equivalent of net radiation. The daily ET estimations by the Penman-Monteith equation are aggregated to annual ET values.

5.4 Results

5.4.1 Daily evapotranspiration by the Penman-Monteith equation

5.4.1.1 Aerodynamic resistance

As shown in Equation (5.2), r_a was dependent on wind speed and land surface roughness which was affected by vegetation height and foliage. When vegetation height is more than 0.7 m, the foliage roughness accounts for a small portion of surface roughness (Järvelä, 2004; Antonarakis et al., 2010). Since the height of willow in this study was around 4.5 m, the impact of herbicides on surface roughness was assumed to be negligible. Therefore, the temporal variation of r_a was mainly driven by wind speed. The mean monthly wind speeds in the two towers at MI and SWC were consistent with each other (Figure 3). The wind speed in the growing season (April to October) was lower than that in the non-growing season. The minimum wind speed at the tower (at a height of 7 m) during the experiment period was 0.7 m s^{-1} in September and the maximum wind speed was 1.5 m s^{-1} in February. Correspondingly, the aerodynamic resistance in the growing season was larger than that in the non-growing season. r_a ranged from 56 s m^{-1} in February to 110 s m^{-1} in September. The typical value of r_a for willow canopy is about 50 s m^{-1} at a wind speed of 1 m s^{-1} and about 150 s m^{-1} at a wind speed of 0.7 m s^{-1} (Lindroth, 1993).

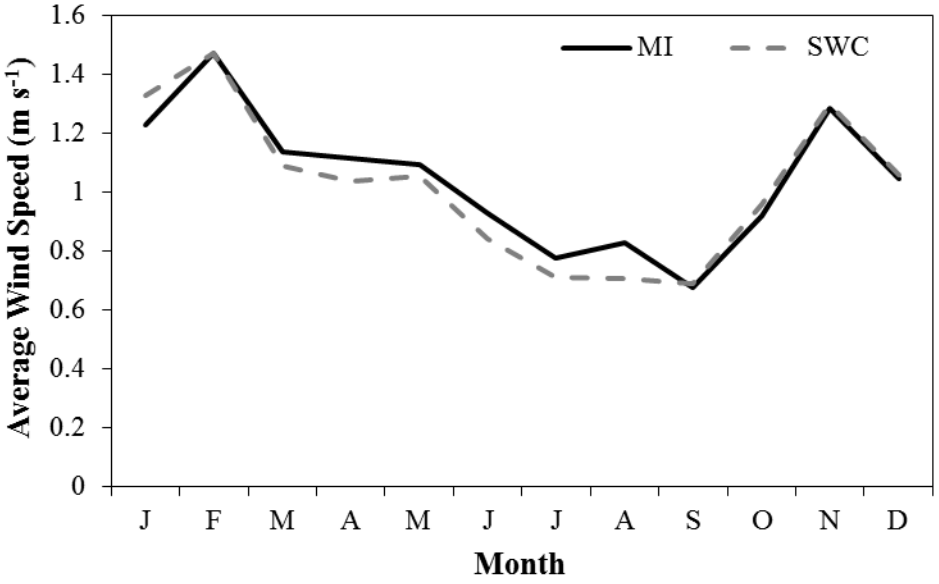

FIGURE 5.3: MEAN MONTHLY WIND SPEED AT THE TWO TOWERS LOCATED IN THE MOCCASIN ISLAND AND SWEETWATER CANAL SITES DURING 9/1/2014-8/31/2016.

5.4.1.2 Leaf area index and surface resistance

The calibrated extinction coefficient *k* varied among the twelve plots from 0.14 in North B to 0.50 in East C and the average value was 0.31 (Table 3). The *k* values ranged from 0.29 to 0.58 for some broad-leaved stands (Bréda, 2003). We computed the daily *LAI* by substituting the calibrated *k* to equation (4). During the pre-treatment period (7/1/2014-7/14/2014), the differences of daily *LAI* among plots were small (Figure 4a). After the first application of herbicide, the average daily *LAI* values during the growing season (7/1/2015-7/14/2015) in the control plots were larger than those in the treated ones, especially for plots sprayed with Clearcast herbicide (Figure 4b). After the second treatment (7/1/2016-7/14/2016), the daily *LAI* in the control plots were still the largest but the differences between treated plots become smaller (Figure 4c). The average daily *LAI* values during 9/1/2014-8/31/2016 were 2.1±0.6 for the control plots, 1.3±0.5 for the treated plots with mixed herbicide, and 1.0±0.4 for the plots treated with Clearcast herbicide, respectively.

The average daily *LAI* values during the growing season were 2.4±0.4 for the control plots, 1.4±0.3 for the treated plots with mixed herbicide, and 1.0±0.2 for the plots treated with Clearcast herbicide, respectively. The average daily *LAI* values during the non-growing season were 1.6±0.3 for the control plots, 1.3±0.4 for the treated plots with mixed herbicides, and 1.0±0.3 for the plots treated with Clearcast herbicide, respectively.

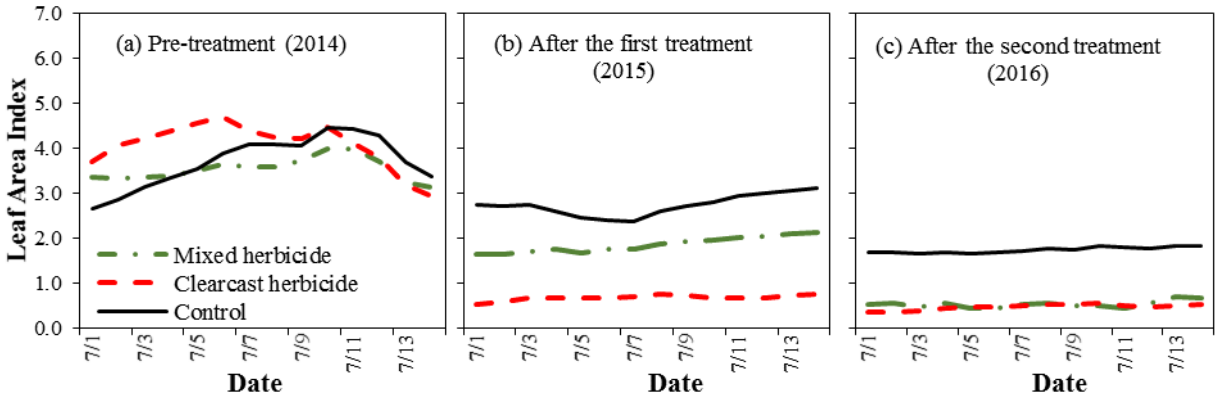

FIGURE 5.4: ESTIMATED DAILY LEAF AREA INDEX (LAI) AVERAGED OVER THE CONTROL PLOTS, THE PLOTS TREATED BY MIXED HERBICIDE, AND THE PLOTS TREATED BY CLEARCAST HERBICIDE DURING JULY 1-14 IN (A) 2014, (B) 2015, AND (C) 2016.

We computed willow surface resistance for each plot by substituting the daily *LAI* in equation (3). The variability of r_s among plots was mainly due to the variation in *LAI*. For the control plots, the average of monthly r_s over blocks ranged from 83 s m^{-1} in September to 200 s m^{-1} in January. For the plot treated by mixed herbicides, r_s ranged from 149 s m^{-1} in September to 283 s m^{-1} in August. For the plot treated by Clearcat herbicide, r_s ranged from 182 s m^{-1} in September to 438 s m^{-1} in June. The reported r_s for willow from Bowen ratio measurements ranged from 40 s m^{-1} to 1000 s m^{-1} corresponding to the variation of *LAI* from 6 to 0.2 (Lindroth, 1993). The recommended r_s value for 95% coverage of marsh in Everglades is 52 s m^{-1} (Jacobs et al., 2008).

5.4.1.3 Daily evapotranspiration by the Penman-Monteith equation

Daily *ET* for the twelve plots during 7/1/2014-8/31/2016 were computed by the PM equation, varying from 0.3 mm day^{-1} to 8.0 mm day^{-1}. The average values of daily *ET* were 3.7±0.1 mm day^{-1} among the control plots, and the maximum values were 5.5±0.6 mm day^{-1} in May as shown in Figure 5a. The observed average daily *ET* for marsh in Everglades in south Florida was 3.9 ± 0.1 mm day^{-1} (Jacobs et al., 2008). The reported transpiration rate of willow in riparian regions was 6.0±0.5 mm day^{-1} during the growing season (Hall et al., 1998). In order to compare the *ET* estimations between control and treated plots, we computed the cumulative *ET* difference between control and treated plots and its slopes for four periods determined by the growing and non-growing seasons (Figure 5b). The 1st slope (Figure 5b) is for the first non-growing season after the first herbicide application (11/1/2014-3/31/2015), the 2nd slope is for the first growing season (4/1/2015-10/31/2015), the 3rd slope is for the second non-growing season (11/1/2015-3/31/2016), and the 4th slope is for the second growing season (4/1/2016/8/31/2016). The slopes reflect the change rate of daily *ET* after willow removal. The four slopes were 0.1 mm day^{-1}, 0.5 mm day^{-1}, 0.4 mm day^{-1}, and 2.1 mm day^{-1} for treated plots with mixed herbicides, and 0.1 mm day^{-1}, 1.5 mm day^{-1}, 0.6 mm day^{-1}, and 2.3 mm day^{-1} for treated plots with Clearcast herbicide. The difference was approximately equal to zero during the pretreatment period and increased slightly during the first non-growing season after herbicide application (i.e., slopes less than 0.1 mm day^{-1}). Starting from the first growing season (4/1/2015), the *ET* difference and slope increased substantially for plots treated by Clearcast herbicide but still slightly for plots treated by mixed herbicide. During the second non-growing and growing seasons (the 3rd slope and the 4th slope), the *ET* change rates were similar for both treated plots. Compared with the first growing

season, the *ET* difference and the slopes for plots treated by mixed herbicides increased substantially.

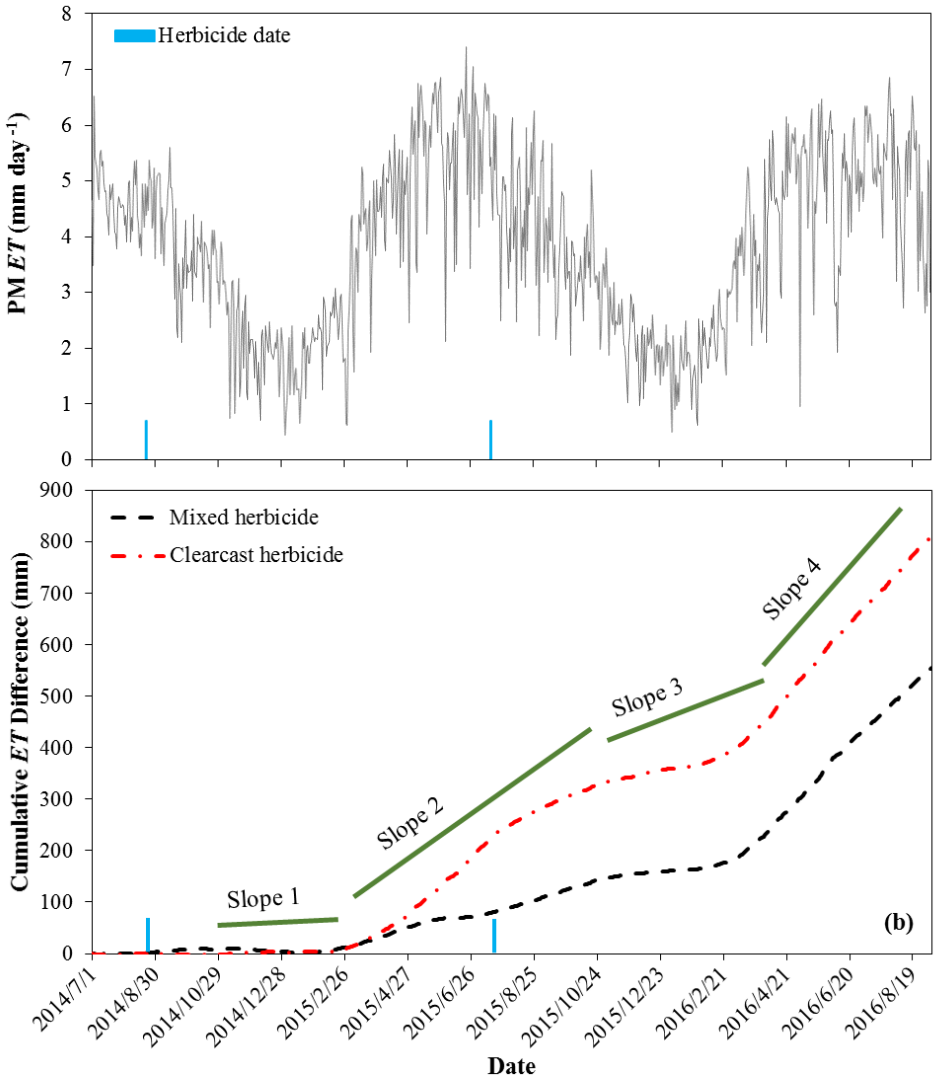

FIGURE 5.5: (A) DAILY PENMAN-MONTEITH (PM) EVAPOTRANSPIRATION (*ET*) AVERAGED OVER THE CONTROL PLOTS; AND (B) THE CUMULATIVE DIFFERENCE (CONTROL MINUS TREATED) OF DAILY EVAPOTRANSPIRATION FOR PLOTS TREATED BY MIXED HERBICIDE AND THE PLOTS TREATED BY CLEARCAST HERBICIDE. BLUE VERTICAL LINES INDICATE THE HERBICIDE APPLICATION DATES. THE GREEN SOLID LINES REPRESENT THE SLOPES OF CUMULATIVE *ET* DIFFERENCE.

5.4.2 Seasonal variations of *LAI* and *ET*

The seasonal variations of *LAI* in the treated plots were quite different compared with the control plot (Figure 5.6a), while the seasonal variations of *ET* were similar among plots (Figure 5.6b). R^2 between observed and modeled monthly *LAI* by the sine model (equation (5.5)) was 0.78 for the control plots, 0.29 for the plots treated by mixed herbicide, and 0.53 for the plots treated by Clearcast herbicide. R^2 between observed and modeled monthly *ET* for both control and treated plots were higher than 0.8. The seasonality of *ET* has been widely used for irrigation and groundwater pumping management in water deficient regions (Zhang and Oweis, 1999).

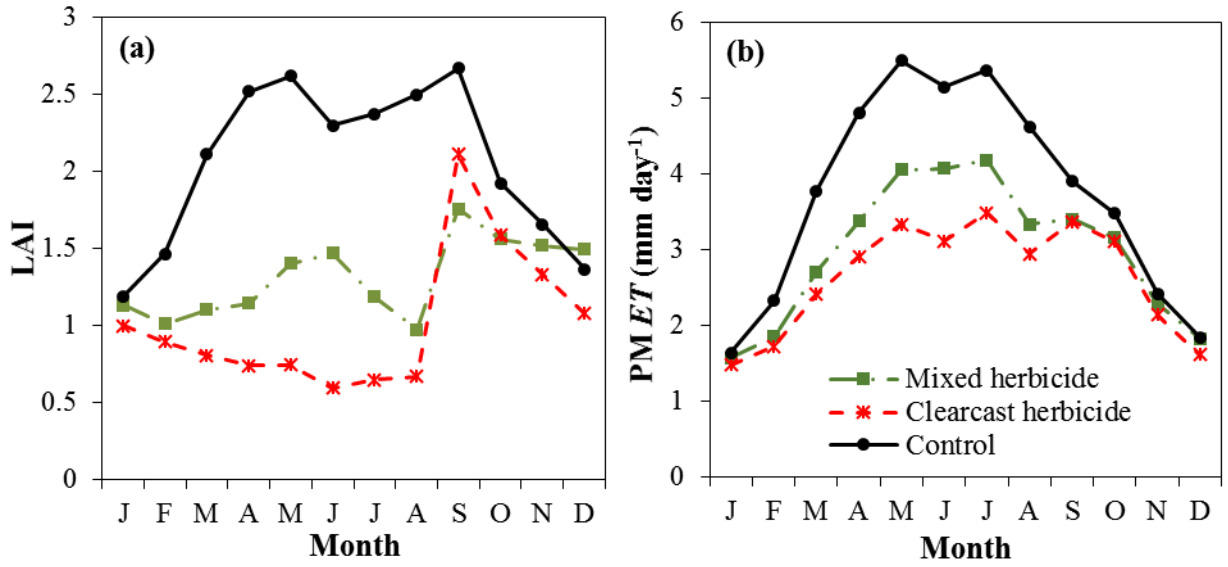

FIGURE 5.6: (A) MEAN MONTHLY EVAPOTRANSPIRATION (*ET*) COMPUTED BY PENMAN-MONTEITH (PM) EQUATION; AND (B) MEAN MONTHLY LEAF AREA INDEX OVER THE CONTROL AND TREATED PLOTS DURING 9/1/2014-8/31/2016.

5.4.3 Annual evapotranspiration model

We used the computed annual *ET* from the daily estimations by PM equation. The aggregated annual *ET* from the twelve plots in two water years varied from 575 mm year^{-1} to 1519

mm year^{-1}. The average annual *ET* rate over the blocks was1368±51 mm year^{-1} for the control plots, 1096±137 mm year^{-1} for the plots treated by mixed herbicides, and 968±117 mm year^{-1} for the plots by Clearcast herbicide. Based on the annual *ET*, we estimated the parameter (ε) of the annual *ET* model (Equation 7) in the two water years. By assuming willow fraction coverage in April of each year (C_w) as an indicator of annual vegetation density for each plot, we identified a strongly positive linear correlation (i.e., r = 0.85, p < 0.01) between ε and C_w (Figure 7), and the relationship follows a natural-logarithm function:

$$\varepsilon = 0.34\text{LN}(C_w) - 0.48 \quad (5.8)$$

The predicted ε by equation (8) can be used to explain 85% of variation (R^2 = 0.85) in the estimated ε among the twelve plots.

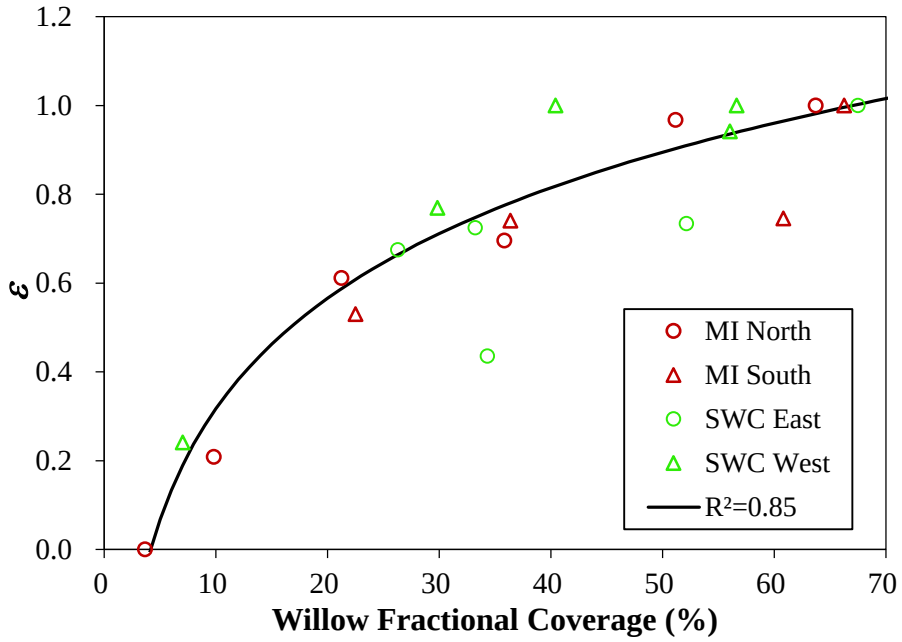

FIGURE 5.7: THE RELATIONSHIP BETWEEN ε IN EQUATION (5) FOR ANNUAL EVAPOTRANSPIRATION AND THE WILLOW FRACTIONAL COVERAGE (C_w) IN APRIL ARE FITTED BY $\varepsilon = 0.34\text{LN}(C_w) - 0.48$.

5.5 Discussion

5.5.1 Performance of daily ET estimation

The PM equation captured the detailed physical processes for *ET* (Cleugh et al., 2007; Leuning et al., 2008). However, a large number of parameters and inputs were required to obtain an accurate estimation of daily *ET* (Beven, 1979; Jacobs et al., 2004). Empirical equations were proposed to estimate the parameters and the applicability to local sites may bring uncertainties (Mu et al., 2007). Some commonly assumed constant parameters (e.g., roughness height and albedo) were also sensitive to the changes in land surface (e.g., willow treatment) (Lindroth, 1993). Additionally, the "big leaf" assumption of PM equation applicable for uniform and dense vegetation surface (Monteith, 1965) might be undermined by our treatments which cause sparse surfaces. For well-watered surface, the actual evapotranspiration is equal to the potential evaporation (Brutsaert and Parlange, 1998). Therefore, in order to validate the performance of PM *ET* in this study, we firstly upscale the point values to block ones by averaging the estimated *ET* over plots in each block. Then, we compared the spatially averaged *ET* with the USGS satellite-based E_p by PT equation in corresponding pixels during 7/1/2014-12/31/2015. Estimates using daily PM *ET* and the USGS satellite-based PT E_p were consistent (Figure 8; $r = 0.91$).

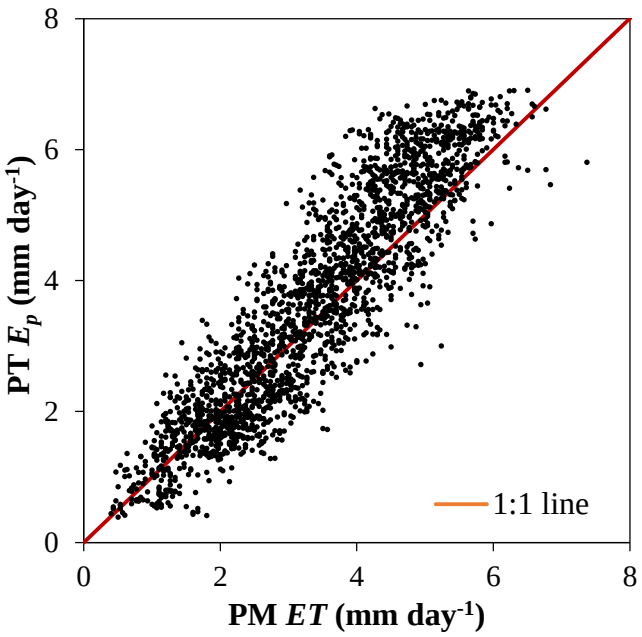

FIGURE 5.8: THE COMPARISON OF SPATIAL AVERAGE VALUES OF DAILY EVAPOTRANSPIRATION (*ET*) COMPUTED BY PENMAN-MONTEITH (PM) EQUATION WITH SATELLITE-BASED POTENTIAL EVAPOTRANSPIRATION (E_P) BY PRESTILEY-TAYLOR (PT) EQUATION FROM USGS.

5.5.2 Impact of willow removal on *ET*

In this study, we emphasized the impact of vegetation change on *ET* through the designed field experiment by ensuring the non-vegetation factor unchanged. For the treated plots, vegetation growth was inhibited for two years after the application of herbicides. Correspondingly, leaf area index decreased substantially especially during the growing season (Figure 5.4) and the seasonal pattern of *LAI* changed (Figure 5.7). As a response, *ET* was the highest in the control plots (3.7 ± 0.1 mm day^{-1}), moderate in the plots sprayed with mixed herbicides (3.0 ± 0.4 mm day^{-1}), and the smallest in the plots sprayed with Clearcast herbicide (2.7 ± 0.3 mm day^{-1}). Differences of *ET* among the control plots and treatment plots were more significant during the growing season (Figure 5.5). However, the seasonal pattern of *ET* was not affected by the willow removal although the seasonality of willow was substantially changed. Therefore, the willow

removal mainly affects the magnitude of *ET* but not its seasonality. The seasonal pattern of *ET* was mainly dependent on the seasonality of *P* and R_n. We computed the correlation coefficient (*r*) between monthly *ET* and three factors (*LAI*, R_n, and *P*) as shown in Table 5.4. It is seen that *r* between *ET* and *LAI* for the treated plots were much smaller than those for R_n and *P*.

5.5.3 Impact of willow removal on annual water yield

ET affects water yield (i.e., runoff and percolation). To assess the secondary impact of willow removal, we computed the annual water yield as the difference between annual precipitation and evapotranspiration. Water yield had a negative correlation with *LAI* as shown in Figure 5.9. This results were in line with the previous findings by Hibbert (1967) and Li et al. (2017). Dugas et al. (1998) showed that potential water yields increased substantially during the short-term period (i.e., less than 2 years) following vegetation removal. When *LAI* decreased by more than a half (*LAI*<1.5) from the natural condition (i.e., controlled plots), the water yield starts to increase significantly. For a long-term period, the removed vegetation may regrow and reach a new equilibrium, and the annual water yield varies considerably from vegetation removal to regrowth (Brown et al., 2005). The regrowth after removal can remain for a long time such as tens and hundreds years (Warren et al., 2001; Zhang and Shangguan, 2016) and the removed vegetation can be replaced by species with rapid and vigorous growth such as herbaceous species (Dugas and Mayeux, 1991). The average daily *ET* values for the control plots (3.7±0.1 mm day^{-1}) were larger than other vegetation surfaces near the USJR marsh, for examples, 3.6 mm day^{-1} for sawgrass and cattail (Mao et al., 2002) and 3.4 mm day^{-1} for mixed marsh in the Lake Okeechobee region (Wu and Shukla, 2014). Therefore, water yield may decrease when new vegetation regrows at the treated willow surface.

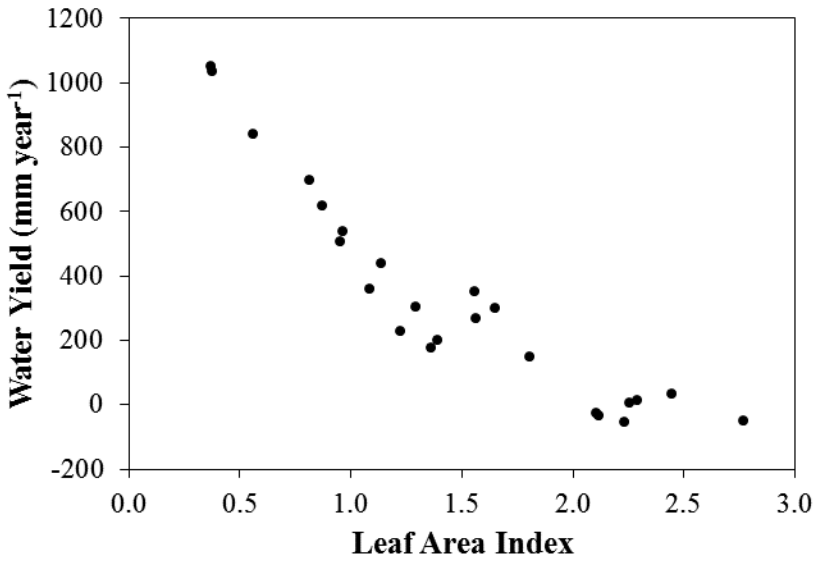

FIGURE 5.9: ANNUAL WATER YIELD (PRECIPITATION MINUS EVAPOTRANSPIRATION) VERSUS LEAF AREA INDEX.

5.5.4 Linking vegetation fractional coverage to annual *ET*

To evaluate the long-term *ET* change due to willow removal, we developed a parsimony annual *ET* model where the model parameter was linked with the fractional willow coverage. Unlike the non-parameter Budyko equation, our equation (Equation (7)) recognizes that annual *ET* from different densities of willow surface could vary and it is in line with the short-term response of *ET*. The parameter (ε) of Equation (7) reflects the effect of landscape characteristics such as vegetation cover on annual evapotranspiration (Zhang et al., 2001; Yang et al., 2007; Donohue et al., 2007; Li et al., 2013). In this experiment, the variability of ε among plots was mainly caused by the application of herbicides to willow. Results suggest a nonlinear relationship between ε and willow fractional coverage (C_w). We used this relationship to evaluate the effect of climate and C_w on annual *ET*:

$$ET = \frac{P+R_n-\sqrt{(P+R_n)^2-4[0.34\mathrm{LN}(C_w)-0.48][2.48-0.34\mathrm{LN}(C_w)]P\times E_p}}{2[0.34\mathrm{LN}(C_w)-0.48][2.48-0.34\mathrm{LN}(C_w)]} \quad (5.9)$$

Vegetation fractional coverage was an important variable to quantify the density of vegetation surface. Vegetation coverage can obtained by field surveying, remote sensing data, or models (Lukina et al., 1999; Chee et al., 2016). Therefore, the developed annual evapotranspiration model provides a useful tool to evaluate and predict the long-term inter-annual variations of *ET* caused by vegetation treatments.

5.6 Conclusion

Vegetation as an important water transition media, largely determines the magnitude of *ET*. To address the ecological and hydrological consequences of willow expansion, vegetation management, such as herbicide, can be potentially applied to the Upper St. Johns River marshes in east central Florida. Therefore, we evaluated the impact of Carolina willow removal by herbicide treatments on evapotranspiration for that region through a field experiment, and the daily evapotranspiration during 7/1/2014-8/31/2016 was calculated using the Penmen-Monteith equation driven by meteorological observations. The leaf area index decreased substantially in the treated plots and the seasonal variation of leaf area index changed after the treatment of willow. From this field experiment, we found that *ET* was 1368±51 mm $year^{-1}$ in the control plots, 1096±137 mm $year^{-1}$ in the plots sprayed with mixed herbicides, and 968±117 mm $year^{-1}$ in the plots sprayed with Clearcast herbicide. The cumulative daily evapotranspiration difference between the control plots and treatment plots were more significant during the growing season. However, the seasonal variation pattern of evapotranspiration was not affected by the willow treatment although the seasonal variation of willow was substantially altered.

ET affects water yield (i.e., runoff and percolation). To assess the subsequent impact of willow removal, we computed the annual water yield as the difference between annual

precipitation and evapotranspiration. A strong negative correlation was identified between water yield and leaf area index. The exponential relation between water yield and leaf area index shows that water yield increased substantially during a short-term period (e.g., about 2 years) following willow removal.

A one-parameter annual evapotranspiration model was applied to the study sites for modeling willow evapotranspiration. The parameter (ε) of the annual evapotranspiration model was estimated for the Upper St. Johns River marshes based on the aggregated annual evapotranspiration from daily values. A natural-logarithm relationship was developed for linking the parameter and willow fractional coverage in April. This empirical relationship provided a useful tool to predict the long-term impact of willow treatment on evapotranspiration for study area.

CHAPTER 6: CONCLUSION AND FUTURE WORK

In this dissertation, a new Budyko-type equations have been derived and applied to watersheds in the United States to disentangle the roles of climate variability, vegetation, soil and topography on long-term water balance, to large-scale irrigation region to reconstruct the historical total water storage change and groundwater storage change and to the Upper St. Johns River marshes to evaluate the impact of willow treatment on annual evapotranspiration.

This dissertation firstly demonstrate the way to derive the one-parameter Budyko-type model from a generalization proportionality relationship for the one-stage partitioning of precipitation. We show that the new model is equivalent to the key equation of the "abcd" model. Theoretical lower and upper bounds of the new model are identified and validated based on previous observations.

Next, a four-parameter Budyko equation was derived by applying the proportionality relationship for the two-stage partitioning of precipitation. The four dimensionless parameters include the Horton index (H, defined as the ratio of evaporation to total wetting) and λ (the ratio of initial evaporation to total wetting) for slow runoff, and β (the ratio of initial wetting to total wetting) and γ (the ratio of total wetting to its potential) for fast runoff. The derived four-parameter equation balances model parsimony and representation of dominant hydrologic processes, and provides a framework to disentangle the roles of climate variability, vegetation, soil and topography on long-term water balance in gauged watersheds. The four parameters are determined for 165 watersheds by using observations of precipitation, potential evaporation, streamflow, and soil properties. Based on the principal component regression analysis, average time interval between rainfall events, slope, normalized difference vegetation index, and wilting point are

identified as the dominant controlling factors on H and λ; saturated hydraulic conductivity and the difference between field capacity and residual soil moisture are identified as the dominant controlling factors on β; and γ is controlled by effective soil water storage capacity, frequency of rainfall events, and climate seasonality. The combination of four-parameter Budyko equation and the principal component regression equations provides a model to assess the long-term responses of evaporation and runoff to climate and watershed property changes in ungauged watersheds.

As the first application for practical problem, the one-parameter Budyko equation has been extended to a two-parameter Budyko model. The extended model can be used to practically and hydrologically reconstruct the historical annual terrestrial water storage change (ΔTWS) and groundwater storage change (ΔGWS). The developed model integrated with the Gravity Recovery and Climate Experiment (GRACE) data was applied to the Punjab in Pakistan as a case study and the ΔTWS and ΔGWS there during 1980-2015 were reconstructed based on multiple input data sources. The model parameters for the Punjab were estimated by minimizing the root-mean-square error between the Budyko-modeled and GRACE-derived ΔTWS during the high data quality period (2004-2010). The ensemble mean of Budyko-modeled ΔTWS correlate well (i.e., r = 0.71) with the ensemble mean of GRACE-derived ΔTWS during 2004-2010. By subtracting the soil moisture storage changes from the Budyko-modeled ΔTWS, the ΔGWS were reconstructed. The reconstructed ΔGWS were validated (i.e., r = 0.64) by the ground-based well observations during the pre-GRACE period (1985-1994). The negative values (i.e., -28.4±19.8 cm) of the cumulative sum of the reconstructed ΔGWS during 1980-2015 indicated the groundwater has been depleted in Punjab. The estimated depletion rates are -0.7±0.6 cm/year during 1980-2015. The depletion has a strongly negative correlation (i.e., r = -0.87) with the total number of tube wells installed in

Punjab. The integration of the developed Budyko model with GRACE data provides a useful tool for the evaluation of long-term groundwater depletion in the large-scale irrigation regions.

As the second application for practical problem, an annual evapotranspiration (*ET*) model has been developed based on the one-parameter Budyko equation. the developed *ET* model was used to quantify the change in evapotranspiration (*ET*) at the community level after removing willow by implementing a field experiment. The experiment includes two sites and each site contains two blocks. A block contains three plots with a size of 150 m × 150 m, one of which is untreated as the control. The other two plots are treated by aerially spraying herbicide(s). Daily *ET* for the twelve plots during 7/1/2014 -- 8/31/2016 is estimated using the Penmen-Monteith equation. The cumulative *ET* difference between control and treated plots increases substantially during the subsequent growing season after herbicide application. The aggregated annual evapotranspiration is 1368±51 mm $year^{-1}$ for the control plots, 1096±137 mm $year^{-1}$ for the plots treated by mixed herbicides, and 968±117 mm $year^{-1}$ for the plots treated by Clearcast herbicide. The water yield increases in the first 2 years following willow treatment due to the decrease of *ET*. A single-parameter annual *ET* model is applied to the study area, and an empirical relationship between the parameter and willow fractional coverage is obtained for predicting *ET* response to willow treatment.

This dissertation reveals the commonality of the one-stage and two-stage partitioning of precipitation, provides a compromised solution to balance the complexity of physical models and the parsimony of empirical Budyko equations, derives two new Budyko-type equations. The derived models can be applied to different spatial (e.g., lakes, watersheds, groundwater basin) for

solving the important theoretical and practical hydrological problems at annual scale. Moreover, they have potential to be extended for other temporal scales (e.g., monthly, seasonal).

APPENDIX A: CURRICULUM VITAE

Yin Tang was born in the city of Guiyang, Guizhou, People's Republic of China. In 2004, she finished secondary school an entered the Beijing Forestry University. Due to her strong interest in natural science, she majored in Soil and Water Conservation. During her bachelors program, she became an undergraduate research assistant and joined to the project: "Non-point source pollution control and management system" funded by Beijing Municipal Science & Technology Commission starting her research career. Based on the work for this project, she published her first journal paper. In 2008, she has been recommended as an exemption helicopter graduate students by the College of Graduate at Beijing Forestry University. She worked for two research projects related to the adaptive watershed management as a graduate research assistant. In 2011, she completed her Master program and delivered a thesis: "The application of SWAT model to small watersheds for assessing hydrologic responses to climate change and land use change" which has been awarded the Best Master Thesis (1%) by Beijing Forestry University. After graduation, she joined the Land Surface Processes and Global Change Research Group at the Institute of Geographic Science and Natural Resources Research (IGSNRR), Chinese Academy of Sciences (CAS) as a postgraduate research assistant. In 2.13, through complete the partial research project: "Study on the regional variation of environmental risk of China and the world", she published her first SCI journal on *Hydrology Earth System Science*. At the same year, she has been admitted by the Civil Engineering Ph.D. program at the University of Central Florida.

In 2014, she started working as a research assistant under the supervision of Dr. Dingbao Wang. Her Ph.D. dissertation is to theoretically derive the new type of annual water balance models. In order to transfer the theoretical findings into practical applications, she applied the

developed model to two projects including the reconstruction of annual total water storage change and groundwater storage change for the large-scale irrigation regions and evaluation the impacts of willow removal on evapotranspiration in the Upper St. Johns River (USJR) Marshes in Florida, the United States. Additionally, she also contributed to the project for the integration of hydrologic and hydrodynamic models to inform an economic valuation of the wetlands as related to flood abatement and flood insurance rates.

As a result of her previous work, she had three first-author manuscripts under reviewed in *Water Resources Research*, *Journal of Hydrology*, and *Agricultural and Forest Meteorology*, one first-author manuscript published to *Hydrology Earth System Science*, and eight co-author manuscripts published in top water-related journals. She will remain working as a postdoctoral fellow for her research career.

APPENDIX B: LIST OF PUBLICATIONS

Under Reviewed Journal Papers:

[1] Tang, Y., Wang, D., Major Revision. Evaluating the roles of watershed properties on long-term water balance through a four-parameter Budyko equation. *Water Resources Research*

[2] Tang, Y., Hooshyar, M., Zhu, T., Ringler, C., Sun, A.Y., Long, D., Wang, D., Second round under review. Reconstruct annual groundwater storage changes in a large-scale irrigation region by integrating GRACE data and Budyko model. *Journal of Hydrology*

[3] Tang, Y., Goodding, D., CaMo, L., Hall, D., Quintana-Ascencio, P. F., Wang, D., Fauth, J., Evaluating the Impact of Willow Treatment on Evapotranspiration in the Upper St. Johns River (USJR) Marshes in Florida. *Agricultural and Forest Meteorology*

Published Journal Papers:

[1] Bacopoulos, P., Tang, Y., Wang, D., Hagen, S., Demissie H., (Accepted). Integrated hydrologic-hydrodynamic modeling of flooding in the lower St. Johns River Basin caused by Tropical Storm Fay (2008). Journal of Hydrologic Engineering

[2] Zhang, C., Ding, W., Li, Y., Tang, Y., Wang D., 2016. Catchments' hedging strategy on evapotranspiration for climatic variability, *Water Resources Research*, 52, 9036–9045, doi:10.1002/2016WR019384.

[3] Wang, D., Zhao, J., Tang, Y., Sivapalan, M., 2015. A thermodynamic interpretation of Budyko and L'vovich formulations of annual water balance: proportionality hypothesis and maximum entropy production, *Water Resources Research*, 51, 3007–3016.

[4] Wang, D., Tang, Y., 2014. A one-parameter Budyko model for water balance captures emergent behavior in Darwinian hydrologic models, *Geophysical Research Letters*, 41, doi:10.1002/2014GL060509.

Conference Proceedings:

[1] Tang, Y., Wang, D., A four-parameter Budyko equation for mean annual water balance. IPWE 2017, Wuhan, Hubei, P. R. China. January 4, 2017.

[2] Tang, Y., Wang, D., Fauth, J., Quintana-Ascencio, P., Hall, D., Ponzio, K., 2016. Quantifying the impact of willow on evapotranspiration in the Upper St. Johns River marshes, Florida, USA. 2016 AWRA Annual Conference, Orlando, Florida, United States. November 18, 2016.

[3] Tang, Y., Wang, D., Zhu, T., Ringler, C., Sun, A.Y., Long, D., Integrating GRACE and a Budyko model to quantify seasonal groundwater depletion in the Indus and Ganges

Basins. EWRI World Environmental & Water Resources Congress 2016, West Palm Beach, Florida, United States. May 23, 2016.

[4] Bacopoulos, P., Tang, Y., Wang, D., Hagen, S., Demissie H., "An Integrated Hydrologic-Hydrodynamic Model for Simulating Floods in the St. Johns River Basin", 31st Annual ASCE Water Resources Seminar, Orlando, Florida, United States. March 27, 2015.

Selected Conference Abstracts:

[1] Tang, Y., Wang, D., A Four-parameter Budyko Equation for Mean Annual Water Balance. AGU Fall Meeting, session H53F. San Francisco, USA. 2016.

[2] Tang, Y., Wang, D., Zhu, T., Ringler, C., Sun, A.Y., Integrating GRACE and Budyko Model to Quantify Groundwater Depletion. AGU Fall Meeting, session H41F. San Francisco, USA. 2015.

[3] Wang, D., Tang, Y., Time-Scale Invariance As an Emergent Property in Water Balance. AGU Fall Meeting, session H43L. San Francisco, USA. 2014.

[4] Tang, Y., Tang, Q., Responses of Hydrological Cycle to Recent Climatic Changes in the Yellow River Basin. AGU Fall Meeting, session H21F. San Francisco, USA. 2012.

[5] Tang Y., Tang, Q., Climate Extremes: Impacts of extreme climate on simulated runoff in the Yellow River Basin. AGU Fall Meeting, session GC51E. San Francisco, USA. 2011.

REFERENCES

Aeschbach-Hertig, W. and T. Gleeson (2012), Regional strategies for the accelerating global problem of groundwater depletion, *Nature Geoscience*, *5*, 853-861, doi:10.1038/ngeo1617.

Alley, W. M. (1985), Water Balance Models in One-Month-Ahead Streamflow Forecasting, *Water Resour. Res.*, *21*(4), 597–606, doi:10.1029/WR021i004p00597.

Barker, R. and F. Molle (2004), *Irrigation management in rice-based cropping systems: issues and challenges in Southeast Asia*, International Water Management Institute, Colombo.

Berghuijs, W., R. Woods, and M. Hrachowitz (2014a), A precipitation shift from snow towards rain leads to a decrease in streamflow, *Nat. Clim. Chang.*, *4*(7), 583–586, doi:10.1038/nclimate2246.

Berghuijs, W. R., M. Sivapalan, R. A. Woods, and H. H. G. Savenije (2014b), Patterns of similarity of seasonal water balances: A window into streamflow variability over a range of time scales, *Water Resour. Res.*, *50*, 5638–5661, doi:10.1002/2014WR015692.

Beven, K. J. (2011). *Rainfall-runoff modelling: the primer*. John Wiley & Sons.

Beven, K. J., and M. J. Kirkby (1979), A physically based variable contributing area model of catchment hydrology, *Hydrol. Sci. Bull.*, *24*, 43-69.

Bhadra, A., N. S. Raghuwanshi, and R. Singh (2012), *Generation of monthly irrigation maps for India using spatial interpolation techniques* in *Sustainable irrigation and drainage IV: management, technologies and policies*, edited by H. Bjornlund et al., pp. 291, WIT Press, Southampton.

Biemans, H., C. Siderius, A. Mishra, and B. Ahmad (2015), Crop-specific seasonal estimates of irrigation water demand in South Asia, *Hydrol. Earth Syst. Sci. Discuss.*, 12, 7843–7873, doi:10.5194/hessd-12-7843-2015.

Biswal, B. (2016), Dynamic hydrologic modeling using the zero-parameter Budyko model with instantaneous dryness index, *Geophys. Res. Lett.*, *43*, 9696–9703, doi:10.1002/2016GL070173.

Blöschl, G. and M. Sivapalan (1995), Scale issues in hydrological modelling: A review, *Hydrol. Process.*, *9*: 251–290, doi: 10.1002/hyp.3360090305.

Briscoe, J. and R. P. S. Malik (2006), *India's water economy: bracing for a turbulent future*, Oxford University Press, New Delhi.

Brooks, P. D., P. A. Troch, M. Durcik, E. Gallo, and M. Schlegel (2011), Quantifying regional scale ecosystem response to changes in precipitation: Not all rain is created equal, *Water Resour. Res.*, 47, W00J08, doi:10.1029/2010WR009762.

Brutsaert, W., and J. L. Nieber (1977), Regionalized drought flow hydrographs from a mature glaciated plateau, *Water Resour*. *Res.*, *13*(3), 637–643, doi:10.1029/WR013i003p00637.

Budyko, M. I. (1958), *The Heat Balance of the Earth's Surface*, translated from Russian by N. A. Stepanova, 259 pp., U.S. Dep. of Commer., Washington, D.C., 1958.

Budyko, M. I. (1974), *Climate and Life*, 508 pp., Academic Press, New York.

Cai, X., B. R. Sharma, M. A. Matin, D. Sharma, S. Gunasinghe (2010), *An assessment of crop water productivity in the Indus and Ganges river basins: Current status and scope for improvement*, pp. 30, International Water Management Institute, Colombo, doi:10.5337/2010.232.

Chen J. L., J. Li, Z. Z. Zhang, S. N. Ni (2014), Long-term groundwater variations in northwest India from satellite gravity measurements. *Global Planet. Change*, 116,130–138, doi:10.1016/j.gloplacha.2014.02.007.

Chen, F., K. Mitchell, J. Schaake, Y. Xue, H. L. Pan, V. Koren, Q. Y. Duan, M. Ek and A. Betts (1996), Modeling of land surface evaporation by four schemes and comparison with FIFE observations. *J. Geophys. Res.*, 101, 7251-7268, doi:10.1029/95JD02165.

Chen, M., P. Xie, J. E. Janowiak, and P. A. Arkin (2002), Global land precipitation: A 50-yr monthly analysis based on gauge observations, *J. Hydrometeor.*, 3, 249-266, doi:http://dx.doi.org/10.1175/1525-7541(2002)003<0249:GLPAYM>2.0.CO;2.

Chen, X., and D. Wang (2015), Modeling seasonal surface runoff and base flow based on the generalized proportionality hypothesis, *J. Hydrol.*, *527*, 367–379, doi:10.1016/j.jhydrol.2015.04.059.

Chen, X., N. Alimohammadi, and D. Wang (2013), Modeling interannual variability of seasonal evaporation and storage change based on the extended Budyko framework, *Water Resour. Res.*, 49, doi:10.1002/wrcr.20493.

Choudhury, B. J. (1999), Evaluation of an empirical equation for annual evaporation using field observations and results from a biophysical model, *J. Hydrol.*, *216*(1–2), 99–110, http://dx.doi.org/10.1016/S0022-1694(98)00293–5.

Dai, Y., X. Zeng, R. Dickinson, I. Baker, G. Bonan, M. Bosilovich, A. Denning, P. Dirmeyer, P. Houser, G. Niu, K. Oleson, C. Schlosser, and Z. Yang (2003), The common land model, *Bull. Am. Meteorol. Soc.*, 84, 1013–1023, doi: http://dx.doi.org/10.1175/BAMS-84-8-1013.

de Linage C., L. Rivera, J. Hinderer, J. Boy, Y. Rogister, S. Lambotte and R. Biancale (2009), Separation of coseismic and postseismic gravity changes for the 2004 Sumatra–Andaman earthquake from 4.6 yr of GRACE observations and modelling of the coseismic change by normal-modes summation, *Geophys. J. Int.*, 176, 695–714, doi:10.1111/j.1365-246X.2008.04025.x.

Donohue, R. J., M. L. Roderick, and T. R. McVicar (2007), On the importance of including vegetation dynamics in Budyko's hydrological model, *Hydrol. Earth Syst. Sci.*, *11*, 983–995, doi:10.5194/hess-11-983-2007.

Donohue, R. J., M. L. Roderick, and T. R. McVicar (2011), Assessing the differences in sensitivities of runoff to changes in climatic conditions across a large basin, *J. Hydrol.*, *406*(3-4), 234-244.

Donohue, R. J., M. L. Roderick, and T. R. McVicar (2012), Roots, storms and soil pores: Incorporating key ecohydrological processes into Budyko's hydrological model, *J. Hydrol.*, *436–437*, 35–50, http://dx.doi.org/10.1016/j.jhydrol.2012.02.033.

Du, C., F. Sun, J. Yu, X. Liu, and Y. Chen (2016), New interpretation of the role of water balance in an extended Budyko hypothesis in arid regions, *Hydrol. Earth Syst. Sci.*, 20, 393-409, doi:10.5194/hess-20-393-2016.

Duan, Q., J. Schaake, V. Andréassian, S. Franks, G. Goteti, H. V. Gupta, Y. M. Gusev, F. Habets, A. Hall, L. Hay, T. Hogue, M. Huang, G. Leavesley, X. Liang, O. N. Nasonova, J. Noilhan, L. Oudin, S. Sorooshian, T. Wagener, and E. F. Wood (2006), The Model Parameter Estimation Experiment (MOPEX): An overview of science strategy and major results from the second and third workshops, *J. Hydrol.*, *320*(1-2), 3-17.

Dunne, T., and R. D. Black (1970), Partial Area Contributions to Storm Runoff in a Small New England Watershed, *Water Resour. Res.*, *6*(5), 1296–1311, doi:10.1029/WR006i005p01296.

Eagleson, P. (1978a), Climate, Soil, and Vegetation 2. The Distribution of Annual Precipitation Derived From Observed Storm Sequences, *Water Resour. Res.*, *14*(5), 713–721, doi:10.1029/WR014i005p00713.

Eagleson, P. (1978b), Climate, Soil, and Vegetation 6. Dynamics of the Annual Water Balance, *Water Resour. Res.*, *14*(5), 749–764, doi:10.1029/WR014i005p00749.

Eastham, J., M. Kirby, M. Mainuddin, and M. Thomas (2010), *Water-use accounts in CPWF basins: simple water-use accounting of the Ganges basin,* in *CPWF Working Paper: Basin Focal Project series BFP05*, pp. 30, The CGIAR challenge program on water and food, Colombo.

Ek, M., K. Mitchell, Y. Lin, E. Rogers, P. Grunmann, V. Koren, G. Gayno, and J. D. Tarpley (2003), Implementation of Noah land surface model advances in the National Centers for Environmental Prediction operational mesoscale Eta model, *J. Geophys. Res.*, 108(D22), 8851, doi:10.1029/2002JD003296.

Fan, Y., and H. van den Dool (2008), A global monthly land surface air temperature analysis for 1948–present, *J. Geophys. Res.*, 113, D01103, doi:10.1029/2007JD008470.

Federer, C. A., C. and B. Fekete (1996), Intercomparison of methods for calculating potential evaporation in regional and global water balance models, *Water Resour. Res.*, 32(7), 2315-2321, doi: 10.1029/96WR00801.

Feng, W., M. Zhong, J. Lemoine, R. Biancale, H. Hsu, and J. Xia (2013), Evaluation of groundwater depletion in North China using the Gravity Recovery and Climate Experiment (GRACE) data and ground-based measurements, *Water Resour. Res.*, 49, 2110-2118, doi: 10.1002/wrcr.20192.

Feng, X., G. Vico, and A. Porporato (2012), On the effects of seasonality on soil water balance and plant growth, *Water Resour. Res.*, *48*, W05543, doi:10.1029/2011WR011263.

Foster, S. S. D., and P. J. Chilton (2003), Groundwater: The processes and global significance of aquifer degradation, *Philos. Trans. R. Soc. Lond B Biol. Sci*., 358(1440), 1957–1972, doi: 10.1098/rstb.2003.1380.

Fowler, H. and D. Archer (2006), Conflicting signals of climatic change in the Upper Indus Basin, *J. Climate*, 19, 4276–4293, doi: http://dx.doi.org/10.1175/JCLI3860.1.

Fu, B. P. (1981), On the calculation of the evaporation from land surface, *Scientia Atmospherica Sinica*, *5*(1), 23–31 (in Chinese).

Garduño, H., S. Romani, B. Sengupta, A. Tuinhof, and R. Davis (2011), *India groundwater governance case study*, World Bank, Washington, D. C.

Gentine, P., D. Entekhabi, and J. Polcher (2010), Spectral behaviour of a coupled land-surface and boundary layer system, *Bound-Lay Meteorol.*, *134*,157–180.

Gentine, P., P. D'Odorico, B. R. Lintner, G. Sivandran, and G. Salvucci (2012), Interdependence of climate, soil, and vegetation as constrained by the Budyko curve, *Geophys. Res. Lett.*, *39*, L19404, doi:10.1029/2012GL053492.

Gerrits, A. M. J., H. H. G. Savenije, E. J. M. Veling, and L. Pfister (2009), Analytical derivation of the Budyko curve based on rainfall characteristics and a simple evaporation model, *Water Resour. Res.*, *45*, W04403, doi:10.1029/2008WR007308.

Giordano, M. (2009), Global groundwater? Issues and solutions, *Annu. Rev. Environ. Resour.*, 34, 153–178, doi: 10.1146/annurev.environ.030308.100251.

Gleeson, T., Y. Wada, M. Bierkens, and L. van Beek (2012), Water balance of global aquifers revealed by groundwater footprint, *Nature*, 488(7410), 197-200, doi:10.1038/nature11295.

Gonzales, A. L., J. Nonner, J. Heijkers, and S. Uhlenbrook (2009), Comparison of different base flow separation methods in a lowland catchment, *Hydrol. Earth Syst. Sci.*, *13*(11), 2055–2068, doi:10.5194/hess-13-2055-2009.

Greve, P., L. Gudmundsson, B. Orlowsky, and S. I. Seneviratne (2015), Introducing a probabilistic Budyko framework, *Geophys. Res. Lett.*, *42*(7), 2261–2269, doi: 10.1002/2015GL063449.

Hamon, W. (1963), Computation of direct runoff amounts from storm rainfall, *Intl. Assoc. Scientific Hydrol. Publ.*, 63, 52-62.

Hamon, W. R. (1961), Estimating Potential Evapotranspiration, *Journal of the Hydraulics Division*, ASCE. 87(HY3):107–120.

Hanasaki, N., S. Kanae, T. Oki, K. Masuda, K. Motoya, N. Shirakawa, Y. Shen, and K. Tanaka (2008), An integrated model for the assessment of global water resources—Part 2: Applications and assessments, *Hydrol. Earth Syst. Sci.*, 12, 1027–1037, doi:10.5194/hess-12-1027-2008.

Hansen, J., R. Ruedy, M. Sato, and K. Lo (2010), Global surface temperature change, *Rev. Geophys.*, 48, RG4004, doi:10.1029/2010RG000345.

Harman, C., and P. A. Troch (2014), What makes Darwinian hydrology "Darwinian"? Asking a different kind of question about landscapes, *Hydrol. Earth Syst. Sci.*, *18*, 417-433, doi:10.5194/hess-18-417-2014.

Harte, J. (2002), Toward a synthesis of the Newtonian and Darwinian worldviews, *Phys. Today*, *55*, 29, doi:10.1063/1.1522164.

Hinkle, D. E., W. Wiersma, S. G. Jurs (2003), *Applied Statistics for the Behavioral Sciences, 5th ed.*, Houghton Mifflin, Boston.

Hooshyar, M., and D. Wang (2016), Analytical solution of Richards' equation providing the physical basis of SCS curve number method and its proportionality relationship, *Water Resour. Res.*, *52*, doi:10.1002/2016WR018885.

Horton, R. E. (1933), The role of infiltration in the hydrologic cycle, *Trans. Amer. Geophys. Union*, *14*, 446–460.

Huang, Y., M. Salama, M. Krol, Z. Su, A. Hoekstra, Y. Zeng, and Y. Zhou (2015), Estimation of human induced changes in terrestrial water storage through integration of GRACE satellite detection and hydrological modeling: A case study of the Yangtze River basin, *Water Resour. Res.*, 51, 8494–8516, doi:10.1002/2015WR016923.

Humphrey, V., L. Gudmundsson, and S. I. Seneviratne (2016), Assessing global water storage variability from GRACE: trends, seasonal cycle, subseasonal anomalies and extremes, *Surv. Geophys.*, 37(2), 357-395, doi: : 10.1007/s10712-016-9367-1.

Jacob, T., J. Wahr, W. Pfeffer, and S. Swenson (2012), Recent contributions of glaciers and ice caps to sea level rise, *Nature*, 482, 514–518, doi:10.1038/nature10847.

Jiang, C., L. Xiong, D. Wang, P. Liu, S. Guo, and C. Y. Xu (2015), Separating the impacts of climate change and human activities on runoff using the Budyko-type equations with time-varying parameters, *J. Hydrol.*, *522*, 326–338, http://dx.doi.org/10.1016/j.jhydrol.2014.12.060.

Jothityangkoon, C., and M. Sivapalan (2009), Framework for exploration of climatic and landscape controls on catchment water balance, with emphasis on inter-annual variability, *J. Hydrol.*, *371*(1), 154–168, http://dx.doi.org/10.1016/j.jhydrol.2009.03.030.

Jury, W. and H. Vaux (2005), The role of science in solving the world's emerging water problems, *PNAS*, 102(44), 15715-15720, doi: 10.1073/pnas.0506467102.

Kemmerikh, A. O. (1972), *Rol lednikov v stoke rek Sredney Asii (Glaciers' part in the stream flow in Central Asia)* (in Russian) in *Data of Glaciological Studies*, vol. 20, pp. 82-94.

Kingston, D. G., M. C. Todd, R. G. Taylor, J. R. Thompson, and N. W. Arnell (2009), Uncertainty in the estimation of potential evapotranspiration under climate change, *Geophys. Res. Lett.*, 36, L20403, doi:10.1029/2009GL040267.

Konikow, L. F., and E. Kendy (2005), Groundwater depletion: A global problem. *Hydrogeol. J.* 13, 317–320, doi:10.007/s10040-004-0411-8.

Koster, R. D., and M. J. Suarez (1994), The components of a SVAT scheme and their effects on a GCMs hydrological cycle, *Adv. Water Resour.*, 17, 61–78, doi:10.1016/0309-1708(94)90024-8.

Koster, R. D., and M. J. Suarez (1996), *Energy and water balance calculations in the Mosaic LSM* in *Technical report series on global modeling and data assimilation, NASA Tech. Memo.*

NASA TM-104606, vol. 9, edited by M. J. Suarez, pp. 60, Goddard Space Flight Center, Greenbelt.

L'vovich, M. I. (1979), World Water Resources and Their Future, 415 pp., *Amer. Geophys. Union*, Washington D. C.

Landerer, F. W., and S. C. Swenson (2012), Accuracy of scaled GRACE terrestrial water storage estimates, *Water Resour. Res.*, 48, W04531, doi:10.1029/2011WR011453.

Li, D., M. Pan, Z. Cong, L. Zhang, and E. Wood (2013), Vegetation control on water and energy balance within the Budyko framework, *Water Resour. Res.*, *49*, 969–976, doi:10.1002/wrcr.20107.

Li, H. Y., M. Sivapalan, F. Tian, and C. Harman (2014), Functional approach to exploring climatic and landscape controls of runoff generation: 1. Behavioral constraints on runoff volume, *Water Resour. Res.*, *50*, 9300–9322, doi:10.1002/2014WR016307.

Li, W., and A. Sankarasubramanian (2012), Reducing hydrologic model uncertainty in monthly streamflow predictions using multimodel combination, *Water Resour. Res.*, *48*, W12516, doi:10.1029/2011WR011380.

Liang, X., D. P. Lettenmaier, E. F. Wood, and S. J. Burges (1994), A simple hydrologically based model of land-surface water and energy fluxes for general-circulation models, *J. Geophys. Res.*, 99(D7), 14415–14428, doi: 10.1029/94JD00483.

Long, D., L. Longuevergne, and B. R. Scanlon (2014), Uncertainty in evapotranspiration from land surface modeling, remote sensing, and GRACE satellites, *Water Resour. Res.*, 50, 1131–1151, doi:10.1002/2013WR014581.

Long, D., L. Longuevergne, and B.R. Scanlon (2015), Global analysis of approaches for deriving total water storage changes from GRACE satellites. *Water Resour. Res.*, 51(4), 2574-2594, doi: 10.1002/2014WR016853.

Long, D., X. Chen, B. R. Scanlon, Y. Wada, Y. Hong, V. P. Singh, Y. Chen, G. Wang, Z. Han, and W. Yang (2016), Have GRACE satellites overestimated groundwater depletion in the Northwest India Aquifer? *Sci. Rep.*, 6, 24398, doi: 10.1038/srep24398.

Longuevergne, L., B. R. Scanlon, and C. R. Wilson (2010), GRACE Hydrological estimates for small basins: Evaluating processing approaches on the High Plains Aquifer, USA, *Water Resour. Res.*, 46, W11517, doi:10.1029/2009WR008564.

Lyne, V., and M. Hollick (1979), *Stochastic time-variable rainfall-runoff modeling*, In: *Proc. Hydrology and Water Resources Symposium*, Perth, 89–92, Inst. Of Engrs, Australia.

MacDonald A. M., H. C. Bonsor, R. Taylor, M. Shamsudduha, W. G. Burgess, K. M. Ahmed, A. Mukherjee, A. Zahid, D. Lapworth, K. Gopal, M. S. Rao, M. Moench, S. H. Bricker, S. K. Yadav, Y. Satyal, L. Smith, A. Dixit, R. Bell, F. van Steenbergen, M. Basharat, M. S. Gohar, J. Tucker, R. C. Calow and L. Maurice (2015), *Groundwater resources in the Indo‐Gangetic Basin: resilience to climate change and abstraction*, pp. 63, British Geological Survey Open Report, OR/15/047.

Margat, J., and J. Gun (2013), *Groundwater around the World*, CRC Press, Balke.

Martinez, G. F., and H. V. Gupta (2011), Hydrologic consistency as a basis for assessing complexity of monthly water balance models for the continental United States, *Water Resour. Res.*, *47*, W12540, doi:10.1029/2011WR011229.

Mekonnen, D., Siddiqi A., and Ringler C. (2016), Drivers of groundwater use and technical efficiency of groundwater, canal water, and conjunctive use in Pakistan's Indus Basin Irrigation System, *Int. J. Water Resour. D.*, doi: 10.1080/07900627.2015.1133402.

Mezentsev, V. S. (1955), More on the calculation of average total evaporation, *Meteorol. Gidrol.*, *5*, 24–26.

Milly, P. C. D. (1993), An analytical solution of the stochastic storage problem applicable to soil water, *Water Resour. Res.*, *29*, 3755–3785, doi:10.1029/93WR01934.

Milly, P. C. D. (1994), Climate, soil water storage, and the average annual water balance, *Water Resour. Res.*, 30, 2143–2156.

Milly, P. C. D., and K. A. Dunne (2002), Macroscale water fluxes 2. Water and energy supply control of their interannual variability, *Water Resour. Res.*, 38(10), 1206, doi:10.1029/2001WR000760.

MoWP. (2012), *Handbook on water statistics of Pakistan*, Ministry of Water and Power Islamabad.

Newman, B. D., B. P. Wilcox, S. R. Archer, D. D. Breshears, C. N. Dahm, C. J. Duffy, N. G. McDowell, F. M. Phillips, B. R. Scanlon, and E. R. Vivoni (2006), Ecohydrology of water limited environments: A scientific vision, *Water Resour. Res.*, *42*, W06302, doi:10.1029/2005WR004141.

Niu, J., C. Shen, S. G. Li, and M. S.Phanikumar (2014), Quantifying storage changes in regional Great Lakes watersheds using a coupled subsurface-land surface process model and GRACE, MODIS products, *Water Resour. Res.*, 50, 7359–7377, doi:10.1002/2014WR015589.

Papa, F., F. Frappart, Y. Malbeteau, M. Shamsudduha, V. Vuruputur, M. Sekhar, G. Ramillien, C. Prigent, F. Aires, R. K. Pandey, S. Bala, and S. Calmant (2015), Satellite-derived surface and sub-surface water storage in the Ganges–Brahmaputra River Basin, *Journal of Hydrology: Regional Studies*, 4, 15-35, doi:10.1016/j.ejrh.2015.03.004.

Pike, J. G. (1964), The estimation of annual runoff from meteorological data in a tropical climate, *J. Hydrol.*, *2*, 116– 123.

Ponce, V. M., and A. V. Shetty (1995), A conceptual model of catchment water balance. 1. Formulation and calibration, *J. Hydrol.*, *173*, 27–40.

Porporato, A., E. Daly, and I. Rodriguez-Iturbe (2004), Soil water balance and ecosystem response to climate change, *American Naturalist*, *164*, 625–632.

Potter, N. J., L. Zhang, P. C. D. Milly, T. A. McMahon, and A. J. Jakeman (2005), Effects of rainfall seasonality and soil moisture capacity on mean annual water balance for Australian catchments, *Water Resour. Res.*, *41*, W06007, doi:10.1029/2004WR003697.

Rawls, W. J., and D. L. Brakensiek (1985), Prediction of soil water properties for hydrologic modeling, *Watershed Management in the Eighties*, ASCE, 293–299.

Repetto, R. (1994), *The "second India" revisited: population, poverty and environmental stress over two decades*, World Resources Institute, Washington, D. C.

Rodell, M., I. Velicogna and J. S. Famiglietti (2009), Satellite-based estimates of groundwater depletion in India, *Nature*, 460, 999-1003, doi:10.1038/nature08238.

Roderick, M. L., and G. D. Farquhar (2011), A simple framework for relating variations in runoff to variations in climatic conditions and catchment properties, *Water Resour. Res.*, *47*, W00G07, doi:10.1029/2010WR009826.

Rui, H. (2015), Readme document for Global Land Data Assimilation System Version 1 (GLDAS-1) products, edited by N. A. a. S. A. GES DISC.

Sankarasubramanian, A., and R. M. Vogel (2002), Annual hydroclimatology of the United States, *Water Resour. Res.*, 38(6), 1083, doi:10.1029/2001WR000619.

Santhi, C., P. M. Allen, R. S. Muttiah, J. G. Arnold, and P. Tuppad (2008), Regional estimation of base flow for the conterminous United States by hydrologic landscape regions, *J. Hydrol.*, *351*(1), 139–153, http://dx.doi.org/10.1016/j.jhydrol.2007.12.018.

Savoskul, O. S., V. Smakhtin (2013a), *Glacier systems and seasonal snow cover in six major Asian river basins: water storage properties under changing climate*, pp. 69, International Water Management Institute, Colombo, doi:10.5337/2013.203.

Savoskul, O. S., V. Smakhtin (2013b), *Glacier systems and seasonal snow cover in six major Asian river basins: hydrological role under changing*, pp. 53, International Water Management Institute, Colombo, doi:10.5337/2013.204.

Scanlon, B. R., C. C. Faunt, L. Longuevergne, R. C. Reedy, W. M. Alley, V. L. McGuire, and P. B. McMahon (2012), Groundwater depletion and sustainability of irrigation in the US High Plains and Central Valley, *PNAS*, 109(24), 9320-9325, doi:10.1073/pnas.1200311109.

Scanlon, B. R., Z. Zhang, R. Reedy, D. R. Pool, H. Save, D. Long, J. Chen, D. M. Wolock, B. D. Conway and D. Winester (2015), Hydrologic Implications of GRACE Satellite Data in the Colorado River Basin (Accepted), *Water Resour. Res.*, 51, 9891–9903, doi:10.1002/2015WR018090.

Schwartz, F. W., and M. Ibaraki (2011), Groundwater: A resource in decline, *Elements*, 7, 175–179, doi:10.2113/gselements.7.3.175.

Scott C. A., and B. Sharma (2009), Energy supply and the expansion of groundwater irrigation in the Indus‐Ganges Basin, *International Journal of River Basin Management*, 7(2), 119-124, doi:10.1080/15715124.2009.9635374.

Shah, T. (2009), *Taming the anarchy: groundwater governance in South Asia*, pp. 26, RFF Press, Washington, D. C.

Shah, T., A. Roy, A. Qureshi, and J. Wang (2003), Sustaining Asia's groundwater boom: An overview of issues and evidence, *Natural Resources Forum*, 27(2), 130-141, doi: 10.1111/1477-8947.00048.

Shah, T., D. Molden, R. Sakthivadivel, D. Seckler (2000), *The global groundwater situation: Overview of opportunities and challenges*, International Water Management Institute, Colombo.

Shamsudduha, M., R. G. Taylor, and L. Longuevergne (2012), Monitoring groundwater storage changes in the highly seasonal humid tropics: Validation of GRACE measurements in the Bengal Basin, *Water Resour. Res.*, 48, W02508, doi:10.1029/2011WR010993.

Sharma, B., U. Amarasinghe, X. Cai, D. de Condappa, T. Shah, A. Mukherji, L. Bharati, G. Ambili, A. Qureshi, D. Pant, S. Xenarios, R. Singh and V. Smakhtin (2010), The Indus and the Ganges: river basins under extreme pressure, *Water International*, 35, 493-521, doi: 10.1080/02508060.2010.512996

Siddiqi A., J. L. Wescoat Jr. (2013), Energy use in large-scale irrigated agriculture in the Punjab province of Pakistan, Water International, 38(5), 571-586, DOI:10.1080/02508060.2013.828671

Siebert, S., J. Burke, J. M. Faures, K. Frenken, J. Hoogeveen, P. Döll, and F. T. Portmann (2010), Groundwater use for irrigation – a global inventory, *Hydrol. Earth Syst. Sci.*, 14, 1863-1880, doi:10.5194/hess-14-1863-2010.

Sivapalan, M. (2005), *Patterns, process and function: Elements of a unified theory of hydrology at the catchment scale, in: Encyclopedia of Hydrological Sciences*, John Wiley and Sons.

Sivapalan, M., M. A. Yaeger, C. J. Harman, X. Xu, and P. A. Troch (2011), Functional model of water balance variability at the catchment scale, 1: evidence of hydrologic similarity and space-time symmetry, *Water Resour. Res.*, *47*, W02522, doi:10.1029/2010WR009568.

Strassberg, G., B. R. Scanlon, and D. Chambers (2009), Evaluation of groundwater storage monitoring with the GRACE satellite: Case study of the High Plains aquifer, central United States, *Water Resour. Res.*, 45, W05410, doi:10.1029/2008WR006892.

Sun, A. Y., R. Green, M. Rodell, S. Swenson (2010), Inferring aquifer storage parameters using satellite and in situ measurements: estimation under uncertainty, *Geophys. Res. Lett.*, 37, L10401, doi:10.1029/2010GL043231.

Sun, A. Y., R. Green, S. Swenson, and M. Rodell (2012), Toward calibration of regional groundwater models using GRACE data, *J. Hydrol.*, 422, 1-9, doi:10.1016/j.jhydrol.2011.10.025.

Swenson, S. C. and J. Wahr (2006), Post-processing removal of correlated errors in GRACE data, *Geophys. Res. Lett.*, 33, L08402, doi:10.1029/2005GL025285.

Swenson, S., and J. Wahr (2002), Methods for inferring regional surface-mass anomalies from Gravity Recovery and Climate Experiment (GRACE) measurements of time-variable gravity, *J. Geophys. Res.*, 107(B9), 2193, doi:10.1029/2001JB000576.

Tang, Q., X. Zhang, and Y. Tang (2013), Anthropogenic impacts on mass change in North China, *Geophys. Res. Lett.*, 40, 3924-3928, doi: 10.1002/grl.50790.

Tapley, B. D., S. Bettadpur, J. C. Ries, P. F. Thompson, and M. M. Watkins (2004), GRACE measurements of mass variability in the Earth system, *Science*, 305, 503–505, doi:10.1126/science.1099192.

Thomas, H. A. (1981), Improved methods for national water assessment: Final report, *U.S. Geol. Surv. Water Resour*. Contract WR15249270, 44 pp.

Tiwari, V. M., J. Wahr, and S. Swenson (2009), Dwindling groundwater resources in northern India, from satellite gravity observations, *Geophys. Res. Lett.*, 36, L18401, doi:10.1029/2009GL039401.

Troch, P. A., G. Carrillo, M. Sivapalan, T. Wagener, and K. Sawicz (2013), Climate-vegetation-soil interactions and long-term hydrologic partitioning: signatures of catchment co-evolution, *Hydrol. Earth Syst. Sci.*, *17*, 2209–2217.

Troch, P. A., G. F. Martinez, V. R. N. Pauwels, M. Durcik, M. Sivapalan, C. Harman, P. D. Brooks, H. Gupta, and T. Huxman (2009), Climate and vegetation water use efficiency at catchment scales, *Hydrol. Process.*, *23*(16), 2409–2414.

Tucker, C. J., J. E. Pinzon, M. E. Brown, D. Slayback, E. W. Pak, R. Mahoney, E. Vermote, and N. El Saleous (2005), An extended AVHRR 8-km NDVI data set compatible with MODIS and SPOT vegetation NDVI data, *Int. J. Remote Sens.*, 26(20), 4485 ‑ 5598.

Turc, L. (1954), Le bilan d'eau des sols Relation entre la précipitation, l'évaporation et l'écoulement, *Ann. Agron.*, *5*, 491– 569.

U.S. Department of Agriculture Soil Conservation Service (SCS) (1972), *National Engineering Handbook, Section 4, Hydrology*, available from U.S. Government Printing Office, Washington, DC.

US Department of Agriculture Soil Conservation Service (SCS) (1985), *National Engineering Handbook, Section 4: Hydrology. SCS*, Washington, DC.

US Department of Agriculture, 2011. Soil Survey Geographic (SSURGO) Database, <http://soildatamart.nrcs.usda.gov>. United States Department of Agriculture, Natural Resources Conservation Service. Washington, DC.

Voepel, H., B. Ruddell, R. Schumer, P. A. Troch, P. D. Brooks, A. Neal, M. Durcik, and M. Sivapalan (2011), Quantifying the role of climate and landscape characteristics on hydrologic partitioning and vegetation response, *Water Resour. Res.*, 47, W00J09, doi:10.1029/2010WR009944.

Vogel, R. M., and A. Sankarasubramanian (2003), Validation of a watershed model without calibration, *Water Resour. Res.*, *39*(10), 1292, doi:10.1029/2002WR001940.

Wada, Y., L. P. H. van Beek, D. Viviroli, H. H. Dürr, R. Weingartner, and M. F. P. Bierkens (2011), Global monthly water stress: 2. Water demand and severity of water stress, *Water Resour. Res.*, 47, W07518, doi:10.1029/2010WR009792.

Wagener, T., M. Sivapalan, P. A. Troch, B. L. McGlynn, C. J. Harman, H. V. Gupta, P. Kumar, P. S. C. Rao, N. B. Basu, and J. S. Wilson (2010), The future of hydrology: An evolving science for a changing world, *Water Resour. Res.*, *46*, 1–10, doi:10.1029/2009WR008906.

Wahr, J., M. Molenaar, and F. Bryan (1998), Time variability of the Earth's gravity field: Hydrological and oceanic effects and their possible detection using GRACE, *J. Geophys. Res.*, 103(B12), 30205– 30229, doi: 10.1029/98JB02844.

Wang D. and M. Hejazi (2011), Quantifying the relative contribution of the climate and direct human impacts on mean annual streamflow in the contiguous United States, *Water Resour. Res.*, 47, W00J12, doi:10.1029/2010WR010283.

Wang, D. (2012), Evaluating interannual water storage changes at watersheds in Illinois based on long-term soil moisture and groundwater level data, *Water Resour. Res.*, 48, W03502, doi:10.1029/2011WR010759.

Wang, D., and N. Alimohammadi (2012), Responses of annual runoff, evaporation, and storage change to climate variability at the watershed scale, *Water Resour. Res.*, *48*, W05546, doi:10.1029/2011WR011444.

Wang, D., and L. Wu (2013), Similarity of climate control on base flow and perennial stream density in the Budyko framework, *Hydrol. Earth Syst. Sci.*, 17, 315–332.

Wang, D., and Y. Tang (2014), A one-parameter Budyko model for water balance captures emergent behavior in darwinian hydrologic models, *Geophys. Res. Lett.*, 41, 4569-4577, doi:10.1002/2014GL060509.

Wang, D., J. Zhao, Y. Tang, and M. Sivapalan (2015), A thermodynamic interpretation of Budyko and L'vovich formulations of annual water balance: proportionality hypothesis and maximum entropy production, *Water Resour. Res.*, *51*, 3007–3016, doi:10.1002/2014WR016857.

Woods, R. (2003). The relative roles of climate, soil, vegetation and topography in determining seasonal and long-term catchment dynamics, *Adv. Water Resour.*, *26*(3), 295–309, http://dx.doi.org/10.1016/S0309-1708(02)00164-1

Xu, X., W. Liu, B. R. Scanlon, L. Zhang, and M. Pan (2013), Local and global factors controlling water-energy balances within the Budyko framework, *Geophys. Res. Lett.*, *40*, 6123–6129, doi:10.1002/2013GL058324.

Yadav, M., T. Wagener, H. Gupta (2007), Regionalization of constraints on expected watershed response behavior for improved predictions in ungauged basins, *Adv. Water Resour.*, *30*, 1756–1774, http://dx.doi.org/10.1016/j.advwatres.2007.01.005.

Yang, D., F. Sun, Z. Liu, Z. Cong, G. Ni, and Z. Lei (2007), Analyzing spatial and temporal variability of annual water-energy balance in nonhumid regions of China using the Budyko hypothesis, *Water Resour. Res.*, *43*, W04426, doi:10.1029/2006WR005224.

Yang, H., D. Yang, Z. Lei, and F. Sun (2008), New analytical derivation of the mean annual water-energy balance equation, *Water Resour. Res.*, *44*, W03410, doi:10.1029/2007WR006135.

Ye, S., H. Y. Li, S. Li, L. R. Leung, Y. Demissie, Q. Ran, and G. Blöschl (2015), Vegetation regulation on streamflow intra-annual variability through adaption to climate variations, *Geophys. Res. Lett.*, *42*, 10,307–10,315, doi:10.1002/2015GL066396.

Yeh, P. J. F., S. C. Swenson, J. S. Famiglietti, and M. Rodell (2006), Remote sensing of groundwater storage changes in Illinois using the Gravity Recovery and Climate Experiment (GRACE), *Water Resour. Res.*, 42, W12203, doi:10.1029/2006WR005374.

Yokoo, Y., M. Sivapalan, and T. Oki (2008), Investigating the roles of climate seasonality and landscape characteristics on mean annual and monthly water balances, *J. Hydrol.*, *357*, 255–269, http://dx.doi.org/10.1016/j.jhydrol.2008.05.010.

Zanardo, S., C. J. Harman, P. A. Troch, P. S. C. Rao, and M. Sivapalan (2012), Intra-annual rainfall variability control on interannual variability of catchment water balance: A stochastic analysis, *Water Resour. Res.*, *48*, W00J16, doi:10.1029/2010WR009869.

Zhang X., Q. Tang, M. Pan, and Y. Tang (2014), A long-term land surface hydrologic fluxes and states dataset for China, *J. Hydrometeor*., 15, 2067–2084, doi:http://dx.doi.org/10.1175/JHM-D-13-0170.1.

Zhang, K., J. S. Kimball, R. R. Nemani, and S. W. Running (2010), A continuous satellite-derived global record of land surface evapotranspiration from 1983 to 2006, *Water Resour. Res.*, *46*, W09522, doi:10.1029/2009WR008800.

Zhang, L., K. Hickel, W. R. Dawes, F. H. S. Chiew, A. W. Western, and P. R. Briggs (2004), A rational function approach for estimating mean annual evapotranspiration, *Water Resour. Res.*, *40*, W02502, doi:10.1029/2003WR002710.

Zhang, L., W. R. Dawes, and G. R. Walker (2001), Response of mean annual evapotranspiration to vegetation changes at catchment scale, *Water Resour. Res.*, *37*(3), 701–708, doi: 10.1029/2000WR900325.

Zhang, S., H. Yang, D. Yang, and A. W. Jayawardena (2016), Quantifying the effect of vegetation change on the regional water balance within the Budyko framework, *Geophys. Res. Lett.*, *43*, 1140–1148, doi:10.1002/2015GL066952.

Zhao, J., D. Wang, H. Yang, and M. Sivapalan (2016), Unifying catchment water balance models for different time scales through the maximum entropy production principle, *Water Resour. Res., 52*, 7503–7512, doi:10.1002/2016WR018977.

Zhou, S., B. Yu, Y. Huang, and G. Wang (2015), The complementary relationship and generation of the Budyko functions, *Geophys. Res. Lett.*, 42, 1781-1790, doi:10.1002/2015GL063511.